Reaction engineering of radical-mediated polymerizations at surfaces and interfaces

A Thesis Submitted to the Faculty of the Graduate School of the
University of Colorado at Boulder
by

Raveesh Shenoy

B.Tech. Indian Institute of Technology Madras, 2007

in partial fulfillment of the requirement for
the degree of Doctor of Philosophy
Department of Chemical and Biological Engineering
2012

This thesis entitled:

Reaction engineering of radical-mediated polymerizations at surfaces and interfaces
written by Raveesh Shenoy
has been approved for the Department of Chemical and Biological Engineering

_____
Christopher N. Bowman, PhD (Committee Chair)

_____
Jeff W. Stansbury; Kristi S. Anseth; Stephanie J. Bryant; Virginia L. Ferguson
(Committee Members)

Date_____

The final copy of this thesis has been examined by the signatories, and we find that both the content and the form meet acceptable presentation standards of scholarly work in the above mentioned discipline

Shenoy, Raveesh (PhD, Chemical Engineering)

Reaction engineering of radical-mediated polymerizations at surfaces and interfaces
Thesis directed by Professor Christopher N. Bowman

Abstract

Polymerization reactions initiated at a surface or interface constitute a class of problems in which the reaction rates are spatially inhomogeneous due to concentration gradients that inevitably arise, thereby requiring an understanding of the coupled reaction behavior and mass transport processes to be able to control the material properties. This thesis is focused on understanding radical-mediated interfacial polymerizations initiated by an enzyme-mediated redox system, which represents a unique design paradigm to form conformal polymeric coatings on 3D substrates. In particular, glucose oxidase catalyzes the reaction between β-D-glucose and oxygen, producing hydrogen peroxide, which in the presence of ferrous ions (Fe^{2+}), generates hydroxyl radicals that are highly efficient for initiating (meth)acrylate polymerization. Interfacial coatings on hydrogel structures using this technique is realized by immersing a glucose-swollen hydrogel into an aqueous solution consisting of monomer, ferrous ion (Fe2+) and glucose-oxidase. The hydrogel serves as a template that spatially confines glucose prior to polymerization. Thus, the locus of the enzymatic reaction involving glucose is initially at the hydrogel boundary but is subsequently delocalized due to the rapid diffusion of glucose into the bulk media. This methodology represents the first instance of the use of interfacial radical polymerization with a non-stationary locus of the initiation reaction. Therefore, the establishment of design principles derived from understanding the reaction engineering aspects of this technique can immensely benefit the utilization of this technique as a material fabrication tool with a variety of monomers and initiating strategies. This thesis

is focused on understanding the factors that influence the reaction delocalization to achieve desired properties of the interfacial film such as thickness, permeability and structure. The relationship between the interfacial film thickness and immersion time, influence of species concentration on coating thickness and the kinetics of enzyme encapsulation by the polymerization front were experimentally investigated to understand the interplay of reaction behavior and mass transport processes. A mathematical model describing the complex coupled reaction-diffusion process through the fundamental steps was developed. The model predictions of the variation of thickness as a function of time and the influence of species concentration on the interfacial film thickness agreed well with the experimental results. In addition, the model was able to characterize interfacial film properties that are difficult to investigate experimentally such as the evolution of polymer density gradients in the coating as well as the factors that can be used to manipulate them. Lastly, the glucose oxidase-mediated redox initiation was engineered to fabricate core-shell microparticles by interfacial polymerization. This investigation broadens the applicability of this technique besides providing a simple reaction engineering tool to tune the surface properties at the micrometer scale.

You live in our hearts, in the happiness we knew
You still speak in the echoes of the words we've heard you say
Your memory is warm in our hearts, comfort in our sorrow.
You are not apart from us, but part of us

Megha, this thesis is dedicated to your memory

For keeping me rooted
And being an unchanging positive force
When it seemed like all was lost

Amma, **Pappa**, **Ganesh** and **Sujal,** this thesis is dedicated to you

Acknowledgements

I would like to express my gratitude to my advisor, Prof. Christopher Bowman whose encouragement, leadership and belief in my abilities helped me grow tremendously as a scientist. Chris has been the catalyst in bringing academic rigor to my efforts and enabling a balanced approach to scientific research.

I would like to express my gratitude to the people I met, friends and colleagues, in whose company I have found strength, vision and encouragement. Particularly, Nava, Vamshi and Shreya who have always been a source of refuge when I felt overwhelmed or lonely. Hugs to all the wonderful people I met: Kushala, Karthik, Abhishek, Monish, Prasanna, Kaniska, Anil, Malar, Parag, Falguni, Tejas, Bala. A huge thanks to my awesome colleagues, Richard Sheridan, Ryan Hansen, Heather Avens, Leah Johnson, Brad Berron, Vaibhav Khire, Mark Tibbitt, Devatha Nair, Tao Gong, Weixian Xi, Chris Fenoli, Ethan Gillett, Alan Aguirre, Abeer Alzahrani, Gayla Berg, Chris Koehler, Megan Cole, Jiancheng Liu, Shunsuke Chatani and Jim Wydra. Thanks to all my wonderful classmates especially Tirzah mills, Katie Rice, Lila Saade, Cole Deforest, Stephanie Lanasa, Pat Hume, Abby Banaszek. Finally, I would like to thank my committee members Kristi Anseth, Jeffrey Stansbury, Ginger Ferguson, Stephanie Bryant for their critique.

Table of Contents

List of Figures

List of Tables

List of schemes

Chapter 1

Introduction and background

1.1 Overview

The interface of material and biological sciences has emerged as a major research focus over the last decade due to significant strides in the ability to tailor the physical, chemical and biological properties of synthetic polymeric materials. Among the techniques used to engineer such materials, free radical polymerization is a powerful tool due to its compatibility with a wide variety of functional groups in addition to the significant body of knowledge that provides the means and understanding to control the reaction kinetics. However, the implementation of radical-mediated polymerizations to provide solutions for new and emerging technologies is not without challenges. This necessitates fundamental insight into these processes through integration of knowledge from several areas, thus allowing one to engineer the polymerization reaction to meet the design criteria for such technologies. Additionally, when polymerization is initiated at a surface or interface, the reaction rates are spatially inhomogeneous due to concentration gradients that inevitably arise, requiring an understanding of the coupled reaction behavior and mass transport processes to be able to control the material properties.

Among the various means available to generate radicals, redox initiation is advantageous in situations where curing of optically thick samples or uniform initiation rates at the interface of 3D objects is required. In such cases photoinitiation, a well-studied and extensively used initiation scheme, is at a major disadvantage due to depth-dependent light attenuation that results in non-uniform conversion profiles. Therefore, redox reactions can be used to initiate interfacial polymerization on complex 3D

substrates as a means to achieve conformal coatings. In particular, glucose oxidase-mediated redox chain initiation is a light-independent radical generation methodology known to efficiently initiate (meth)acrylate polymerization in addition to being impervious to oxygen inhibition. Furthermore, this approach represents the ideal reaction

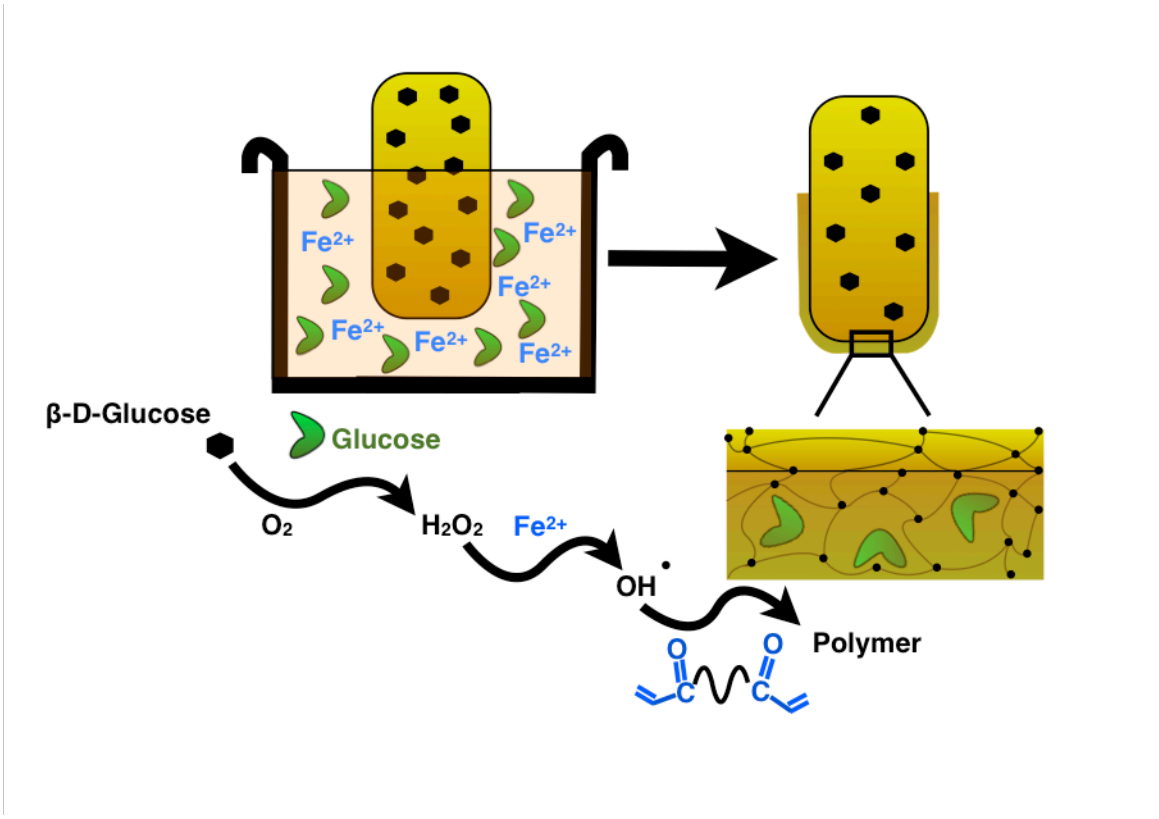

Figure 1.1: Schematic illustrating the formation of coating on hydrogel substrates by interfacial polymerization initiated by a glucose oxidase-mediated system. Reaction between GOx and glucose that subsequently triggers polymerization initially occurs near the hydrogel boundary but becomes delocalized due to rapid diffusion of glucose.

to facilitate interfacial polymerization as it necessitates multiple components to achieve rapid, successful polymerization. As such, this technique can be used to form conformal coatings on complex 3D substrates quite simply by immersion of the desired substrate into a precursor solution (Figure 1), resulting in polymerization initiation at the substrate boundary since contact between the various necessary components for initiation exists

only there. Polymerization occurs initially at the interface due to the reaction between glucose in the supporting hydrogel substrate and glucose oxidase in the immersing solution. However, due to the rapid diffusion of glucose and hydrogen peroxide into the bulk media, the initiation reaction becomes delocalized and as a result

capable of fabricating coatings that are much thicker than radical or other conventional interfacial polymerization strategies. This methodology represents the first

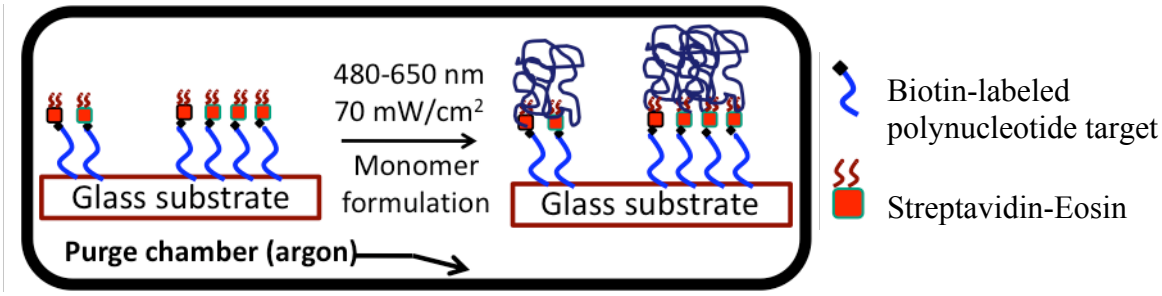

Figure 2: Schematic depicting surface-initiated photopolymerization for amplification of biorecognition events. The recognition reaction between biotin-labeled polynucleotide and the macrophotoinitiator, Streptavidin-Eosin is rendered visible upon polymer formation

instance of the use of interfacial radical polymerization with a non-stationary locus of the initiation reaction. Therefore, the establishment of design principles derived from understanding the reaction engineering aspects of this technique can immensely benefit the utilization of this technique as a material fabrication tool with a variety of monomers and initiating strategies. Chapter 3 of this thesis establishes an experimental basis for the conceptualization of the mechanistic aspects of the interfacial polymerization on macroscopic hydrogel substrates while chapter 4 implements this understanding to develop a generalized kinetic model used to predict the polymer formation and species

concentration gradients. This network characterization capability of the model is immensely useful in understanding the mass transport properties of the coating. Chapter 5 demonstrates the ability to enable conformal coatings on hydrogel substrates whose dimensions are in the sub-millimeter range.

Photoinitiation is a light-dependent technique that affords spatiotemporal control over polymerization and lead to rapid reactions that occur at ambient conditions. These benefits enable photopolymerization to be used extensively in biological applications, including in the surface-initiated photopolymerization-based amplification of molecular recognition events. In this technique, photoinitiators are allocated in proportional amounts to the target material attached to a solid substrate by means of a biorecognition reaction between the photoinitiator and target. This reaction is followed by formation of highly crosslinked polymeric material which occurs only in regions where the photoinitiators are allocated based on biospecific molecular interactions. This biospecific polymerization renders the initially invisible biomolecular recognition event, visible due to the macroscopic nature of the polymer gel that is formed as a result of the radical photoinitiation (Figure 2). However, this process necessarily is performed in an atmosphere devoid of oxygen, due to its inhibiting effect on radical polymerizations. Additionally, a cost-intensive light source that delivers high power output is employed to create favorable photopolymerization conditions.

In considering such a technique for biodetection in resource-limited settings, infectious diseases that are otherwise treatable continue to pose a major challenge. Their existence makes it imperative to design diagnostic tests that are user-friendly, affordable, equipment-free and readily deliverable to the point of care in addition to ensuring high

sensitivity and specificity. Therefore, there is a need to design a photoinitiation scheme that would enable suppression of oxygen inhibition in parallel with photopolymerization, thereby eliminating the necessity to purge oxygen from the sample. Chapter 6 of this dissertation investigates such a photoinitiation strategy to overcome oxygen inhibition in addition to demonstrating the ability to conduct bulk radical polymerization of acrylates in the extreme condition of oxygen-purged formulations. The optimized conditions are then implemented in the surface grafting of highly crosslinked polymers from ultra low concentrations of surface-bound photoinitiators without the need to use purge chambers or high power light sources. This aspect is discussed in chapter 7 and provides a foundation for future directions in using surface-initiated photopolymerization as a tool to amplify molecular recognition events without purging of oxygen from the vicinity.

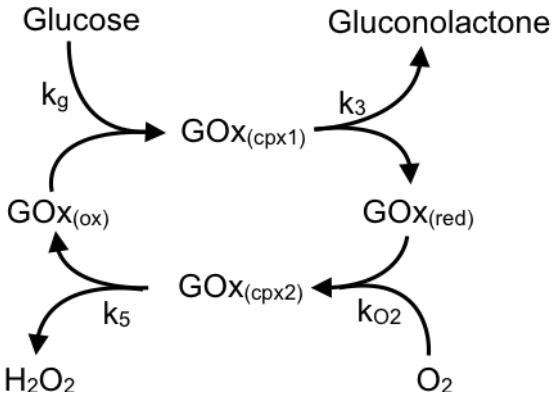

Scheme 1.1: Ping-pong mechanism of action of glucose oxidase (GOx). The glucose oxidase reciprocates between the oxidized state ($GOx_{(ox)}$) and the reduced state ($GOx_{(red)}$) as a result of being reduced by glucose and oxidized by oxygen in alternation. The intermediates in these transformations are the complexed states ($GOx_{(cpx1)}$ and $GOx_{(cpx1)}$)

1.2 Conformal coating of 3D hydrogel substrates by interfacial radical polymerization

1.2.1 Glucose oxidase mediated reaction

The enzyme, glucose oxidase (GOx), is an oxido-reductase, meaning it catalyzes the transfer of electrons between molecules. It is widely used in glucose biosensors[1,2] due to its rapid and specific reaction with -D-Glucose producing hydrogen peroxide that can subsequently be used in colorimetric determination of glucose levels. The specificity of this enzymatic reaction enables its use in quantitative determination of glucose in blood, urine, foods and other biological systems. The ability of the enzyme to catalyze the formation of hydrogen peroxide from glucose also enables its use as an antibacterial agent and an oxidant in food processing[3,4]. Glucose is slowly oxidized by oxygen to gluconolactone producing hydrogen peroxide, but is accelerated significantly in the presence of GOx. The best-studied enzyme is glucose oxidase from the fungi, *Aspergillus Niger*. It has a molecular weight of 186,000 and the mechanism of its action is shown in Scheme 2. The enzyme alternates between the oxidized and the reduced states as a result of being reduced by glucose and oxidized by oxygen in alternation. This mechanism has been comprehensively elucidated in the seminal work of Gibson *et al.*[5].

In addition to the GOx reaction involving glucose, the enzyme also reacts with other monosaccharides such as D-Mannose and Xylose (~100 times less reactive), and β-D-Galactose (~200 times less reactive). Besides oxygen, other hydrogen acceptors such as thionine, methylene blue and quinones can also be used; however, these substrates do not result in hydrogen peroxide generation. Hydrogen peroxide can also be generated by enzymatic reactions involving other enzymes such as amine oxidases[6,7], glycolate oxidase[8] and xanthine oxidase[9]. This thesis is focused on using the GOx-mediated reaction involving glucose and oxygen as the two substrates used to produce hydrogen peroxide.

1.2.2 Redox reaction

Hydrogen peroxide generated from the enzymatic reaction can participate in electron transfer reactions with a donor to generate radicals. The most commonly employed redox reaction involving hydrogen peroxide for radical generation is the Fenton's reaction proposed by Fenton in 1894[10]. This reaction is an electron transfer reaction between hydrogen peroxide and Fe^{2+} to generate hydroxyl radicals. In fact, the hydroxyl radicals responsible for the oxidative capability of the Fenton's reagent (H_2O_2 and Fe^{2+}), were implicated 40 years later by Haber *et al.*[11] and is comprehensively described in the highly cited review article on the Fenton's reagent[12]. Other reductants such as Cr^{2+}, V^{2+}, Ti^{3+}, Co^{2+}, and Cu^{+} can also be used instead of iron [13]. Hydroxyl radicals are an extremely reactive species[14] that are very efficient in initiating (meth)acrylate polymerization.

The advantage of radical generation resulting from coupling the redox reaction with the enzymatic generation of hydrogen peroxide is manifold. Firstly, other enzymatic reactions that use hydrogen peroxide directly as the substrate to generate radicals suffer from long and irregular inhibition times likely due to the dismutation of H_2O_2 to form oxygen, which has a strong inhibitory effect on radical polymerizations. In this technique, H_2O_2 is not present at high concentration to begin with and is rapidly consumed by Fe^{2+} as it is generated. Secondly, high levels of hydrogen peroxide that result from its use directly as a substrate prevents its applicability in biological systems due to the cytotoxic nature of H_2O_2. Thirdly, the enzymatic reaction provides an additional level of control over initiation kinetics, and this overcomes challenges in controlling the rapid reaction between iron salts and hydrogen peroxide when it is the sole initiation step. Most

importantly, coupling of the enzymatic and redox reactions necessitates the use of multiple components to achieve rapid, successful polymerization, thereby presenting a simple opportunity to conduct interfacial polymerization by bringing into contact initiating species that are spatially isolated. By confining glucose in the hydrogel support phase and the complimentary initiating species (GOx, Fe^{2+}) in the bulk media, the initial locus of reaction initiation is limited to the interface. Since the immersing solution (Figure 1) also consists of the monomer, poly(ethylene glycol) diacrylate, rapid reaction ensues between the hydroxyl radicals and the carbon-carbon double bonds of the acrylate functionality to result in interfacially-confined polymer formation.

1.2.3 Interfacial radical-mediated polymerization

Glucose oxidase-mediated redox initiation is appropriate for implementation as an interfacial polymerization technique due to the relative simplicity with which the components of the initiation system are separated. These components can be spatially organized in different phases such that contact between the initiating species arises only at the interface. Glucose is poorly soluble in organic media and glucose oxidase (GOx) shows reduced reactivity in non-aqueous solvents. Therefore, the reaction between glucose and GOx is most efficient when water is used as the solvent. Hydrogels are water-swollen porous substrates that are insoluble in water and are therefore an ideal phase to confine one of the initiating species, particularly considering they offer a significant transport barrier to large molecules such as GOx. By confining glucose in the hydrogel and having GOx, Fe^{2+} and an acrylic monomer such as poly(ethylene glycol) diacrylate in an external aqueous phase, interfacial polymerization is accomplished simply by immersion of the hydrogel substrate in the aqueous precursor solution. Upon

contacting the two phases, the initiating components are free to diffuse in the direction of their concentration gradient, thereby resulting in the delocalization of the initiation reaction. Due to the delocalization resulting from the mobility of the radical generating species, films much thicker than those films formed by conventional interfacial polymerizations are formed.

The absence of immobilization also affords the fabrication of multiple polymeric layers without complicated multiple surface attachment/immobilization of radical generating species. For example, multilayered interfacial films are enabled simply by immersion of the substrate successively in liquid phases containing different monomers. This outcome occurs because the initiating species confined in the porous substrate (glucose in this investigation) diffuse through the first layer to react with initiating species in the bulk, leading to surface radical generation and the formation of a second layer. Additionally, this polymerization mode is compatible with a wide variety of monomers and functional groups that are used to influence the properties of the resulting polymeric material such as permeability, crosslink density, mechanical integrity and various chemical or biological properties. The following sections discuss some of the applications that could benefit from using radical-mediated interfacial polymerization.

1.3 Applications

1.3.1 Biocompatible coatings

Hydrogels have been widely used as a synthetic extracellular matrix to organize cells in a 3-D environment because of their hydrophilic nature, mild fabrication conditions and biocompatibility[15,16,17]. In spite of the relatively biocompatible nature of hydrogels compared to metal implants, without systemic immunosuppression, graft

failure can result partly because small molecules such as cytokines and reactive oxygen species diffuse into the hydrogel and compromise the integrity of the cells. Unfortunately, this immunosuppression strategy results in undesirable side effects and the risk of infection. One approach to overcoming these biocompatibility issues is surface functionalization of hydrogel implants to enable implant isolation and prevent the invasion of the hydrogel structures by destructive small molecules. Additionally, surface modification prevents undesirable interactions between the biological functionalities responsible for immunoprotection and the encapsulated cells as a result of the spatial separation. Researchers have used various methods to tune the surface properties of hydrogels such as layer-by-layer fabrication of hydrogels by photopolymerization[18] and photolithographic patterning of hydrogel surfaces[19]. These methods suffer from the inability to form conformal coatings on complex 3D hydrogel substrates because of depth-dependent light attenuation that results in non-uniform light intensity distribution to the surface. The GOx-mediated redox initiation of interfacial polymerization is a light-independent process, takes place under mild aqueous conditions, and is ideally suited to the fabrication of conformal 3D coatings on such hydrogel structures. Furthermore, the radical nature of the polymerization process is compatible with a wide variety of monomers and functional groups and enables tailoring of the physical, chemical and biological properties of the coating by physical entrapment of biological moieties or covalent incorporation of molecules through copolymerization.

1.3.2 Drug Delivery

Traditional drug delivery methods use oral, intravenous or subcutaneous routes that generally result in the distribution of drug throughout the body through the systemic

blood circulation. However, this approach can result in unfavorable pharmacokinetics due to the rapid clearance of the drug by the kidney. Drugs that have widespread distribution in the body can affect normal tissues resulting in dose-limiting side effects. Drugs derived from proteins or peptides are prone to proteolytic degradation and hence have extremely short circulation times that often require multiple injections or large doses to maintain the drug concentration in the therapeutic window. Many of these pharmacological properties can be significantly improved through the use of drug delivery carriers[20-30]. Specifically, hydrogels are ideal carriers for the delivery of bioactive materials due to the 3D nature of the polymer network, well-defined physicochemical properties, mild network fabrication techniques and drug encapsulation conditions and reproducible drug release profiles[20,31-35]. In addition, materials used to construct such hydrogels can be designed to respond to external stimuli such as heat, light, pH, current, and/or magnetic field, and therefore, facilitate not only the release of such active materials at a characteristic rate but also provide spatiotemporal control over its delivery under some circumstances[36-42]. This ability to manipulate the controlled release behavior is one of the primary objectives of any drug delivery system to sustain the drug concentration in the therapeutic window for an extended period. The geometry of the architectures also plays a critical role in being able to tune the release rate of the encapsulated material. Researchers have used a variety of geometries such as triangular, hemispherical, donut–shaped devices to tune the release rates to the desired profiles[43-52]. The versatility of hydrogels can be combined with surface modification techniques to enable many advantageous characteristics. Coatings can be designed to function as time-dependent, stimuli-responsive degradable barriers that delay the release of molecules

encapsulated within the core or any layer. Multilayer coatings with diverse physicochemical properties also enable more complex release profiles such as bimodal or pulsatile release. Additionally, compartmentalization of multiple drugs is achieved with multilayered coatings.

The mild fabrication conditions and the 3D hydrophilic nature of the hydrogel substrate and coating formed by this method are ideally suited to encapsulate bioactive molecules such as proteins and peptides as well as to enable homogeneous dispersion of hydrophilic drugs for delivery. The ability to form complex 3D structures stratified with assorted characteristics benefits the fabrication of drug- delivery devices that deliver multiple drugs which are spatially isolated before delivery. The ability to fabricate coatings on complex geometries provides an additional handle in tuning the release profiles of these bioactive materials. The rapid formation of coatings ranging from as thin as 20 microns to several millimeters can be useful to increase drug loading, delay drug release or enhance the mechanical properties of the construct without sacrificing permeability.

In these applications, it is important to have the means and the understanding to control the interfacial film properties such as thickness, permeability and the structure. Coating thickness is a critical factor that dictates the size of hydrogel implants. Permeability influences the diffusion of molecules into and out of the coated construct, and thus, the viability of encapsulated cells or release profiles of therapeutic molecules. The film structure such as the presence of gradients in the concentration of polymer can enable the fashioning of chemical or biological property gradients in the coating by copolymerization. However, investigations on interfacial polymerization reported in the literature focus on the condensation reaction between two monomers, and no work exists

that describe the nature of interfacial polymerization initiated by radical forming reactions. Mechanistic insight into the process can enable materials and process design of appropriate monomers, initiating systems and conditions necessary for optimizing this interfacial radical polymerization based coating process and predicting the kinetics of film growth. Chapter 3 of this thesis attempts to understand the interplay of the coupled reaction diffusion process in the glucose oxidase-mediated interfacial polymerization of macroscopic hydrogel substrates through design of experiments. Chapter 4 focuses on building a mathematical model based on this developed understanding that can predict not only the kinetics of film growth but determine factors that can be used to enable control over the physicochemical properties of the interfacial coating.

1.3.3 Small-scale drug delivery systems

Currently, a typical dose of a potent drug is tens to hundreds of micrograms. For example, epinephrine, which is used to treat anaphylactic shock delivers an injection of 300 micrograms of the drug. Fentanyl, a potent narcotic used for anesthesia is given in doses of 25 micrograms for adults. Antibiotics such as penicillin and amoxillin are given in doses exceeding 1 gram per day for adults. This highlights the importance of the scale of drug delivery systems designed for such uses. Efforts to miniaturize drug delivery devices from the macroscale (>1mm) to the microscale (<1mm) are the subject of emerging research and offer several benefits in addition to the ability to use small quantities of drug payloads[54,55]. Micro-engineered devices can be delivered, by non-surgical means such as injections, to areas of the body not accessible by macroscopic devices. Submicron carriers smaller than a few microns can be internalized by cells and deliver small amounts of bioactive materials such as proteins, peptides and nucleic acids

directly to the cytoplasm of the cells for cell-based prophylactic and therapeutic treatments. The micro-scale size of the carrier also enhances diffusion of nutrients and other factors that are essential to maintain the function of the encapsulated cells or biological moiety. Micron-scale carriers greater than 10 microns act as depots for drug delivery while simultaneously displaying longer circulation times due to minimal phagocytosis, a process in which macrophages internalize solid particles and clear them from the body[53]

Chapter 5 of this thesis demonstrates the ability to form conformal coatings on sub-millimeter hydrogel particles thereby broadening the applicability of this technique besides providing a simple reaction engineering tool to tune the surface properties at the micrometer scale.

1.4 Photopolymerization-based amplification: A molecular diagnostic tool

1.4.1 Introduction to molecular diagnostics

Molecular diagnostics is a field concerned with identifying biomarkers such as nucleic acids, proteins and other metabolites well known as molecular signatures for the onset of disease that leads to timely treatments. Early diagnosis holds promise for greatly improving patient prognosis and aiding in the administration of preventive medicine; however, this approach demands highly sensitive detection of ultra-low concentrations of target materials. One approach is creating multiple copies of the target material and subsequent detection of the amplified products[56,57,58]. The second approach is the establishment of an amplified signal from molecular recognition events[59-66]such as the hybridization reactions between complimentary polynucleotides, by coupling the molecular recognition reaction to a magnified auxiliary response. Photopolymerization-

based amplification is based on exactly such an approach.

1.4.2 Photopolymerization-based amplification

Free radical polymerization is a process that transforms low molecular weight monomers into high molecular weight polymers as a result of a chain reaction initiated by radicals. These radicals can be generated as a result of a number of different means with one of the most common being photoinitiation where a photon directly or indirectly leads to radical generation. However, every radical that is generated can initiate a chain reaction that consumes a vast number of monomer molecules. This inherent amplification

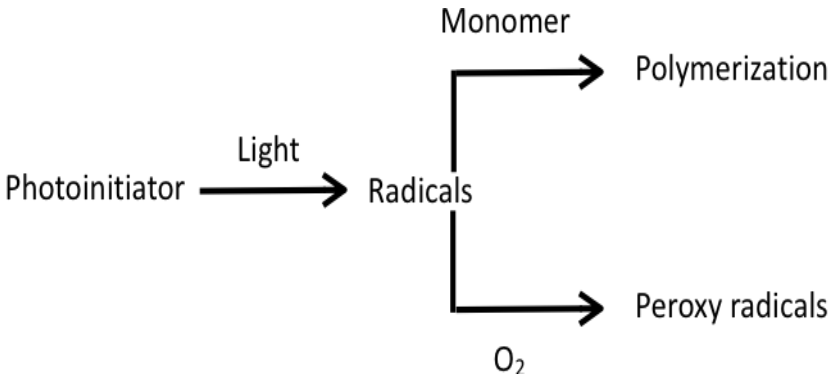

Scheme 1.2: Schematic of oxygen inhibition which is the classical issue facing radical polymerizations. The radical consumption reaction by oxygen competes with the desired chain initiating reaction with monomer. The resulting peroxy radicals formed by reactions with oxygen are poor initiators of polymerization.

present in photopolymerization is precisely what is exploited in the visual biodetection in a highly sensitive manner[67-70]. By coupling photoinitiators to recognition events followed by polymerization in the presence of monomer, visual detection is accomplished due to the macromolecular nature of the polymer that is formed. The high sensitivity afforded by this strategy is directly related to the ability to initiate polymerization from extremely low concentrations of photoinitiators, and this sensitivity is intimately connected with the

ability to prevent radical reactions that do not contribute to polymerization. Unfortunately, oxygen limits radical polymerizations by acting as a powerful radical scavenger, consuming radicals on a one radical to one oxygen molecule basis to form peroxy radicals that are practically incapable of continuing the polymerization, particularly in the absence of any chain transfer agents such as thiols or amines[71,72]. This behavior is shown in Scheme 1. Since the inhibition reaction is much more rapid than the radical propagation reaction with monomer, polymerization does not begin until nearly all of the oxygen is consumed. To enable high sensitivity, surface-initiated photopolymerization must be conducted in the absence of oxygen in the monomer formulation as well as in the vicinity because oxygen can diffuse rapidly into the monomer formulation. Oxygen elimination is accomplished by enclosing the process in a chamber that is continuously purged with an inert gas such as argon or nitrogen that does not react with radicals. Without this modification, surface-initiated polymerization is completely suppressed, an indication of the drastic inhibitory effect of oxygen. In addition, photoinitiation rates must be maintained sufficiently high in order to minimize the inhibitory contribution from remnant oxygen as it diffuses from the bulk media to the radical generation site. High initiation rates are usually accomplished by utilizing a high power light source such as that from a mercury vapor lamp.

1.4.3 Molecular diagnostics in resource-limited settings

Infectious diseases that are otherwise treatable are a major source of concern in the developing world. For example, several studies in Africa, that is most burdened by Malaria[73,74,75], have shown that for every case of fever-related illness diagnosed in a healthcare facility, five others remain untreated in the outlying areas[75]. Pneumonia and

Table 1: Characteristics of an ideal diagnostic test for the developing world

ASSURED

- **A**ffordable by those at risk of infection
- **S**ensitive (Few false-negative results)
- **S**pecific (Few false-positive results)
- **U**ser-friendly (no trained personnel required)
- **R**apid treatment at first visit
- **E**quipment-free (No large electricity dependence, portability)
- **D**elivered to those in need

other respiratory illnesses are the major source of child mortality in these countries[76,77]. A critical factor in reducing infections in the developing world is the ability to provide accurate diagnosis and monitor the patient response to such treatments. The World Health Organization (*WHO*) has developed a list of criteria for the feasibility of a diagnostic technology in resource-limited settings prevalent in the developing world[78]. These are abbreviated by the acronym ASSURED and shown in Table 1. It is not only necessary for the detection scheme to be highly sensitive and specific but also be simple enough to be operated by personnel not experienced in laboratory settings, affordable, equipment-free and readily deliverable at the point of care.

A portion of this thesis (Chapter 6) is focused on developing a strategy to suppress oxygen inhibition while simultaneously performing photopolymerization without the need to physically eliminate the oxygen from the monomer formulation. In this chapter, the strategy is presented and the hypothesis of the mechanism is validated

through a series of experimental strategies and mathematical modeling. The capability of this technique is then demonstrated by conducting bulk polymerization in the extreme condition of a monomer formulation that is equilibrated with pure oxygen. Chapter 7 discusses future directions concerning this suppression technique in the context of surface-initiated photopolymerization. Specifically, the ability to conduct surface-initiated photopolymerization uninhibited by oxygen is demonstrated without the need to use purge chambers or high power light sources.

1.5 References

1. Gregg BA, Heller A. Cross-linked redox gels containing glucose oxidase for amperometric biosensor applications. Analytical Chemistry. 1990;62(3):258-63.

2. Wilson R, Turner APF. Glucose oxidase: an ideal enzyme. Biosensors and Bioelectronics. 1992;7(3):165-85.

3. Gujral HS, Rosell CM. Improvement of the breadmaking quality of rice flour by glucose oxidase. Food Research International. 2004;37(1):75-81.

4. Tiina M, Sandholm M. Antibacterial effect of the glucose oxidase-glucose system on food-poisoning organisms. International Journal of Food Microbiology. 1989;8(2):165-74.

5. Gibson QH, Massey V, Swoboda BEP. Kinetics and mechanism of action of glucose oxidase Journal of Biological Chemistry. 1964;239(11):3927-&.

6. Cona A, Rea G, Angelini R, Federico R, Tavladoraki P. Functions of amine oxidases in plant development and defence. Trends in Plant Science. 2006;11(2):80-8.

7. Brazeau BJ, Johnson BJ, Wilmot CM. Copper-containing amine oxidases.

Biogenesis and catalysis; a structural perspective. Archives of Biochemistry and Biophysics. 2004;428(1):22-31.

8. Blanchard M, Green DE, Nocitocarroll V, Ratner S. L-HYDROXY ACID OXIDASE. Journal of Biological Chemistry. 1946;163(1):137-44.

9. Lacy F, Gough DA, Schmid-Schonbein GW. Role of xanthine oxidase in hydrogen peroxide production. Free Radical Biology and Medicine. 1998;25(6):720-7.

10. Fenton HJH. LXXIII.-Oxidation of tartaric acid in presence of iron. Journal of the Chemical Society, Transactions. 1894;65:899-910.

11. Haber F, Weiss J. The Catalytic Decomposition of Hydrogen Peroxide by Iron Salts. Proceedings of the Royal Society of London Series A - Mathematical and Physical Sciences. 1934;147(861):332-51.

12. Walling C. Fenton's reagent revisited. Accounts of Chemical Research. 1975;8(4):125-31.

13. Odian GG. Principles of Polymerization: Wiley-Interscience; 2004.

14. Pryor WA. Oxy-Radicals and Related Species: Their Formation, Lifetimes, and Reactions. Annual Review of Physiology. 1986;48(1):657-67.

15. Slaughter BV, Khurshid SS, Fisher OZ, Khademhosseini A, Peppas NA. Hydrogels in Regenerative Medicine. Advanced Materials. 2009;21(32-33):3307-29.

16. Jagur-Grodzinski J. Polymers for tissue engineering, medical devices, and regenerative medicine. Concise general review of recent studies. Polymers for Advanced Technologies. 2006;17(6):395-418.

17. Drury JL, Mooney DJ. Hydrogels for tissue engineering: scaffold design variables and applications. Biomaterials. 2003;24(24):4337-51.

18. Weber LM, Cheung CY, Anseth KS. Multifunctional Pancreatic Islet Encapsulation Barriers Achieved Via Multilayer PEG Hydrogels. Cell Transplantation. 2007;16(10):1049-57.

19. Hynd MR, Frampton JP, Burnham M-R, Martin DL, Dowell-Mesfin NM, Turner JN, et al. Functionalized hydrogel surfaces for the patterning of multiple biomolecules. Journal of Biomedical Materials Research Part A. 2007;81A(2):347-54.

20. Lin C-C, Metters AT. Hydrogels in controlled release formulations: Network design and mathematical modeling. Advanced Drug Delivery Reviews. 2006;58(12–13):1379-408.

21. Langer R. NEW METHODS OF DRUG DELIVERY. Science. 1990;249(4976):1527-33.

22. Rojanasakul YY. Antisense oligonucleotide therapeutics: Drug delivery and targeting. Advanced Drug Delivery Reviews. 1996;18(2):115-31.

23. Pierige F, Serafini S, Rossi L, Magnani A. Cell-based drug delivery. Advanced Drug Delivery Reviews. 2008;60(2):286-95.

24. Charman WN. Lipids, lipophilic drugs, and oral drug delivery - Some emerging concepts. Journal of Pharmaceutical Sciences. 2000;89(8):967-78.

25. Delehanty JB, Boeneman K, Bradburne CE, Robertson K, Medintz IL. Quantum dots: a powerful tool for understanding the intricacies of nanoparticle-mediated drug delivery. Expert Opinion on Drug Delivery. 2009;6(10):1091-112.

26. Lee HJ. Protein drug oral delivery: The recent progress. Archives of Pharmacal Research. 2002;25(5):572-84.

27. Menjoge AR, Kannan RM, Tomalia DA. Dendrimer-based drug and imaging

conjugates: design considerations for nanomedical applications. Drug Discovery Today. 2010;15(5-6):171-85.

28. Muller RH, Mader K, Gohla S. Solid lipid nanoparticles (SLN) for controlled drug delivery - a review of the state of the art. European Journal of Pharmaceutics and Biopharmaceutics. 2000;50(1):161-77.

29. Meisner D, Mezei M. LIPOSOME OCULAR DELIVERY SYSTEMS. Advanced Drug Delivery Reviews. 1995;16(1):75-93.

30. Wilson-Welder JH, Torres MP, Kipper MJ, Mallapragada SK, Wannemuehler MJ, Narasimhan B. Vaccine Adjuvants: Current Challenges and Future Approaches. Journal of Pharmaceutical Sciences. 2009;98(4):1278-316.

31. Peppas NA, Bures P, Leobandung W, Ichikawa H. Hydrogels in pharmaceutical formulations. European Journal of Pharmaceutics and Biopharmaceutics. 2000;50(1):27-

32. Ganji F, Vasheghani-Farahani E. Hydrogels in Controlled Drug Delivery Systems. Iranian Polymer Journal. 2009;18(1):63-88.

33. Kashyap N, Kumar N, Kumar M. Hydrogels for pharmaceutical and biomedical applications. Critical Reviews in Therapeutic Drug Carrier Systems. 2005;22(2):107-49.

34. Gupta P, Vermani K, Garg S. Hydrogels: from controlled release to pH-responsive drug delivery. Drug Discovery Today. 2002;7(10):569-79.

35. Hoffman AS. Hydrogels for biomedical applications. Advanced Drug Delivery Reviews. 2002;54(1):3-12.

36. Bajpai AK, Shukla SK, Bhanu S, Kankane S. Responsive polymers in controlled drug delivery. Progress in Polymer Science. 2008;33(11):1088-118.

37. Qiu Y, Park K. Environment-sensitive hydrogels for drug delivery. Advanced

Drug Delivery Reviews. 2001;53(3):321-39.

38. Soppimath KS, Aminabhavi TM, Dave AM, Kumbar SG, Rudzinski WE. Stimulus-responsive "smart" hydrogels as novel drug delivery systems. Drug Development and Industrial Pharmacy. 2002;28(8):957-74.

39. Kurisawa M, Yui N. Dual-stimuli-responsive drug release from interpenetrating polymer network-structured hydrogels of gelatin and dextran. Journal of Controlled Release. 1998;54(2):191-200.

40. Kulkarni RV, Biswanath S. Electrically responsive smart hydrogels in drug delivery: a review. Journal of Applied Biomaterials & Biomechanics. 2007;5(3):125-39.

41. Kikuchi A, Okano T. Pulsatile drug release control using hydrogels. Advanced Drug Delivery Reviews. 2002;54(1):53-77.

42. Gil ES, Hudson SM. Stimuli-reponsive polymers and their bioconjugates. Progress in Polymer Science. 2004;29(12):1173-222.

43. Mishra DS, Yalkowsky SH. A Flat Circular Hole Device for Zero-Order Release of Drugs: Characterization of the Moving Dissolution Boundary. Pharmaceutical Research. 1990;7(11):1195-7.

44. Narasimhan B, Langer R. Zero-order release of micro- and macromolecules from polymeric devices: the role of the burst effect. Journal of Controlled Release. 1997;47(1):13-20.

45. Sangalli ME, Maroni A, Zema L, Cerea M, Conte U, Gazzaniga A. A study on the release mechanism of drugs from hydrophilic partially coated perforated matrices. Il Farmaco. 2003;58(9):971-6.

46. Qiu Y, Chidambaram N, Flood K. Design and evaluation of layered diffusional

matrices for zero-order sustained-release. Journal of Controlled Release. 1998;51(2–3):123-30.

47. Lu S, Ramirez WF, Anseth KS. Photopolymerized, multilaminated matrix devices with optimized nonuniform initial concentration profiles to control drug release. Journal of Pharmaceutical Sciences. 2000;89(1):45-51.

48. Kim C-j. Release kinetics of coated, donut-shaped tablets for water soluble drugs. European Journal of Pharmaceutical Sciences. 1999;7(3):237-42.

49. Kim C-j. Compressed Donut-Shaped Tablets with Zero-Order Release Kinetics. Pharmaceutical Research. 1995;12(7):1045-8.

50. Karasulu HY, Ertan G. Different geometric shaped hydrogel theophylline tablets: statistical approach for estimating drug release. Il Farmaco. 2003;57(11):939-45.

51. Hsieh DST, Rhine WD, Langer R. Zero-order controlled-release polymer matrices for micro- and macromolecules. Journal of Pharmaceutical Sciences. 1983;72(1):17-22.

52. Conte U, Maggi L, Colombo P, La Manna A. Multi-layered hydrophilic matrices as constant release devices (GeomatrixTM Systems). Journal of Controlled Release. 1993;26(1):39-47.

53. Champion JA, Walker A, Mitragotri S. Role of particle size in phagocytosis of polymeric microspheres. Pharmaceutical Research. 2008;25(8):1815-21.

54. Putnam D. Polymers for gene delivery across length scales. Nat Mater. 2006;5(6):439-51.

55. Raemdonck K, Demeester J, De Smedt S. Advanced nanogel engineering for drug delivery. Soft Matter. 2009;5(4):707-15.

56. Heid CA, Stevens J, Livak KJ, Williams PM. Real time quantitative PCR.

Genome Research. 1996;6(10):986-94.

57. Parsons G. Development of DNA Probe-Based Commercial Assays. Journal of Clinical Immunoassay. 1988;11(4):152-60.

58. Saiki RK, Gelfand DH, Stoffel S, Scharf SJ, Higuchi R, Horn GT, et al. Primer-Directed Enzymatic Amplification of DNA with a Thermostable DNA-Polymerase. Science. 1988;239(4839):487-91.

59. Adams JC. Biotin amplification of biotin and horseradish peroxidase signals in histochemical stains. Journal of Histochemistry & Cytochemistry. 1992;40(10):1457-63.

60. Baggerly K, Mitra R, Grier R, Medhane D, Lozano G, Kapoor M. Comparison of sample-labeling techniques in DNA microarray experiments. Analytica Chimica Acta. 2004;506(2):117-25.

61. Jenison R, Yang S, Haeberli A, Polisky B. Interference-based detection of nucleic acid targets on optically coated silicon. Nature Biotechnology. 2001;19(1):62-5.

62. Tsongalis GJ. Branched DNA technology in molecular diagnostics. American Journal of Clinical Pathology. 2006;126(3):448-53.

63. Elghanian R, Storhoff JJ, Mucic RC, Letsinger RL, Mirkin CA. Selective colorimetric detection of polynucleotides based on the distance-dependent optical properties of gold nanoparticles. Science. 1997;277(5329):1078-81.

64. Taton TA, Mirkin CA, Letsinger RL. Scanometric DNA array detection with nanoparticle probes. Science. 2000;289(5485):1757-60.

65. Goluch ED, Nam JM, Georganopoulou DG, Chiesl TN, Shaikh KA, Ryu KS, et al. A bio-barcode assay for on-chip attomolar-sensitivity protein detection. Lab on a Chip. 2006;6(10):1293-9.

66. Hsing IM, Xu Y, Zhao WT. Micro- and nano-magnetic particles for applications in biosensing. Electroanalysis. 2007;19(7-8):755-68.

67. Hansen RR, Johnson LM, Bowman CN. Visual, base-specific detection of nucleic acid hybridization using polymerization-based amplification. Analytical Biochemistry. 2009;386(2):285-7.

68. Hansen RR, Avens HJ, Shenoy R, Bowman CN. Quantitative evaluation of oligonucleotide surface concentrations using polymerization-based amplification. Analytical and Bioanalytical Chemistry. 2008;392(1-2):167-75.

69. Hansen RR, Sikes HD, Bowman CN. Visual detection of labeled oligonucleotides using visible-light-polymerization-based amplification. Biomacromolecules. 2008;9(1):355-62.

70. Sikes HD, Hansen RR, Johnson LM, Jenison R, Birks JW, Rowlen KL, et al. Using polymeric materials to generate an amplified response to molecular recognition events. Nature Materials. 2008;7(1):52-6.

71. Decker C, Jenkins AD. Kinetic approach of oxygen inhibition in ultraviolet- and laser-induced polymerizations. Macromolecules. 1985;18(6):1241-4.

72. Hoyle CE, Bowman CN. Thiol–Ene Click Chemistry. Angewandte Chemie International Edition. 2010;49(9):1540-73.

73. Rutstein SO. Factors associated with trends in infant and child mortality in developing countries during the 1990s. Bulletin of the World Health Organization. 2000;78(10):1256-70.

74. Snow RW, Guerra CA, Noor AM, Myint HY, Hay SI. The global distribution of clinical episodes of Plasmodium falciparum malaria. Nature. 2005;434(7030):214-7.

75. Breman JG, Alilio MS, Mills A. Conquering the intolerable burden of malaria: What's new, what's needed: A summary. American Journal of Tropical Medicine and Hygiene. 2004;71(2):1-15.

76. Mulholland K. Global burden of acute respiratory infections in children: Implications for interventions. Pediatric Pulmonology. 2003;36(6):469-74.

77. Bryce J, Boschi-Pinto C, Shibuya K, Black RE. WHO estimates of the causes of death in children. Lancet. 2005;365(9465):1147-52.

78. Mabey D, Peeling RW, Ustianowski A, Perkins MD. Diagnostics for the developing world. Nature Reviews Microbiology. 2004;2(3):231-40.

Chapter 2

Objectives

Free radical-mediated polymerization is compatible with a wide range of monomers, functional groups and initiating systems. This technique offers good control over the polymerization kinetics through alteration of the initiation kinetics and enables the tuning of the physical, chemical and biological properties of the polymer through selection of appropriate monomers. Interfacial radical polymerization combines these advantages and provides a facile way of tuning the surface properties of substrates independently from the fabrication procedures of the construct. Glucose oxidase-mediated redox initiation is an ideal reaction to conduct interfacial polymerization due to the multiple components involved in the achievement of rapid and successful polymerization. The mild conditions of temperature and pressure and the absence of oxygen inhibition allow its application in biological systems. Other methods of surface modification such as surface-initiated photopolymerization or photolithographic patterning use light distributed to the surface to cause reaction and therefore incapable of achieving uniformity in modification when optically thick substrates or complex geometrical configurations are employed. The technique discussed in this work is light-independent and therefore able to achieve conformal coatings on complex 3-dimensional substrates[1]. Additionally, unlike other interfacial polymerizations that use a condensation reaction between monomers or interfacially-immobilized radical source to confine the polymerization, the initiating species here are free to diffuse into the different phases and the ensuing delocalization is able to generate thicker films ranging in the hundreds of microns. However, not much work exists in the literature that describes the nature of the

radical interfacial polymerization process. The overarching objective of this thesis is to understand the factors that influence the reaction delocalization and achieve heightened capabilities of the technique. The specific aims pertaining to this goal are as follows,

Specific aim 1: Experimentally investigate the influence of interfacial reaction delocalization on the kinetics of film formation

Specific aim 2: Build a mathematical model of the coupled-reaction diffusion process at the interface that fundamentally describes the reaction delocalization and its influence on the interfacial film properties

Specific aim 3: Engineer the glucose-oxidase mediated redox initiation reaction to fabricate coatings on microscopic substrates by interfacial polymerization

In specific aim 1, the understanding of the interplay of reaction behavior and mass transport process that underpins the polymerization delocalization is accomplished by investigating the relationship between the interfacial film thickness and the time of immersion of the substrate into the coating solution. The factors that influence the reaction delocalization such as species concentration and enzyme encapsulation by the propagating polymerization front were investigated by studying how these parameters affect the rate of growth of the interfacial film.

In specific aim 2, a mathematical model was developed by solving the partial differential equations describing the coupled reaction-diffusion process and incorporating a polymer concentration dependent diffusion coefficient to accurately reflect the changing mass transport conditions. The experimental results from specific aim 1 were used to obtain

values for unknown constants as well as for model validation. The model was then used to highlight the ability of the enzyme-mediated initiation system to effect extensive delocalization and hence thick interfacial coatings by comparing it to a two-component system involving only the redox reaction. The model was also used to determine the factors that affect the interfacial film properties such as permeability and the polymer density gradients.

In specific aim 3, the means and the understanding to control the reaction delocalization was used to develop conditions that enable conformal coatings on hydrogel substrates whose dimensions are in the sub-millimeter range. Additionally, the ability of the coating to be self-sustaining is tested by dissolving the solid core after the coating process.

Photopolymerization has been demonstrated to be a viable technique in the detection of biomarkers by signal amplification. By allocating photoinitiators in proportional amounts to the target attached to the surface, surface-initiated polymerization can be enabled by exposing the surface to a monomer solution and shining light thereby enabling macroscopic polymer formation and hence visual detection. However, the competitive features of this technology such as high sensitivity is achieved by minimizing oxygen inhibition, a classical issue facing radical polymerization, by means of high light intensities that enable favorable photoinitiation kinetics and oxygen elimination from the vicinity by enclosing the sample in a chamber containing an inert gas such as argon. In the absence of these measures, polymerization is completely suppressed owing to the significantly lower concentration of photoinitiators on the surface. The viability of this technique to provide diagnostic solutions in resource-limited settings preclude the use of expensive equipments as well as procedures that

require trained personnel. The goal of this project was to design a photoinitiation scheme that suppresses oxygen inhibition in parallel with photopolymerization such that surface-initiated polymerization based amplification could be conducted without the need to physically eliminate the oxygen. The specific aim pertaining to this goal is as follows,

Specific aim 4: Understand and implement the oxygen sensitizing mechanism of Zinc phthalocyanine to reduce the inhibition times of the bulk polymerization of acrylates

In this specific aim, the relationship between the phthalocyanine concentration and inhibition time is studied and the mechanism of action is proposed. A mathematical equation describing the nature of the photochemical reactions was developed and fit to the experimental results to validate the mechanism. The polymerization conditions were then optimized to enable oxygen inhibition suppression in the extreme case of a sample saturated with oxygen.

Chapter 3

Kinetics of interfacial radical polymerization initiated by a glucose-oxidase mediated redox system

The reaction and coating kinetics for the glucose oxidase initiated interfacial polymerization are elaborated. The interfacial film grows rapidly and linearly with time, producing time-dependent controllable conformal coating thicknesses of up to a millimeter in less than 4 minutes. Bulk polymerization was only observed when the immersing media was stirred to induce higher mass transport rates. The dramatically different film thicknesses observed between different concentrations of glucose in the hydrogel and iron in the bulk media are demonstrated to be a result of an initial rapid growth phase following which the film grows at the same rate nearly independent of either the glucose or iron concentration. The polymerization rate and hence the thickness growth rate in this initial phase saturate at glucose and iron concentrations above 0.8 M and 0.63 mM, respectively. At iron concentrations above 0.05 mM, the film thickness at the end of 3 hours of reaction monotonically decreased with increasing iron concentration from 5.7 mm to 4.2 mm. The glucose oxidase is trapped by the growing polymerization front and can be used as the sole enzymatic precursor to coat a second polymeric layer. However, the rate of film growth of the second layer is 14-fold lower than the rate of film growth when bulk enzyme is present during the second stage coating process.

3.1. Introduction

Glucose oxidase-mediated initiation of radical polymerization reactions, first reported by Iwata *et al.* [1], has the advantage of being resistant to oxygen inhibition, the

classical issue facing radical polymerizations [2], while proceeding rapidly at ambient temperature and pressure. Further, this technique represents an ideal biological reaction to use to facilitate interfacial polymerizations as it necessitates multiple components to achieve rapid, successful polymerization. In particular, glucose oxidase catalyzes the reaction between -D-glucose and oxygen, producing hydrogen peroxide, which in the presence of ferrous ions (Fe^{2+}), generates hydroxyl radicals that are highly efficient for

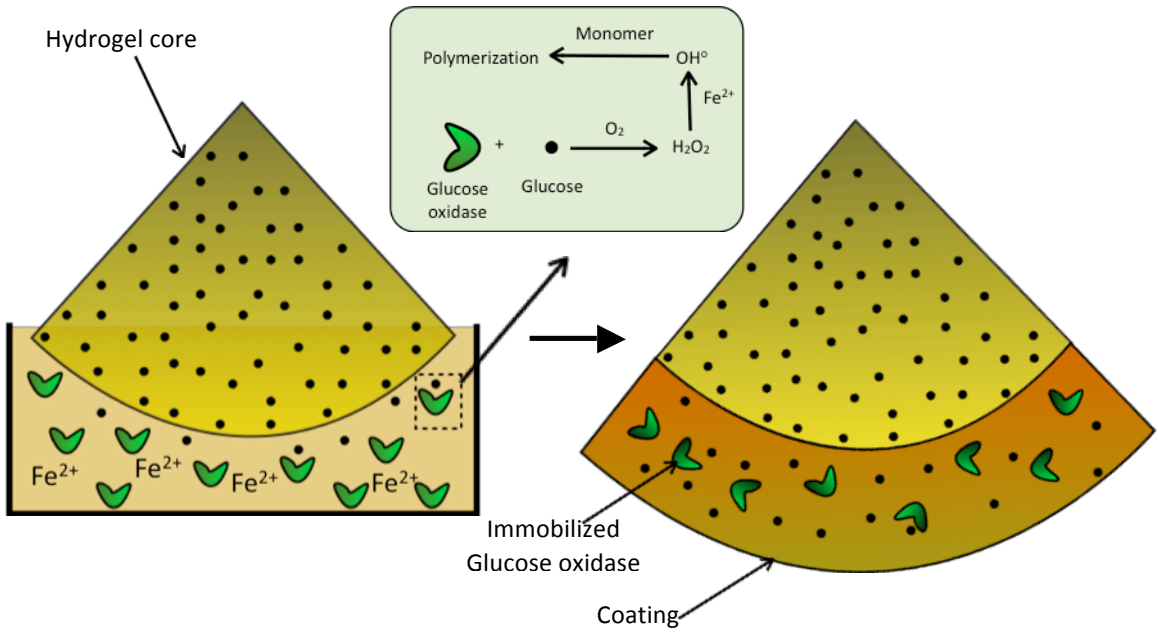

Figure 3.1: Schematic illustrating the formation of coating on hydrogel substrates by interfacial polymerization initiated by a glucose oxidase-mediated system. Reaction between GOx and glucose that subsequently triggers polymerization initially occurs near the hydrogel boundary but becomes delocalized due to rapid diffusion of glucose.

initiating (meth)acrylate polymerization [3]. Since its original demonstration, this technique has been applied in a variety of systems that exploit the unique aspects of the initiation system. The light independent mechanism and absence of oxygen inhibition

was utilized in fabricating hydrogels for cellular encapsulation that were several millimeters thick [3]. The ability of glucose oxidase to participate in radical generation while continually regenerating was used to fabricate highly sensitive polymerization-based amplification devices [4]. Recently, this initiation system was used to fabricate conformal coatings on 3-dimensional hydrogel structures by interfacial polymerization [5]. Unlike interfacial condensation polymerizations that result in polymer growth in an uncontrollable fashion, radical chain polymerizations allow for good control of polymerization kinetics to be achieved by simply changing the initiator concentration, whose effect on polymerization rate is very well understood. In addition, initiation reactions capable of generating radicals are compatible with a wide variety of monomers, and molecular design of chemical or biological properties of the resulting polymer is enabled by copolymerization of the desired functional monomers. This behavior was demonstrated recently in the fabrication of immunoactive barriers for implantable devices by covalent incorporation of thiolated-biomolecules as achieved by this interfacial polymerization method [6].

One method for forming interfacial coatings on hydrogel structures using this technique is realized by immersing a glucose-swollen hydrogel into an aqueous solution consisting of monomer, ferrous ion (Fe^{2+}) and glucose-oxidase as shown in Figure 1. The hydrogel serves as a template that spatially confines glucose prior to polymerization. Thus, the locus of the enzymatic reaction involving glucose is initially at the hydrogel boundary but is subsequently delocalized due to the rapid diffusion of glucose into the bulk media. Depending on the conditions and species concentrations, hydrogen peroxide generated by this reaction can also diffuse into the surrounding media before reacting

with ferrous ion to produce the hydroxyl radicals responsible for initiating the polymerization. The rapid mass transport of the initiating species results in the reaction zone extending well into the bulk, thereby enabling conformal coatings that are several hundreds of micrometers thick [5]. This outcome is difficult to achieve using conventional or other interfacial radical polymerizations that confine the initiator to the surface or interface [7-13] primarily because radicals have a very short lifetime and hence have significantly smaller diffusion length scales. However, if the interfacial polymerization process is reaction-controlled, high mass transport rates can cause undesired bulk polymerization. This behavior arises because the initiating species can avoid reaction at the interface and diffuse into the bulk, resulting in polymerization throughout the immersing solution. The choice of monomer that is used to fabricate the hydrogel and the polymeric coating also affects the resulting crosslinking density and hence the diffusion coefficient of the initiating species and the film growth rate. The efficiency of glucose oxidase encapsulation or capture by the propagating polymerization front influences the diffusion length of glucose and hence the degree of delocalization of the initiating reactions. The species concentrations affect the polymerization rate and consequently the likelihood of bulk polymerization induced by rapid diffusion of glucose and hydrogen peroxide. The current investigation attempts to understand the interplay of reaction and mass transport rates of this interfacial polymerization process as a means for controlling the physical, biological and chemical attributes of the coating process and achieving heightened capabilities from this technique.

3.2. Experimental

3.2.1 Materials

Poly(ethylene glycol) diacrylate, MW 575 ($PEGDA_{575}$), Iron (II) sulfate heptahydrate, glucose oxidase (GOx) from *Aspergillus Niger*, and D-(+)-glucose solutions were obtained from Sigma-Aldrich. 4-(2-Hydroxyethoxy) phenyl-(2-hydroxy-2-propyl) ketone (Irgacure 2959) was obtained from BASF. 2-(N-Morpholino)ethanesulfonic acid (MES) buffer pH 4.5 was obtained from Teknova. Methacryloxyethyl thiocarbamoyl rhodamine B (Rhodamine B acrylate) was obtained from Polysciences and suspended in DMSO before using volumes necessary to achieve the desired target concentration. The final volumes of DMSO in the precursor solution were 0.5 to 1 vol%. The hydrogen peroxide detection kit was obtained from Enzo Life Sciences.

3.2.2 Polymerization and formation of the core hydrogel substrate

The monomer formulation used was an aqueous solution of 15wt% $PEGDA_{575}$, 0.1wt% Irgacure 2959 and glucose in appropriate quantities to achieve the final desired glucose concentration. This precursor solution was placed in a cylindrical mold (4mm diameter and 2 mm height) and polymerized by exposing to 320-390 nm light from an Acticure 4000 (Exfo) at an intensity of 15 mW/cm^2 for 10 minutes.

3.2.3 Interfacial polymerization of hydrogel coating and characterization

The hydrogel substrates were immersed in a coating solution comprised of an aqueous solution of 15 wt% $PEGDA_{575}$, 3.1M GOx, 0.005wt% rhodamine-B acrylate and 10 mM MES pH 4.5, glucose and iron at the desired concentrations. The immersion process was carried out in an automated fashion using a VersArray ChipWriter Pro system (Bio-Rad laboratories). The pin that was used to hold the hydrogel substrate was punctured through the center of the substrate before being immersed into the bulk media. After the coating process, the hydrogels were thinly sliced to obtain a cross section followed by storage in

water until further characterization. The coatings consisting of covalently immobilized fluorescent molecules, particularly rhodamine-B, were imaged using a Zeiss Pascal LSM 5 confocal microscope. The gels were excited with a 543 nm helium neon laser and fluorescence was monitored from 547-680nm.

3.3 Results and Discussion

Interfacial polymerizations were conducted by immersing the hydrogel core in the bulk media for various times followed by evaluation of the coating extent and process. The coating thickness as a function of the immersion time is shown in Figure 2 for different concentrations of glucose present in the hydrogel precursor solution. The film growth rate, as measured by the slope of the thickness profile as a function of time, is a measure of the average polymerization rate within the coating. It is instructive to note that the polymerization reaction at the moving interface, which is defined as the transition from the gelled to the viscous region, contributes predominantly to film growth. The polymerization reactio

n happening within the coating increases the crosslinking density and hence alters the swelling and transport properties but is assumed to contribute minimally to the thickness,

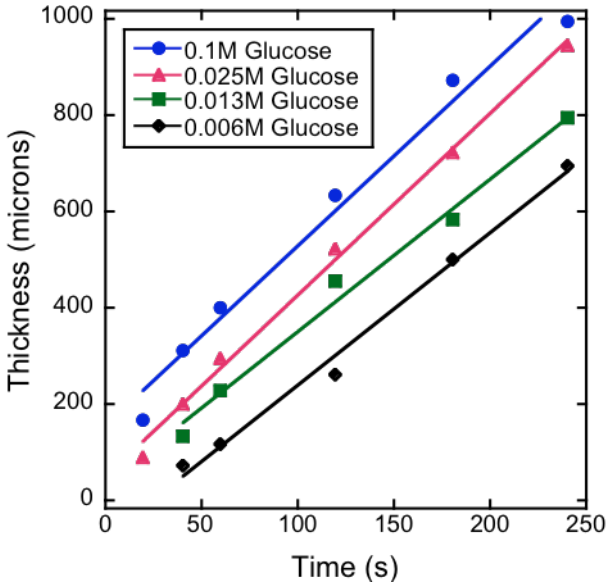

Figure 3.2: Film thickness vs. time for various concentrations of glucose in the core hydrogel. The conditions used were: 3.1µM GOx, 0.25mM Fe^{2+}, 0.005wt% rhodamine-B acrylate, 10 mM MES pH 4.5 and 15wt% $PEGDA_{575}$

for the sake of interpretation of the experiments. After an initial period, the pseudo-linear dependence of film thickness on time indicates sufficiently rapid diffusion of glucose to the interface to maintain the average polymerization rate at a nearly constant level. The near-constant film growth rate could also be due to the rapid diffusion to the interface of hydrogen peroxide generated by the reaction between glucose and the enzyme trapped in the coating. In reality, the diffusion of both glucose and hydrogen peroxide influence the film growth rate. However the relative contributions depend on the thickness of the film, the fraction of glucose oxidase encapsulated within the already formed coating, and the concentration of iron in the bulk media. This complex interplay will be discussed later in this manuscript. In either case, the film growth rate is not limited by species diffusion. It is clear from Figure 2 that the film growth rate is nearly the same for different glucose concentrations and that the dramatically different thicknesses achieved at different glucose concentrations are a result of different initial film formation rates. For many of the conditions evaluated, at early times the absence of a

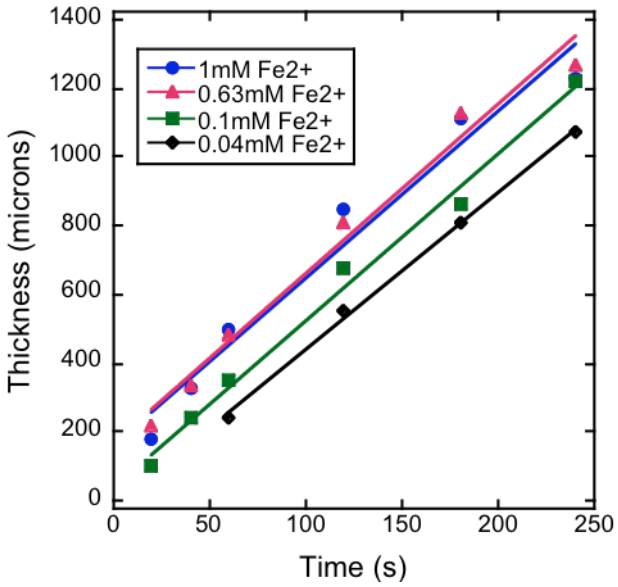

Figure 3.3: Film thickness vs. time for various concentrations of iron in the bulk media. The conditions used were: 3.1µM GOx, 0.1M Glucose, 0.005wt% rhodamine-B acrylate, 10 mM MES pH 4.5 and 15wt% $PEGDA_{575}$

significant coating results in lower resistance to mass transfer and hence a more rapid rate of film growth. Following this initial phase, the interfacial radical

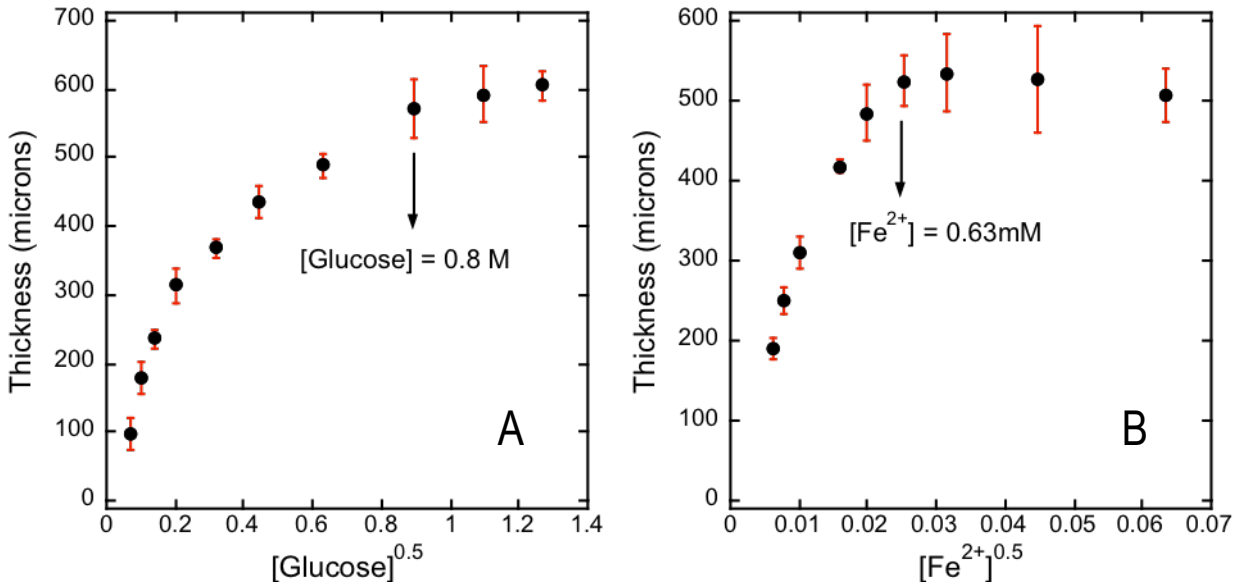

Figure 3.4: Variation of film thickness with square root of glucose concentration (a) and iron concentration (b) after 1 min immersion to form the coating. The conditions used were 3.1µM GOx, 0.005wt% rhodamine-B acrylate, 10 mM MES pH 4.5 and 15 wt% $PEGDA_{575}$, and either 0.25 mM Fe^{2+} (Figure 4a) or 0.1 M glucose (Figure 4b)

generation rate reaches a steady state as indicated by the constant rate of film growth, where this rate is almost independent of the initial glucose concentration. At lower glucose concentrations, the slower initiation rate delays gelation implying an effective inhibition time for the initial coating formation.

The thickness as a function of time for different iron solution concentrations is shown in Figure 3 with similar overall kinetic behavior observed. Furthermore, at the two highest iron concentrations, the thickness profiles overlap indicating that even the initial rapid initial growth phase is similar. This behavior is likely due to the presence of a rate-limiting reaction that does not involve iron and arises prior to the reaction of iron with the

hydrogen peroxide to form the hydroxyl radicals. To explore further the reaction kinetics in this initial film growth region, the film thickness is plotted after 1 minute of immersion for different concentrations of glucose and iron, as shown in Figures 4a and 4b, respectively. Here, the abscissa is plotted as the square root of the species concentration. The exponent of 0.5 was chosen because previous studies on the bulk polymerization kinetics of a similar system indicated that the polymerization rate scaled with the half power of glucose and iron concentrations over a wide range of concentrations, likely due to bimolecular termination [3]. Therefore, the concentrations of these components of the initiation system are scaled to account for their influence on the ideal, bulk polymerization rate. It is seen that at glucose concentrations higher than 0.8 M and iron concentrations higher than 0.63 mM, the average polymerization rate in the rapid growth phase saturates. When the concentrations of iron, glucose and oxygen were increased further (not shown), there was no significant change in the film thickness, indicating that none of the abovementioned species limit the reaction rate. Thus, it appears that the turnover rate of the enzyme, a measure of the maximum substrate conversion rate achievable has been attained. In all these experiments, bulk polymerization was a minimal concern in spite of rapid diffusion rates of glucose and hydrogen peroxide. Bulk polymerization occurs if the initiating species escapes reaction at the interface and diffuses to the bulk causing polymerization in isolation from the adhered coating. Interestingly, when the bulk media is stirred at various rates (60, 150 and 400 rpm), an interfacial coating was not formed. Instead polymerization of the entire immersing solution occurred. This outcome represents a case where the interfacial mass transport rates are much higher than reaction rates at the interface. Without stirring, the interfacial

reaction rate is fast enough to form an attached polymer at the interface prior to bulk diffusion of the initiating species. Therefore, if one were to use monomers with a much higher molecular weight to form the hydrogel, the resulting crosslinking density would be much lower, consequently increasing the likelihood of bulk polymerization due to lower mass transfer resistance. This pitfall can readily be countered simply by using a more viscous bulk solution or otherwise by enabling higher interfacial reaction rates.

3.3.1 Encapsulation of glucose oxidase (GOx) by the polymerization front

Glucose oxidase is a bulky enzyme (Hydrodynamic radius ~ 43A^{o}) compared to the mesh size of the polymer network formed using $PEGDA_{575}$ (<20A^{o}). Once encapsulated by the growing polymerization front, the enzyme is effectively trapped.

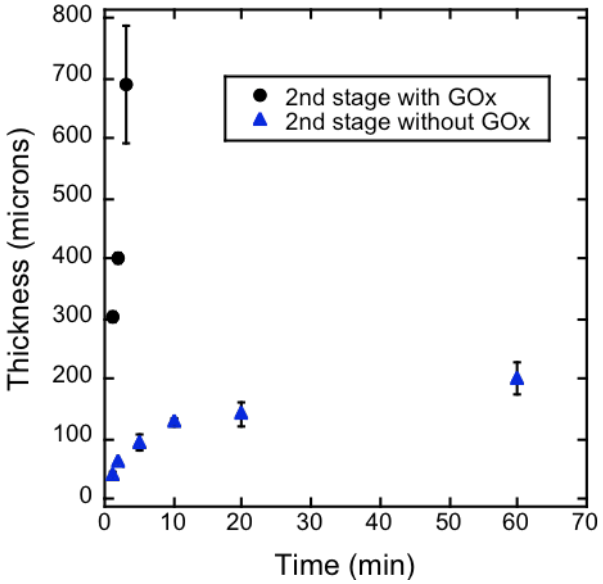

Figure 3.5: 2nd stage film thickness vs. time with GOx (O) and without GOx (Δ) in the bulk media. The conditions used were: 3.1μM GOx, 0.005wt% rhodamine-B acrylate, 10 mM MES pH 4.5 and 15wt% $PEGDA_{575}$, 0.05mM Fe^{2+}, 0.1M glucose. The first stage thickness was 600 microns

Immobilized glucose oxidase is capable of enzymatic activity associated with its reaction with glucose [14]. However, hydrogen peroxide generated by the initiation reaction is also capable of reacting with glucose-oxidase and rendering it inactive [15-17].

Therefore, the efficiency of glucose oxidase encapsulation in addition to enzyme inactivation by hydrogen peroxide dictates the effective active enzyme concentration trapped within the dynamically forming coating. To understand the trapped enzymatic activity, a two-stage interfacial coating was performed. In the first stage, a coating 600 microns thick is formed in the same manner as earlier. In the second stage, the coated hydrogel is immersed in a monomer solution without bulk enzyme. Therefore, for this particular experimental approach, any additional coating formation or polymerization that occurs during the 2nd stage would be entirely a result of the enzyme encapsulated within the coating formed during the 1st stage polymerization. The 2nd stage thickness profile as a function of time was plotted and compared to the control experiment, where the bulk enzyme was present in both stages (Figure 5). It is clearly seen that the interfacial polymerization rate without bulk GOx in the second stage is dramatically lower compared to when bulk GOx is present. This behavior indicates that the film growth is predominantly due to the diffusion of glucose to the interface and subsequent reaction with GOx in the bulk. It is also observed that the film growth rate, when bulk GOx is absent, decreases with increasing time. The locus of the initiation reaction

$[Fe^{2+}]$ in bulk	Thickness
0.05 mM	5.7 mm
0.25 mM	4.6 mm
2 mM	4.2 mm

Table 3.1: Thickness of the interfacial film after 3 hours of reaction for three different bulk iron concentrations. The conditions used were: 3.1μM GOx, 0.005wt% rhodamine-B acrylate, 10 mM MES pH 4.5 and 15wt% $PEGDA_{575}$, 0.1M glucose.

in the 2nd stage that generates hydrogen peroxide is always within the 1st stage coating. This behavior means that, as the thickness in the 2nd stage process increases, the distance that H_2O_2 has to diffuse to reach the interface increases. The reaction of H_2O_2 with iron to produce hydroxyl radicals (OH^o) is most productive at the interface and contributes least to the thickness when taking place far from the interface. This limitation arises because OH^o generated within the coating take part in radical termination or chain transfer reactions with abstractable hydrogens on the polymer backbone in the absence of significant monomer. Furthermore, it is known that OH^o are an extremely reactive species and cannot diffuse farther than 1-5 times their molecular diameter without reaction [18] and hence have minimal potential to diffuse to the interface. The result is a steadily decreasing film growth rate with increasing thickness. Additional evidence of the decreased contribution of OH^o generated within the coating comes from Table 1. When the interfacial polymerization is allowed to proceed for 3 hours at three different iron concentrations, the thickness monotonically decreased with increasing iron concentration. At higher iron concentrations, H_2O_2 generated within the coating would not be able to diffuse far before reacting with iron to form OH^o, and this reaction thus increases the likelihood of radicals being generated within the coating rather than at the interface.

A persistent issue remains as to whether the low concentration of active GOx in the coating is due to an inefficient encapsulation process or due to deactivation of the enzyme. Alternatively, the enzyme activity might be negligible and the film growth in the 2nd stage without GOx in the bulk media is entirely as a result of the remnant hydrogen peroxide (H_2O_2) from the 1st stage coating process. To explore whether residual hydrogen peroxide was present and initiating the reaction, the coated hydrogel from the first stage was investigated for enzymatic activity. This evaluation was performed simply by immersing the hydrogel in water and evaluating the H_2O_2 released into the bulk by the coating. Figure 6 shows a plot of H_2O_2 concentration in the bulk as a function of time for just such a system. The circles represent the release from a coated construct just after the coating process. The triangles represent the release from the coated construct after it has been allowed to stand in an aqueous solution containing 0.5mM Fe^{2+} for 15 minutes before being investigated for H_2O_2 release. The purpose was to decompose any remnant hydrogen peroxide within the

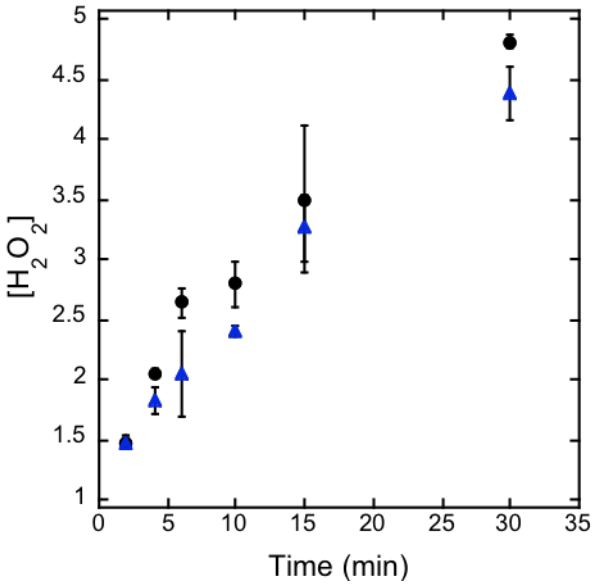

Figure 3.6: Hydrogen peroxide concentration released into the bulk vs. time when the coated hydrogel construct is immersed in water just after the coating process (O) or after allowing the hydrogel to stand in a 0.05 mM Fe^{2+} solution for 15 min (Δ). The coating was 600 µm thick

coating so that further H_2O_2 released would be due to the continuing reaction of glucose with the encapsulated enzyme. The similar slopes of the two curves indicate that the enzymatic reaction is predominantly responsible for the H_2O_2 release. The slightly lower concentration detected when the hydrogel is immersed in an iron solution before H_2O_2 release, is most likely due to the consumption of the remnant H_2O_2 by iron. The work of Hume *et al.* [6] provides additional evidence of encapsulated enzyme activity. In their work, when the coated hydrogel containing cells were placed in a cell culture media (containing glucose) overnight, low cell viability was observed, likely due to the reaction of encapsulated GOx with bulk glucose which generates H_2O_2 that is cytotoxic. This behavior implies that the 2nd stage coating thickness profile without bulk enzyme (Figure 5,) is predominantly due to the encapsulated enzyme itself. The choice of monomers used for coating the hydrogel influences the glucose oxidase kinetics as well as its relative propensity to become trapped within the growing polymer film.

3.4 Conclusions

The film formed by the interfacial glucose oxidase-mediated polymerization grows linearly with time for different concentrations of glucose and iron indicating that the interfacial polymerization process is not limited by the diffusion of glucose to the interface. The initial rapid film growth is due to the absence of significant polymer film at short times, thereby resulting in lower resistance to mass transfer. The diffusive flux of the initiating species to the interface reaches a steady state following this initial rapid growth phase and this behavior leads to a constant film growth rate that is independent of the initial concentrations of glucose and iron. The film thickness at the end of this initial rapid growth phase saturates at higher concentrations of iron and glucose, likely due to

the enzymatic reaction achieving its maximum substrate conversion rate. When the interfacial polymerization is allowed to proceed for long times, higher bulk iron concentration leads to lower film thickness because the diffusion distance of hydrogen peroxide within the coating is significantly limited by reaction with iron to form hydroxyl radicals within the film rather than at the interface. Glucose oxidase that is trapped by the propagating polymerization front is active but significantly lower in overall activity as compared to the enzyme in the bulk media. This reduction results in a 14-fold lower initial film growth rate when the bulk enzyme is absent and the trapped enzyme is used as the sole precursor for further coating formation.

Acknowledgements

This work has been supported by the National Institutes of Health (Grant R21 EB 012188)

3.5 References

1. Iwata H, Hata Y, Matsuda T, Ikada Y. Initiation of Radical Polymerization by Glucose-Oxidase Utilizing Dissolved-Oxygen. Journal of Polymer Science Part a-Polymer Chemistry 1991;29(8):1217-1218.

2. Decker C, Jenkins AD. Kinetic approach of oxygen inhibition in ultraviolet- and laser-induced polymerizations. Macromolecules 1985;18(6):1241-1244.

3. Johnson LM, Fairbanks BD, Anseth KS, Bowman CN. Enzyme-Mediated Redox Initiation for Hydrogel Generation and Cellular Encapsulation. Biomacromolecules 2009;10(11):3114-3121.

4. Berron BJ, Johnson LM, Ba X, McCall JD, Alvey NJ, Anseth KS, et al. Glucose Oxidase-Mediated Polymerization as a Platform for Dual-Mode Signal Amplification and

Biodetection. Biotechnology and Bioengineering 2011;108(7):1521-1528.

5. Johnson LM, DeForest CA, Pendurti A, Anseth KS, Bowman CN. Formation of Three-Dimensional Hydrogel Multilayers Using Enzyme-Mediated Redox Chain Initiation. Acs Applied Materials & Interfaces 2010;2(7):1963-1972.

6. Hume PS, Bowman CN, Anseth KS. Functionalized PEG hydrogels through reactive dip-coating for the formation of immunoactive barriers. Biomaterials 2011;32(26):6204-6212.

7. Scott C, Wu D, Ho CC, Co CC. Liquid-core capsules via interfacial polymerization: A free-radical analogy of the nylon rope trick. Journal of the American Chemical Society 2005;127(12):4160-4161.

8. Luo YW, Gu HY. A general strategy for nano-encapsulation via interfacially confined living/controlled radical miniemulsion polymerization. Macromolecular Rapid Communications 2006;27(1):21-25.

9. Jiang D, Huang X, Qiu F, Luo C, Huang LL. Synthesis of Polymer Thin Film Gradient with Nanometer Thickness through Water Diffusion Controlled Surface Polymerization. Macromolecules 2009;43(1):71-76.

10. von Werne TA, Germack DS, Hagberg EC, Sheares VV, Hawker CJ, Carter KR. A Versatile Method for Tuning the Chemistry and Size of Nanoscopic Features by Living Free Radical Polymerization. Journal of the American Chemical Society 2003;125(13):3831-3838.

11. Sikes HD, Hansen RR, Johnson LM, Jenison R, Birks JW, Rowlen KL, et al. Using polymeric materials to generate an amplified response to molecular recognition events. Nature Materials 2008;7(1):52-56.

12. Yoshikawa C, Goto A, Tsujii Y, Fukuda T, Yamamoto K, Kishida A. Fabrication of High-Density Polymer Brush on Polymer Substrate by Surface-Initiated Living Radical Polymerization. Macromolecules 2005;38(11):4604-4610.

13. Kizilel S, Perez-Luna VH, Teymour F. Photopolymerization of poly(ethylene glycol) diacrylate on eosin-functionalized surfaces. Langmuir 2004;20(20):8652-8658.

14. Fortier G, Belanger D. Characterization of the Biochemical Behavior of Glucose-Oxidase Entrapped in a Polypyrrole Film. Biotechnology and Bioengineering 1991;37(9):854-858.

15. Krishnaswamy S, Kittrell JR. Deactivation Studies of Immobilized Glucose Oxidase. Biotechnology and Bioengineering 1978;20(6):821-835.

16. Tse PHS, Gough DA. Time-Dependent Inactivation of Immobilized Glucose-Oxidase and Catalase. Biotechnology and Bioengineering 1987;29(6):705-713.

17. Greenfield PF, Kittrell JR, Lawrence RL. Inactivation of Immobilized Glucose Oxidase by Hydrogen-Peroxide. Analytical Biochemistry 1975;65(1-2):109-124.

18. Pryor WA. Oxyradicals and Related Species - Their Formation, Lifetimes, and Reactions. Annual Review of Physiology 1986;48:657-667.

Chapter 4

A comprehensive kinetic model of free radical-mediated interfacial polymerization

A mathematical model describing interfacial radical polymerization-based film formation on hydrogel substrates is elucidated. The initiation reaction comprises a glucose oxidase-mediated generation of hydrogen peroxide coupled to a redox reaction involving Fe^{2+} that generates hydroxyl radicals capable of initiating polymerization of poly (ethylene glycol) diacrylate. Radical formation is interfacially-confined by immersing the glucose-swollen hydrogel into an aqueous precursor solution containing the complementary initiating species and monomer so that contact between the species exists initially only at the interface. The ensuing diffusion of the initiating species results in delocalization of the polymerization reaction thereby influencing the properties of the interfacial film such as thickness, permeability and the presence of polymer concentration gradients. The model provides mechanistic insight into the reaction delocalization, accomplished by solving the partial differential equations that describe coupled reaction-diffusion process and incorporating a polymer concentration-dependent diffusion coefficient to reflect accurately the changing mass transport conditions in the growing film. Model predictions of the film thickness as a function of time and concentrations of glucose and iron agree well with the experimental results. The predicted thickness for the same bulk iron concentration and immersion time is almost 3-fold greater for the enzyme-mediated redox initiation system compared to the thickness for a two-component system involving only the redox reaction. The model predicts that the average diffusion coefficient of a non-reactive molecule such as rhodamine-B decreases with increasing thickness, an

indication of the gradual densification of the membrane after it has formed. The densification rate is strongly influenced by the bulk iron concentration, allowing the tuning of the membrane permeability at a given thickness. The model is also useful to determine the nature of polymer density gradients within the polymer film and the factors that affect such properties. The model predictions indicate that, depending on the initial location and the concentration of iron, membranes that show improved adhesion to the substrate or asymmetric polymer density gradients are fabricated.

4.1. Introduction

Free radical polymerization offers the ability to control the polymerization kinetics by altering the conditions of the participating initiation reactions whose effect on polymerization reaction is well understood. Additionally, this polymerization mode is compatible with a wide variety of monomers and functional groups, thereby enabling the selection of starting materials that can influence the properties of the resulting polymeric material such as permeability, mechanical integrity and chemical or biological behavior. These advantageous characteristics have motivated the development of interfacial radical polymerization approaches to fabricate thin film membranes that coat porous or solid substrates like hydrogels[1,2] or even encapsulate liquid cores[3,4]. In these previous efforts, interfacially-confined polymerization is accomplished either by initiating contact between two or more components separated in two different phases to generate radicals at the interface[1,2] or by the immobilization of radical generating species at the interface of two immiscible phases[3,4] . The coatings can function as a barrier membrane that isolates the substrate or core from harsh external environments such as pH, physiological or biochemical stress, serve as a barrier membrane that controls the release of encapsulated

molecules, provide a means to achieve integration of multiple components with spatial separation, or to alter the surface characteristics (energy, chemistry, biology, etc.) without impacting the bulk material properties. These characteristics are useful in areas such as tissue engineering[6], drug delivery[7,8], catalysis[9], and autonomic healing[10] among others. The optimal functioning of these devices would require the means and understanding to control the interfacial film properties such as thickness, permeability and the structure.

The current investigation describes the nature of interfacial polymerization initiated by radicals through a mathematical model and focuses on the recent development and capacity for utilizing a multistage initiation process that enables delocalization of the initiation reaction and the formation of films of controlled thickness. The initiating reactions that generate radicals are generally confined to the interface by spatially isolating the initiating components in immiscible phases such that contact between them initially exists only at the interface. Subsequently, the initiating species are free to diffuse into both phases resulting in delocalization of the polymer film formation. The degree of delocalization is dependent on viscosity of the phases, reaction rates, size of the initiating species, choice of monomer used to fabricate the polymeric film, and the crosslink density, all of which are coupled to affect the mass transport and reaction processes. The properties of the interfacial film such as the thickness, permeability and polymer concentration are dictated by this reaction delocalization.

The primary initiation system used in this work comprises the specific reaction between glucose and glucose oxidase that generates hydrogen peroxide, which, in the presence of $Fe2^{+}$, forms hydroxyl radicals capable of efficiently initiating (meth)acrylate polymerization. Glucose is initially confined in a hydrogel support phase and glucose

oxidase (GOx), $Fe2^{+}$ and poly(ethylene glycol) diacrylate are present in the aqueous phase. Subsequent immersion of the hydrogel into the aqueous phase results in rapid diffusion of glucose into the bulk media to initiate the polymerization reaction. Experimental work on this technique[5] has investigated the factors that determine the degree of reaction delocalization and its influence on the kinetics of film growth. The model enables materials and process design with selection of appropriate monomers, initiating systems and conditions necessary for optimization of this interfacial polymerization process. In addition, the model provides understanding of the characteristics of the interfacial film such as the existence of polymer concentration gradients which is useful in the fabrication of membranes that possess gradients in the physical, biological and chemical properties.

Generally, mathematical models describing the interfacial polymerization process reported in the literature focus on using a condensation reaction between two monomers at the interface of immiscible phases which is mechanistically different from the radical-mediated interfacial polymerization described here [11-17]. The model presented in this manuscript provides insight into the reaction delocalization as a result of the complex coupled reaction-diffusion process through an understanding of the fundamental steps involved in the film formation.

4.2. Experimental

4.2.1 Interfacial polymerization

Two distinct designs were used to coat hydrogel constructs by interfacial polymerization. In the first a hydrogel was fabricated in the shape of a rectangular cuboid by photopolymerization of the hydrogel precursor solution between two glass slides

separated by a 1 mm spacer. The aqueous precursor solution consisted of 15wt% poly(ethylene glycol) diacrylate, MW 575 ($PEGDA_{575}$, Sigma Aldrich), 0.1wt% Irgacure 2959 (BASF) and 0.1M D-(+)-glucose (Sigma Aldrich). This formulation was exposed to 320-390 nm light from an Acticure 4000 (Exfo) at an intensity of 15 mW/cm^2 for 10 minutes. The hydrogel formed was removed and inserted between two glass slides with a 1mm spacer. The coating solution was rapidly injected into the space between glass slides resulting in contact with the hydrogel at the boundary and subsequent interfacial polymerization. The coating solution consisted of an aqueous solution of 15 wt% PEGDA, MW 574, 3 μM Glucose oxidase (Sigma Aldrich), 10mM 2-(*N*-morpholino)ethanesulfonic acid (MES) buffer pH 4.5 (Teknova), 0.005wt% methacryloxyethyl thiocarbamoyl rhodamine B (rhodamine B acrylate) (Polysciences) and iron(II) sulfate (Fe^{+2}) (Sigma-Aldrich) at the desired concentrations. The presence of rhodamine B acrylate in the coating allowed fluorescence based confocal microscopy using a Zeiss Pascal LSM 5 confocal microscope. The gels were excited with a 543 nm helium neon laser and fluorescence was monitored from 547-680nm. The coated construct fabricated using this design was primarily used for interface characterization studies. In the second design, a cylindrical hydrogel 2 mm in diameter and 15 mm in height was fabricated by injecting the hydrogel precursor solution into a capillary tube with the same dimensions and exposing to the same light conditions as before. The hydrogel precursor solution consisted of 15wt% poly(ethylene glycol) diacrylate, MW 575, 0.1wt% Irgacure 2959, 0.1M D-(+)-glucose and 0.01 wt% rhodamine B (Sigma Aldrich). The presence of non-reactive rhodamine in the hydrogel was used subsequently in controlled release experiments. After polymerization, the hydrogel was pushed out

from one side so that it just hangs out of the other opening. This structure was then immersed in the coating solution to trigger rapid polymerization at the hydrogel boundary. The coating solution consisted of an aqueous solution of 15 wt% PEGDA, MW 574, 3 µM glucose oxidase, 10mM 2-(*N*-morpholino)ethanesulfonic acid (MES) buffer pH 4.5 and iron(II) sulfate (Fe^{+2}) (Sigma-Aldrich) at the desired concentration. The coated construct fabricated using this design was primarily used for controlled release studies.

4.2.2 Diffusion controlled release measurements

The coated cylindrical construct described earlier was immersed in distilled water to release the dye, rhodamine B, into the bulk solution. The fluorescence of the solution was measured at 580 nm and correlated to the concentration of the rhodamine B in the bulk solution. The fractional release of the dye as a function of time was plotted and the numerical solution of equation 1 was fit to the experimental data to obtain the average value of the diffusion coefficient of the dye within the coating ($D_{coating}$) .

$$\frac{\partial c}{\partial t} = \frac{1}{r}\frac{\partial}{\partial r} rD\frac{\partial c}{\partial r} \quad (1)$$

$$D = \begin{cases} D_{core} & r < a \\ D_{coat} & r > a \end{cases} \quad (2)$$

Here, c is the concentration of the dye, r is the radial distance, t is the time, D is the diffusion coefficient of the dye, which takes the value of D_{core} ($2x10^{-7}$ cm^2. s^{-1}) within the core and $D_{coating}$ within the coating, a is the radius of the cylindrical hydrogel core.

4.3. Model development

4.3.1 Catalytic cycle of glucose oxidase

The mechanism of the enzymatic reaction between glucose and glucose oxidase has been extensively investigated in the seminal work of Gibson *et al.*[19]. Shown in

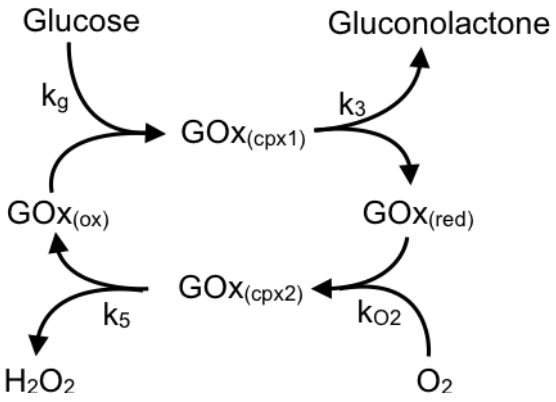

Scheme 4.1: Ping-pong mechanism of action of glucose oxidase (GOx). The glucose oxidase osciallates between the oxidized state ($GOx_{(ox)}$) and the reduced state ($GOx_{(red)}$) as a result of being reduced by glucose and oxidized by oxygen. The intermediates in these transformations are the complexed states ($GOx_{(cpx1)}$ and $GOx_{(cpx1)}$).

Scheme 1 is the ping-pong mechanism of action of this enzymatic reaction that generates hydrogen peroxide which here is used to form initiating radicals. Glucose oxidase moves from an oxidized state to the fully reduced form by reacting with glucose, and the reduced state then reacts with molecular oxygen to form hydrogen peroxide and return glucose oxidase to its oxidized, enzymatic state. The isomerization and subsequent dissociation of both complexed enzyme states are so rapid that the catalytic cycle is far from equilibrium. Therefore, material balances on all the species involved are created and

$$[E_{ox}] = \left[\frac{k_{cat}k_{O_2}c_{O_2}}{k_{cat}k_{O_2}c_{O_2} + k_{cat}k_g c_g + k_g k_{O_2} c_g c_{O_2}}\right] c_{E_o} = f_{ox} c_{E_o} \quad (3)$$

$$[E_{red}] = \left[\frac{k_{cat}k_g c_g}{k_{cat}k_{O_2}c_{O_2} + k_{cat}k_g c_g + k_g k_{O_2} c_g c_{O_2}}\right] c_{E_o} = f_{red} c_{E_o} \quad (4)$$

$$[E_{cplx}] = \left[\frac{k_g k_{O_2} c_g c_{O_2}}{k_{cat}k_{O_2}c_{O_2} + k_{cat}k_g c_g + k_g k_{O_2} c_g c_{O_2}}\right] c_{E_o} = f_{cplx} c_{E_o} \quad (5)$$

where,

$$k_{cat} = \frac{k_3 k_5}{k_3 + k_5}$$

solved by taking into consideration kinetic constants of each individual reaction. The concentrations of the different enzyme states are shown in equations 3-5.

Here, k_{cat} is the catalytic constant, k_3 and k_5 are the kinetic constants of dissociation of complexed states 1 and 2, respectively, k_g and k_{O2} are the kinetic constants of glucose and oxygen reaction, respectively, c_g and c_{O2} are the concentrations of glucose and oxygen, respectively, C_{Eo} is the total concentration of the enzyme, and $f_{ox,}$ f_{red} and f_{cpx} are the fractions of the enzyme in the oxidized, reduced and complexed states, respectively. These fractions represent the corresponding terms in the parenthesis.

4.3.2 Redox reactions and polymerization

$$H_2O_2 + Fe^{2+} \xrightarrow{k_{redox}} OH^{o} + Fe^{3+} + OH^{-} \quad (6)$$

$$Fe^{2+} + OH^{o} \xrightarrow{k_{inh1}} Fe^{3+} + OH^{-} \quad (7)$$

$$OH^{o} + M \xrightarrow{k_i} {}^{o}MOH \xrightarrow{M,k_p} \xrightarrow{M,k_p} \ldots {}^{o}M_n \quad (8)$$

$${}^{o}M_n + Fe^{3+}OH^{-} \xrightarrow{k_{inh2}} Fe^{2+} + M_nOH \quad (9)$$

$${}^{o}M_n + {}^{o}M_m \xrightarrow{k_t} M_n\text{-}M_m \quad (10)$$

The redox reaction between H_2O_2 and Fe^{2+}, widely known as "Fenton's reagent", is a well-studied reaction[20] leading to the generation of hydroxyl radicals where these radicals are extremely efficient in initiating (meth)acrylate polymerization. In addition, Fe^{2+} is also an inhibitor of hydroxyl radicals; however, the kinetic constant of this inhibition reaction is significantly lower than the initiation reaction between OH^{o} and monomer. A byproduct of these reactions is the Ferric ion (Fe^{3+}), which is also a known inhibitor of the propagating radicals. These reactions are shown in equations 6-10.

Here, k_{redox} is the kinetic constant of the redox reaction between H_2O_2 and Fe^{2+}, k_{inh1} and k_{inh2} are the kinetic constants of inhibition by Fe^{2+} and Fe^{3+}, respectively, k_i is the kinetic constant of reaction between carbon-carbon double bonds and primary radicals, k_p and k_t are the kinetic constants of propagation and termination, respectively, M represents the monomer and ${}^{o}M_n$ represents the propagating radical.

Oxygen inhibition in radical-mediated polymerizations involving the enzymatic initiation system investigated here is significantly lower than those involving conventional initiating systems (e.g. UV/Visible light initiation) because the enzymatic reaction of oxygen with glucose oxidase is kinetically more favorable than the radical reaction with oxygen. Therefore, inhibition of the polymerization by oxygen is neglected.

4.3.3 Enzyme encapsulation and inactivation

In our earlier investigation[5], we reported that glucose oxidase is trapped by the propagating polymerization front; however, the concentration of the active enzyme is significantly lower than the concentration of the bulk enzyme. This outcome arises as a result of inefficiency in encapsulation as well as inactivation of the enzyme by hydrogen peroxide where the inactivation by hydrogen peroxide has been extensively investigated in the literature[21-24]. H_2O_2 affects the enzyme activity; however, the severity of that reaction depends on whether it is in its oxidized, reduced or complexed state. The model developed in this work incorporates the kinetics of inactivation as a time dependent total concentration of the enzyme determined by the deactivation kinetics. The mathematical representation is shown in equation 11. The fraction of the initial bulk enzyme concentration that is encapsulated (f_{trap}) by the polymerization front is incorporated into the equation. The value of f_{trap} is obtained by fitting the model to experimental data as discussed later in this manuscript.

$$\frac{dc_E}{dt} = \frac{d[E_{red}]}{dt} + \frac{d[E_{cpx}]}{dt} = (k_{red} f_{red} + k_{cpx} f_{cpx}) c_{Enz} c_{H_2O_2} \quad (11)$$

$$c_{Enz} = f_{trap} c_E \quad \mathrm{x} < \mathrm{T}$$

$$c_{Enz} = c_E \quad \mathrm{x} > \mathrm{T}$$

Here, k_{red} and k_{cpx} are the kinetic constants of inhibition of the reduced and complexed states of the enzyme by hydrogen peroxide, and T is the thickness of the coating. Since inactivation of the oxidized state is negligible compared to the reduced and the complexed states, the kinetics of deactivation for the oxidized state are not considered.

A schematic of the physical picture describing the interfacial polymerization on a

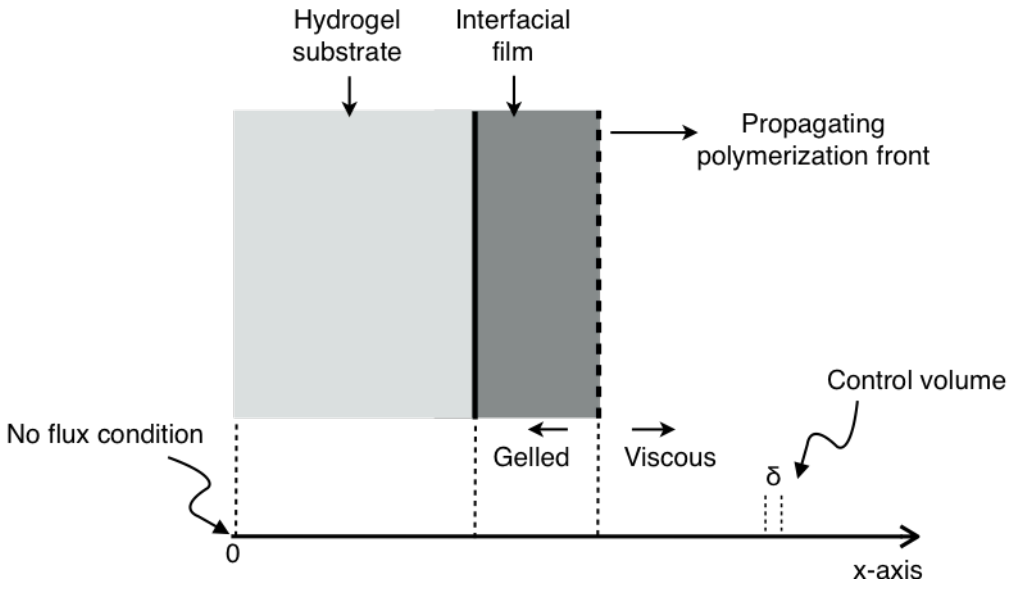

Figure 4.1: Schematic of the physical picture of 1-D interfacial polymerization on a hydrogel substrate at time t. The distance axis (x-axis) originates at the center of the hydrogel and extends into the bulk media

hydrogel substrate is presented in figure 1. The model describes the reaction-diffusion process in 1-dimension. However, this approach is readily extended to diffusion in more than one dimension by establishing appropriate boundary conditions and rewriting the differential mass balances appropriately. The reaction-diffusion system is modeled as a semi-infinite system whose distance coordinate originates at the center of the hydrogel core and extends outward into the surrounding media. At any point on the distance axis

(x-axis), there exists a value of concentration for all the species involved, and this value is determined by the consumption and/or generation rate due to reaction and the species diffusion into and out of an infinitesimal control volume (δ). The concentration is assumed to be uniform in this control volume. The value for the species diffusion coefficient in this control volume is dependent on the time-dependent polymer concentration in the control volume. This dependence is modeled by using the Cukier hydrodynamic theory, which represents mathematically the relationship between species diffusion coefficient and the hydrodynamic drag experienced by the species due to the macromolecular polymer chains. This prediction is shown in equation 12, and this theory has been used previously to model the diffusion of small molecules in hydrogels[25-27].

$$D_s = D_s^w e^{-k_c r_H \Phi^{0.75}} \quad (12)$$

Here, D_s and D_s^w are the species diffusion coefficient in the polymer and water, respectively, r_h is the hydrodynamic radius of the species, ϕ_p is the polymer volume fraction and k_c is a polymer specific constant. The value of k_c was determined to be 1.5.

$$\frac{\partial c_g}{\partial t} = \frac{\partial}{\partial x} D_g(x) \frac{\partial c_g}{\partial x} - k_g c_g [E_{ox}] \quad (13)$$

$$\frac{\partial c_{H_2O_2}}{\partial t} = \frac{\partial}{\partial x} D_{H_2O_2}(x) \frac{\partial c_{H_2O_2}}{\partial x} + k_{O_2} c_{O_2} [E_{red}] - k_{redox} c_{Fe^{2+}} c_{H_2O_2} - \frac{dc_E}{dt} \quad (14)$$

$$\frac{\partial c_{Fe^{2+}}}{\partial t} = \frac{\partial}{\partial x} D_{Fe^{2+}}(x) \frac{\partial c_{Fe^{2+}}}{\partial x} - k_{redox} c_{Fe^{2+}} c_{H_2O_2} - k_{inh1} c_{Fe^{2+}} c_{OH^-} + k_{inh2} c_{Fe^{3+}} c_{M_n^\circ} \quad (15)$$

Performing a mass balance for all the species in the control volume and generalizing for the entire domain, we can obtain the partial differential equations that describe the reaction-diffusion system as shown in equations 13-18. The local radical concentration is

obtained by locally making the pseudo steady state approximation and solving for the resulting equation. (equation 19)

$$\frac{\partial c_{OH^\circ}}{\partial t} = \frac{\partial}{\partial x} D_{OH^\circ}(x) \frac{\partial c_{OH^\circ}}{\partial x} + k_{redox} c_{Fe^{2+}} c_{H_2O_2} - k_i c_{OH^\circ} c_M \quad (16)$$

$$\frac{\partial c_M}{\partial t} = \frac{\partial}{\partial x} D_M(x) \frac{\partial c_M}{\partial x} - k_p c_M c_{M_n^\circ} \quad (17)$$

$$\frac{\partial c_{Fe^{3+}}}{\partial t} = \frac{\partial}{\partial x} D_{Fe^{3+}}(x) \frac{\partial c_{Fe^{3+}}}{\partial x} + k_{inh1} c_{Fe^{2+}} c_{OH^\circ} - k_{inh2} c_{Fe^{3+}} c_{M_n^\circ} \quad (18)$$

$$k_i c_{OH^\circ} c_M = k_t (c_{M_n^\circ})^2 + k_{inh2} c_{Fe^{3+}} c_{M_n^\circ} \quad (19)$$

Here, $D_g(x)$, $D_{H2O2}(x)$, $D_{Fe2+}(x)$, $D_{Fe3+}(x)$, $D_{OHo}(x)$, $D_M(x)$ are the position-dependent diffusion coefficients of glucose, hydrogen peroxide, ferrous ion, ferric ion, hydroxyl radicals and monomer, respectively; and c_{Fe3+}, c_{OHo} and c_{oMn} are the concentrations of ferric ion, hydroxyl radicals and propagating radicals, respectively. The oxygen concentration is assumed to be constant as a result of rapid diffusion from the surrounding atmosphere, and bulk diffusion of the polymeric radicals, terminated polymer and glucose oxidase is neglected.

4.3.4 Modeling the coating thickness

Initial conditions	x < 2000 μm	x > 2000 μm
[Glucose]	0.1 M	0
[Fe^{2+}]	0	0.25 mM
[Glucose oxidase]	0	3.1 μM
[Monomer]	0	0.27 M
OH^o	0	0
[Fe^{3+}]	0	0
[H_2O_2]	0	0
[O_2]	1 mM	1 mM
Polymer volume fraction	0.14	0

Boundary conditions	
x = 0	Diffusive flux for all species is zero i.e. $D_i(x)\frac{\partial c_i}{\partial x} = 0 \; \forall \; i$
x = ϖ	Concentration of all the species is equal to the initial value

Table 4.1: Initial and boundary conditions for the reaction-diffusion model for interfacial reactive coating.

When the hydrogel core is immersed in the precursor solution, rapid diffusion of glucose into the bulk media causes the initiation reactions to be delocalized. This behavior results in a gradient in the polymerization rate, and therefore in the conversion of carbon-carbon double bonds, which decreases as the distance from the hydrogel boundary increases. For these circumstances, there exists a critical conversion for

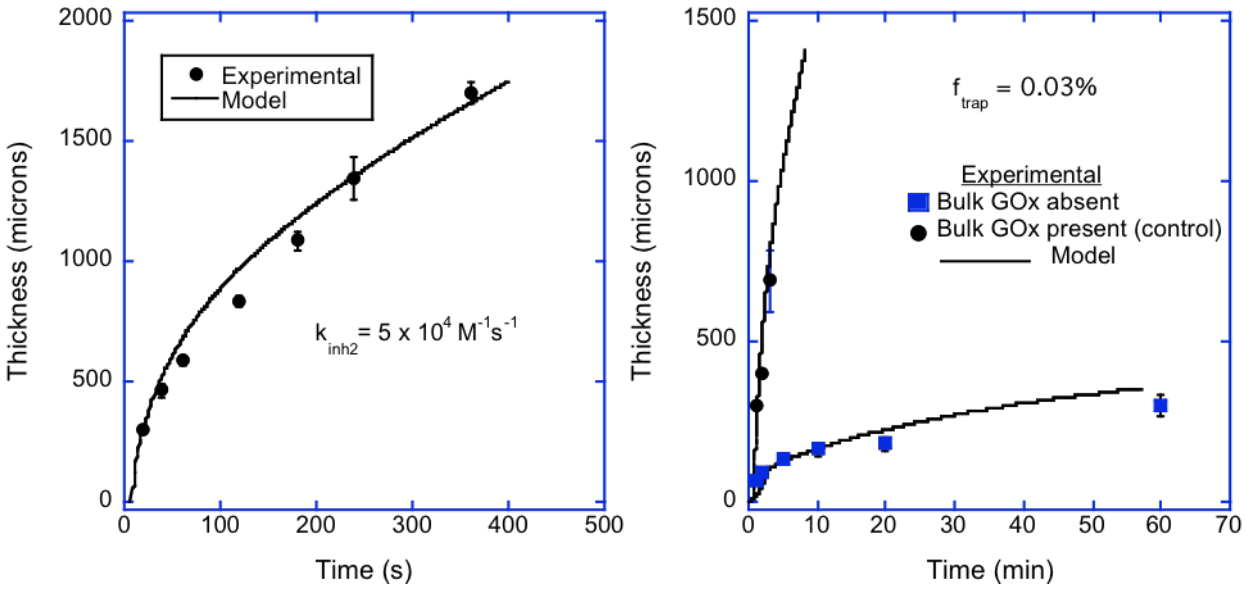

Figure 4.2: Experimental and predicted film thickness as a function of time for two cases: a) Coating of a hydrogel core with GOx in the bulk media b) 2nd stage coating of a previously coated hydrogel core with and without GOx in the bulk. The conditions used for the coating solution were 15 wt% $PEGDA_{575}$, 3 µM glucose oxidase, 0.1M Glucose, 10 mM MES buffer pH 4.5, 0.005 wt% rhodamine acrylate and 2 mM Fe^{2+} (a), 0.25 mM Fe^{2+} (b). The coating thickness of the hydrogel used in (b) was 600 microns

gelation below which the solution is viscous rather than gelled. The boundary between the gelled and the viscous region is the polymerization front, as illustrated in figure 1. The distance from the hydrogel boundary to this region is assumed to be the instantaneous thickness of the coating.

4.3.5 Initial and boundary conditions

The initial and boundary conditions for the coating model are given in Table 1 for one particular set of initiation conditions. As a result of symmetry of the hydrogel geometry, the diffusive flux of all the species is zero at the origin. A value for the distance coordinate nearly 2 orders of magnitude greater than the average diffusion distance of the species during the timescale of the experiments is chosen to represent infinity. The effect of the reactions and species diffusion on the species concentration at this coordinate is assumed to be negligible.

4.4. Results and Discussion

4.4.1 Parameter estimation and model validation

To solve the model, the spatial domain (x-axis in figure 1) is partitioned using a 1-dimensional mesh that is fixed to this axis and originates at the center of the hydrogel.

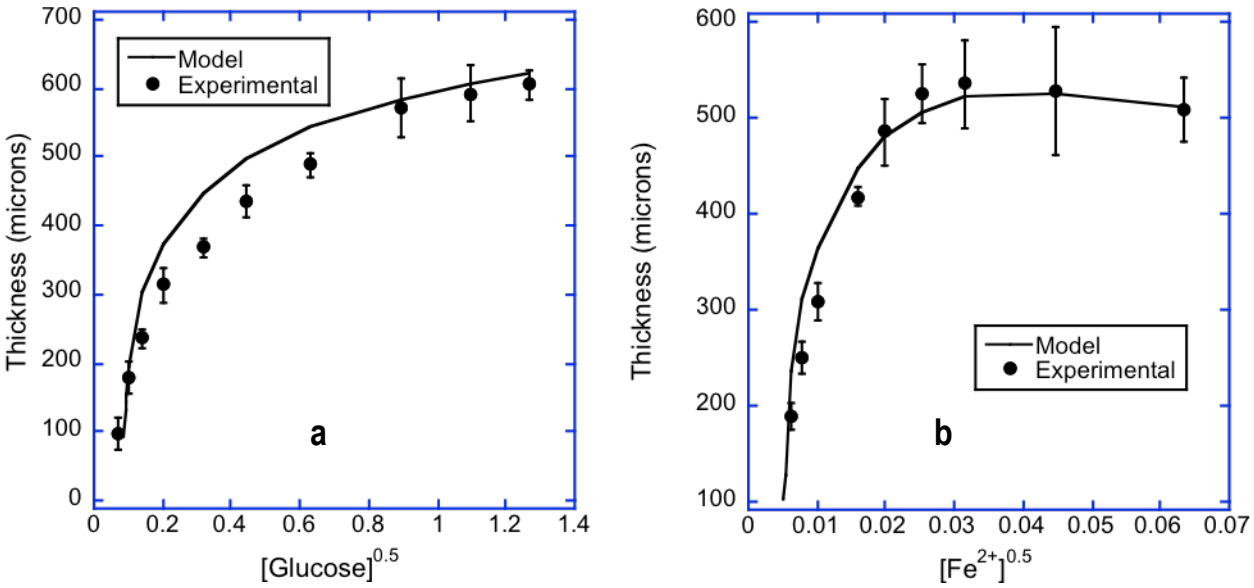

Figure 4.3: Experimental and predicted film thickness as a function of square root of glucose (a) and iron (b) concentrations at the end of 1 minute of immersion into the coating solution. The conditions used for the coating solution were 15 wt% $PEGDA_{575}$, 3 µM glucose oxidase, 0.1M Glucose (b), 0.25 mM Fe^{2+} (a), 10 mM MES buffer pH 4.5 and 0.005 wt% rhodamine acrylate

The thickness of the interfacial film is obtained by tracking the coordinate on the x-axis at which the value of the carbon-carbon double bond conversion reaches the critical conversion for gelation, which is reasonably assumed to be 0.2. As the polymerization proceeds, this coordinate "moves" further away from the interface and is used to represent the propagating polymerization front. Every coordinate on this axis is associated with a dynamic polymer volume fraction, which is used to obtain the polymer concentration dependent diffusion coefficient. In this manner, a stationary mesh is used to model accurately the changing mass transport conditions as the polymerization proceeds and the coating thickness changes as a function of time. Values for many of the parameters used in the model are obtained from the literature as listed in Tables 2 and 3. Other parameters that are not reported in the literature include the kinetic constant of inhibition of propagating radicals by ferric ion ($FeOH^{2+}$, k_{inh2}) and the fraction of the bulk enzyme encapsulated by the propagating polymerization front (f_{trap}). This latter parameter is obviously specific to the system investigated here and is dependent on the reaction rates employed. However, one representative value for the enzyme fraction trapped is used for all experimental conditions. To obtain the values for these unknown constants, the model prediction for the time-dependent thickness was fit to the experimental data reported earlier for two cases[5]. In the first case, the enzymatic precursor for film formation is the glucose oxidase (GOx) in the bulk media (Figure 2a). In the second, only GOx that is trapped by the coating in the first stage is used to initiate film formation in the second stage (Figure 2b). The value for k_{inh2} is close to other similar values reported in the literature for inhibition of propagating radicals in the polymerization of acrylamide

in aqueous solution[37]. It is possible that this model overpredicts this value because factors such as volume shrinkage due to polymerization and evaporation of water from the hydrogel coating have not been accounted for and could contribute to reducing the film thickness. However, the evaporation of water is not an issue during the polymerization because the hydrogel is completely submerged in the coating solution and evaporation occurs only at the air-water interface. The low value for the fraction of enzyme trapped (f_{trap}) (0.03% of bulk enzyme concentration) is an indication of the resistance of glucose oxidase in binding to the polymer and instead remaining in solution. Moreover, the enzyme is a glycoprotein of molecular weight 160kDa having a hydrodynamic radius of 43 Angstroms, almost twice as large as the mesh size of the polymer network. Therefore, it is not surprising that the polymer network nearly excludes the enzyme during its formation. However, GOx reacts with glucose in catalytic amounts and despite the low value of f_{trap}, hydrogen peroxide is generated in sufficient amounts to initiate the polymerization, albeit at a significantly lower rate. These estimated parameters together with the previously reported values were incorporated into the model to predict the film thickness as a function of the concentrations of glucose and iron and compare to the experimental data that were reported earlier[5] (Figures 3a and 3b).

4.4.2 Kinetics of interfacial film formation

The delocalization of hydrogen peroxide generation, which is a product of the glucose reaction with glucose oxidase, is a result of the rapid diffusion of glucose out of the substrate and into the bulk. The generated H_2O_2 can also diffuse into the bulk thereby delocalizing the generation of hydroxyl radicals that initiate polymerization. The degree of delocalization in the above cases is strongly dependent on the relative diffusion and

reaction rates of glucose and hydrogen peroxide with glucose oxidase and Fe^{2+}, respectively. Specifically, an increase in the reaction rate results in the decreased likelihood of either species escaping reaction and diffusing into the bulk. Glucose is readily able to escape the substrate and diffuses even more rapidly once it escapes the substrate and enters the bulk. While it is not feasible for glucose oxidase to diffuse into the coating and little of it becomes trapped therein, Fe^{2+} does readily diffuse into the

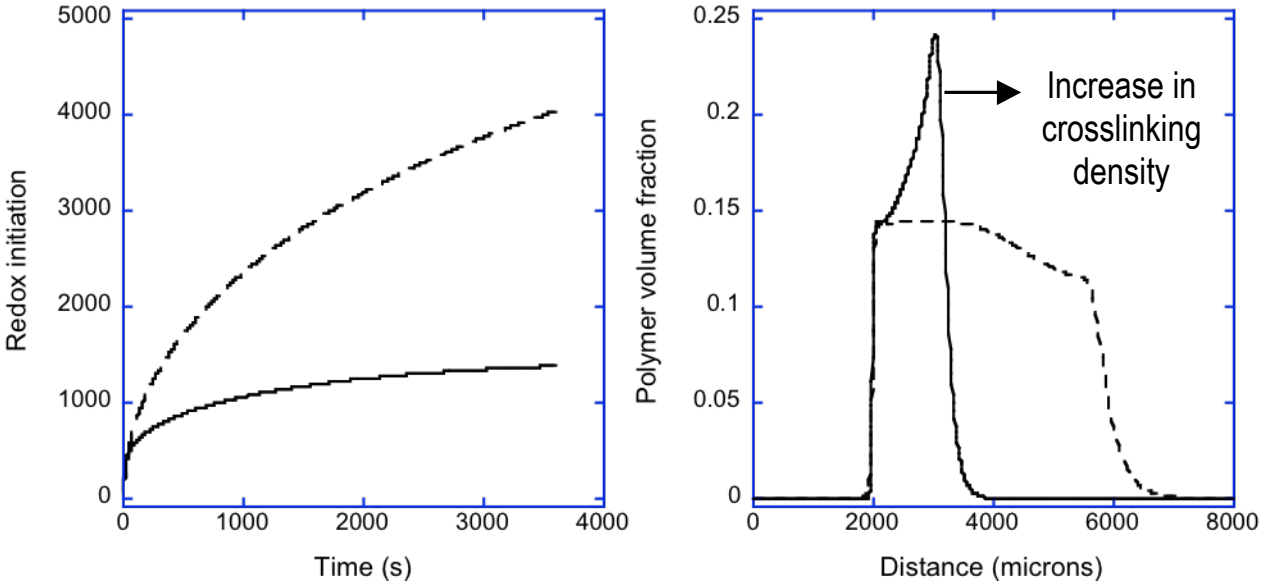

Figure 4.4: Predicted thickness as a function of time (left) and polymer fraction as a function of distance when the interfacial polymerization is initiated by an enzyme-mediated redox system (-----) and in a two-component redox system (——). The conditions used in the simulation were 3 μM GOx, 0.1 M glucose, 2 mM Fe^{2+}, 15 wt.% $PEGDA_{575}$ and immersion time of 1 hour.

coating. The implications of the interpenetration of reactive components on the thickness of the interfacial film are significant. Figure 4 (left) highlights this by comparing the predicted thickness as a function of time for the glucose oxidase-mediated initiation with an otherwise similar initiation system that does not involve an enzyme. For example, one might encapsulate H_2O_2 in one phase and Fe^{2+} in the other prior to initiation. The film thickness for similar species concentrations at the end of 1 hour is significantly higher for

the glucose oxidase-mediated initiation system. This outcome arises because in the enzyme-mediated system H_2O_2 can continue to be generated at the moving interface as a result of the delocalization of glucose without being hindered significantly by the reaction with glucose oxidase within the coating. However, for the pure redox initiation system, the increased hindrance to diffusion of H_2O_2 within the coating means that as the coating thickness increases, the likelihood of continued radical generation at the interface decreases. When the diffusion timescale of H_2O_2 to the moving interface increases above

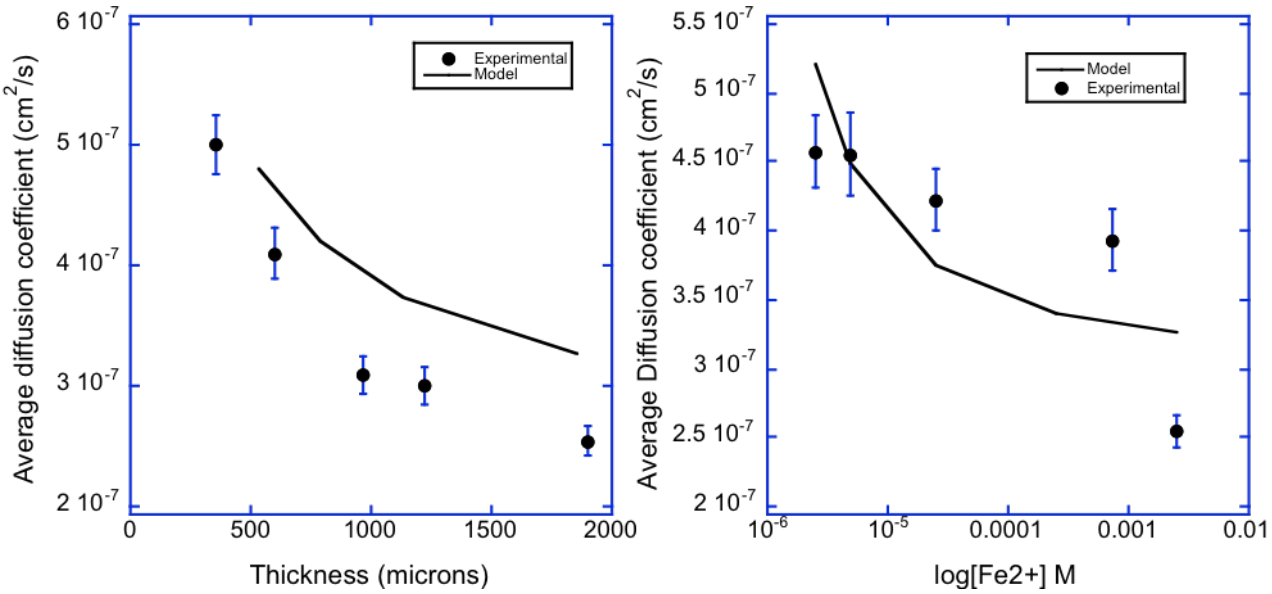

Figure 4.5: Experimental and predicted average diffusion coefficient of the coating as a function of thickness (left) and initial iron concentration (right). The conditions used were 3µM GOx, 0.1M Glucose, 15 wt% PEGDA, 10 mM MES buffer ph 4.5, 2.5mM Fe^{2+}(left) and 1.9 mm thickness (right).

the timescale of monomer diffusion from the bulk to the interface, further polymerization predominantly increases the crosslinking density of the coating adjacent to the interface rather than contributing to the film growth (Figure 4, right).

A particular implication of the rapid delocalization of the enzyme-mediated initiation reactions is the continued densification of the interfacial film after it has

formed. The model can be used to determine the factors that influence the extent of reaction within the membrane film and therefore the overall membrane permeability. Figure 5 (left) shows the variation of the average diffusion coefficient of a non-reactive dye, rhodamine-B within the coating as a function of the film thickness. With increasing coating thickness, the diffusion coefficient approaches the theoretical value at complete conversion i.e. 2 x $10^{-7}$$cm^2$/s because the increased polymerization time leads to complete reaction and network formation within the coating. By ensuring higher initiation rates within the coating, the rate of densification of the coating and hence the extent of the reaction at a given thickness can be increased. This behavior is shown in Figure 5 (right), where the coating becomes less permeable as the bulk iron concentration is increased to enable higher initiation rates within the coating. The experimentally determined values for diffusion coefficient indicate that the model predicts qualitatively, the variation as a function of thickness and bulk iron concentration. The quantitative disparity between the experimental values and the model is likely due to non-specific interactions of the dye, Rhodamine-B with the polymer and has not been accounted for in the model. Specifically, in equation 12 that describes the variation of diffusion coefficient with polymer volume fraction, a single value for the polymer-specific constant (k_c) was used. While the experiments enable investigation of permeability, the determination of polymer concentration gradients as a result of reaction delocalization is not straightforward. The model can be used to investigate the nature of these gradients and determine the factors that influence them as discussed in the following section.

4.4.3 Influence of iron concentration on reaction delocalization

The rapid diffusion of glucose into the bulk media inevitably causes a gradient in the initiation rates resulting in the polymerization rate dependence as a function of distance from the hydrogel substrate. Therefore, the interfacial film formed is not homogeneous with respect to the extent of the polymerization reaction.

The concentration of iron in the bulk media plays a critical role in determining the

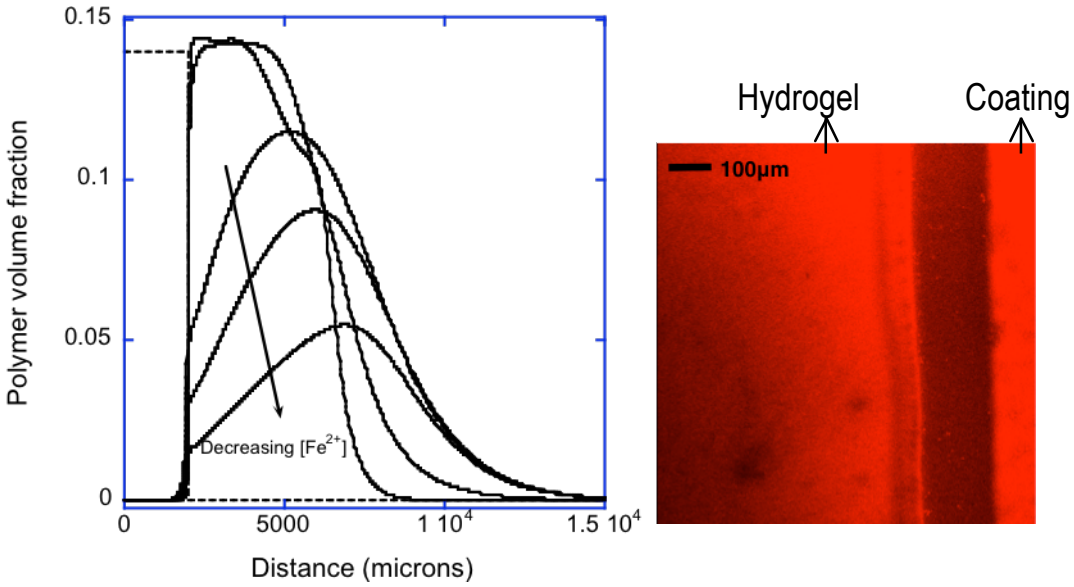

Figure 4.6: Predicted polymer volume fraction as a function of distance for various iron concentrations in the bulk (left). The solid lines represent the newly formed interfacial film and the dashed line represents the initial hydrogel polymer network substrate. Fluorescence image of a coated hydrogel showing the cross-section of the interface between the hydrogel and the coating(right). The dramatically lower extent of reaction adjacent to the hydrogel compared to the bulk results in the decreased immobilization of the fluorescent co-monomer rhodamine-B acrylate. The conditions used were 3 µM GOx, 0.1 M glucose, 2.5 µM Fe^{2+}, 15 wt% $PEGDA_{575}$, 10 mM MES buffer pH4.5, 0.005wt% rhodamine-B acrylate and immersion time of 1 hour

degree of delocalization of the initiation reaction. The predicted polymer volume fraction, a measure of the extent of reaction, as a function of distance from the center of the hydrogel at the end of 3 hours of coating, is shown in Figure 6 (left). The dashed line

represents the initial polymer core, and the solid lines indicate the coating polymer volume fraction (Φ_p). The interfacial polymer spans both the hydrogel core (interpenetrating network) while also penetrating into the surrounding media. Outside the hydrogel, at higher concentrations of iron in the bulk media, the polymer density monotonically decreases as the distance from the interface increases as a result of the decrease in glucose concentration and hence the initiation rate. However, at lower iron concentrations, the polymer fraction reaches a maximum some distance away from the core before decreasing as the distance from the hydrogel boundary increases. This behavior is due to the fact that, in the incipient stages of coating formation, iron is rapidly consumed, resulting in significant amounts of polymer formed, albeit incompletely. For further polymer formation, iron from the bulk media must diffuse into this partially formed film and initiate further polymerization.

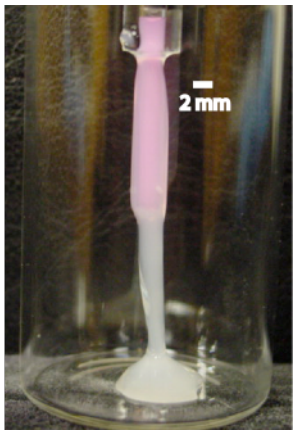

Figure 4.7: Gravity-induced settling of polymer coating as a result of interface weakening at low iron concentrations due to low conversion and coupling at the interface as predicted by the model. Shown here is a coated cylindrical hydrogel for the following condition of the coating formulation: 25 μM Fe^{2+}, 3 μM GOx, 0.1M Glucose and 15wt% $PEGDA_{575}$, 10 mM MES buffer pH = 4.5 and immersion time of 10 min.

However, this must occur in the face of increasing diffusion resistance from the growing polymer film, in addition to escaping reaction with the rapidly generated hydrogen peroxide from the enzymatic reaction. This effect is exacerbated at very low iron concentration, and as a consequence the region adjacent to the interface never

reaches complete conversion of carbon-carbon double bonds. This results in the formation of an asymmetric interfacial film that gets progressively denser away from the hydrogel boundary before decreasing again. Figure 6 (right) experimentally validates this

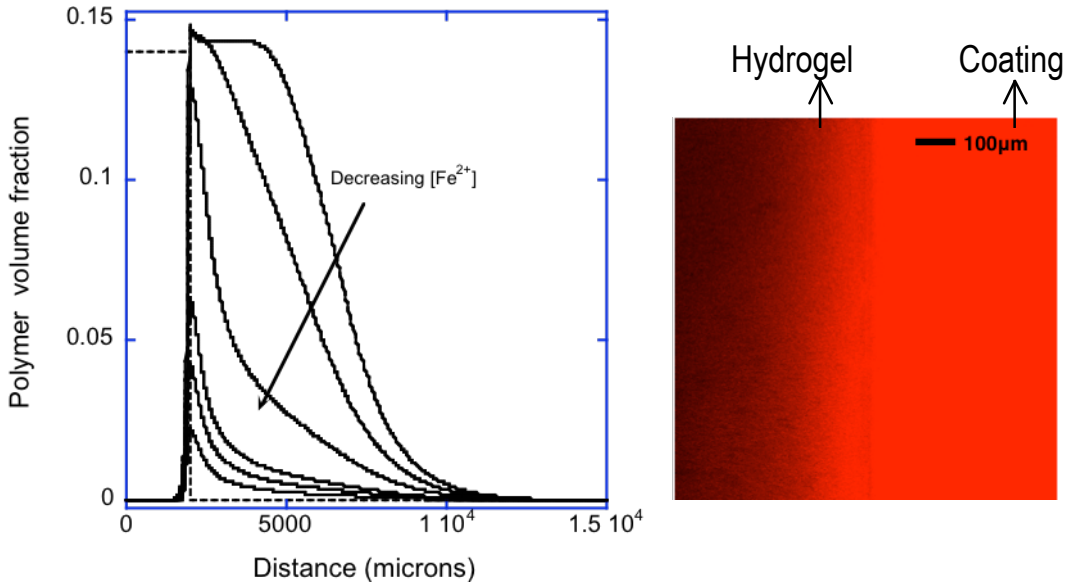

Figure 4.8: Predicted polymer volume fraction as a function of distance for various iron concentrations in the hydrogel (left). The solid lines represent the interfacial membrane and the dashed line represents the hydrogel polymer network. Fluorescence image of a coated hydrogel showing the cross-section of the interface between the hydrogel and the coating (right). The higher extent of reaction adjacent to the hydrogel compared to the bulk results in the elimination of the "dips" in the polymer volume fraction .The condition used was 3 µM GOx, 0.1 M glucose, 2.5 µM Fe^{2+}, 15 wt% $PEGDA_{575}$, 10 mM MES buffer pH4.5, 0.005wt% rhodamine-B acrylate and immersion time of 1 hour.

hypothesis. It is clearly seen that there exists a region of dramatically decreased immobilization of the fluorescent co-monomer, rhodamine-B acrylate adjacent to the interface.

Additional evidence comes from the fact that when the interfacial polymerization is conducted in a manner such that there is a net force on the interfacial polymer layer due to the opposing nature of gravity and buoyancy, a film much thicker than predicted by diffusion alone results, as shown in Figure 7. It is clearly seen that the cylindrical shaped hydrogel is coated with a "tapering" polymer film on the curved surface area and a "stretched" polymer film on the lateral surface area. This outcome arises because the mechanical integrity of the interface is severely undermined by the low conversion and coupling that occur at that interface. Therefore, the relatively dense polymer is shed as it forms and settles to the bottom. As the settling process occurs, counter diffusion of the initiating species and monomer towards the hydrogel boundary occurs. The rapid reaction adjacent to the interface results in crosslink formation that subsequently causes the non-stationary coating to eventually adhere to the surface. When the reaction rates were decreased as a result of decreasing the bulk iron concentration b y two orders of magnitude, this feature was not observed. Instead, macrogels of polymer at the bottom of the immersing solution were observed, indicating that the settling velocity exceeded the rate of polymer formation adjacent to the interface. This phenomenon also did not occur when the cylindrical hydrogel was coated at conditions of significantly higher bulk iron concentration.

The lack of interfacial adhesion resulting from the significantly decreased polymerization rate adjacent to the interface at lower iron concentrations can be overcome by generating radicals persistently in this region. This solution is accomplished by ensuring that iron can diffuse into this region without being hindered by the redox reaction with H_2O_2. Since the presence of iron in the bulk media is what is driving this

behavior, inclusion of iron in the hydrogel initially, instead of the bulk means that Fe^{2+}must diffuse through the region adjacent to the hydrogel boundary before diffusing into the bulk media. Figure 8 (left) conceptualizes this hypothesis. It is clearly seen that these "dips" in the polymer volume fraction are eliminated at lower iron concentrations. Figure 8 (right) which represents interfacial polymerization on a hydrogel substrate when iron is in the hydrogel initially, validates this hypothesis.

4.5 Conclusions

A mathematical model was developed that describes the nature of film formation by radical-mediated interfacial polymerization. The delocalization of the initiation reactions as a result of rapid diffusion strongly influences the properties of the interfacial film properties such as thickness, permeability and the presence of polymer concentration gradients. The influence of the glucose and iron concentration on the interfacial film thickness predicted by the model agrees well with the experiments. The model predicts that, using an enzyme-mediated redox initiation system produces 3-fold thicker coatings compared to a simple, two-component redox initiation system. This is because the enzyme is significantly excluded from the coating thereby decreasing the reactivity of glucose within the coating and leading to a higher degree of reaction delocalization. This delocalization implies that the membrane gradually densifies after it has formed. The model correctly predicts that the average diffusion coefficient of a non-reactive molecule such as rhodamine-B decreases with increasing thickness, which is a result of the increased time for membrane densification. The iron concentration in the bulk determines the rate of densification and therefore the permeability characteristics at a given thickness. The model was also used to provide insight into the gradients in the

polymer density and determine the conditions that affect such properties. The model predicts that at lower iron concentrations, the depletion of iron within the membrane and the resistance to bulk iron diffusion into this region lowers the polymer density adjacent to the hydrogel. In situations where the adhesion of the membrane to the substrate is important, higher bulk iron concentrations or inclusion of iron initially in the hydrogel instead of the bulk ensures higher initiation rates adjacent to the interface and therefore better adhesion.

Acknowledgements

This work has been supported by the National Institutes of Health (GrantR21 EB 012188)

Species diffusion coefficient in water	Value ($cm^2. s^{-1}$)	Reference
Glucose (D_g)	$7x10^{-6}$	29
Ferrous (D_{Fe2+})	$7x10^{-6}$	30
Ferric (D_{Fe3+})	$6x10^{-6}$	30
Hydrogen peroxide (D_{H2O2})	$1.4x10^{-5}$	31
Hydroxyl radical ($D_{OH^{\cdot}}$)	$7.1x10^{-5}$	35
Monomer (D_M)	$4x10^{-6}$	32

Table 4.2:Values for the diffusion coefficients used in the model

Kinetic constants	Value	Reference
k_{cat}	$1x10^{3}\ s^{-1}$	19
k_{g}	$1x10^{4}\ M^{-1}.\ s^{-1}$	19
k_{O2}	$2x10^{6}\ M^{-1}.\ s^{-1}$	19
k_{redox}	$76\ M^{-1}.\ s^{-1}$	20
k_{inh1}	$3x10^{8}\ M^{-1}.\ s^{-1}$	20
k_{i}	$10^{9}\ M^{-1}.\ s^{-1}$	34
k_{p}	$2x10^{4}\ M^{-1}.\ s^{-1}$	28
k_{t}	$0.7x10^{6}\ M^{-1}.\ s^{-1}$	28
k_{red}	$0.02\ M^{-1}.\ s^{-1}$	21
k_{cpx}	$0.76\ M^{-1}.\ s^{-1}$	21

Table 4.3: Values for the kinetic constants used in the model and their corresponding references

4.6. References

1. Scott, C.; Wu, D.; Ho, C.-C.; Co, C. C., (2005). "Liquid-Core Capsules via Interfacial Polymerization:, A Free-Radical Analogy of the Nylon Rope Trick." Journal of the American Chemical Society 127(12): 4160-4161.
2. Luo, Y. W. and H. Y. Gu (2006). "A general strategy for nano-encapsulation via interfacially confined living/controlled radical miniemulsion polymerization." Macromolecular Rapid Communications 27(1): 21-25.
3. Johnson, L. M.; DeForest, C. A.; Pendurti, A.; Anseth, K. S.; Bowman, C. N., (2010). "Formation of Three-Dimensional Hydrogel Multilayers Using Enzyme-Mediated Redox Chain Initiation." ACS Applied Materials & Interfaces 2(7): 1963-1972.
4. Hume, P. S.; Bowman, C. N.; Anseth, K. S., (2011). "Functionalized PEG hydrogels through reactive dip-coating for the formation of immunoactive barriers." Biomaterials 32(26): 6204-6212.
5. Shenoy R, Bowman CN, Kinetics of interfacial radical polymerization initiated by a glucose oxidase-mediated redox system, Biomaterials (2012), http://dx.doi.org/10.1016/j.biomaterials.2012.06.014
6. Langer, R. (1999). "Biomaterials in Drug Delivery and Tissue Engineering: One Laboratory's Experience." Accounts of Chemical Research 33(2): 94-101.
7. Freiberg, S. and X. X. Zhu (2004). "Polymer microspheres for controlled drug release." International Journal of Pharmaceutics 282(1–2): 1-18.
8. Zhu, Y.; Shi, J.; Shen, W.; Dong, X.; Feng, J.; Ruan, M.; Li, Y., (2005). "Stimuli-Responsive Controlled Drug Release from a Hollow Mesoporous Silica

Sphere/Polyelectrolyte Multilayer Core–Shell Structure." Angewandte Chemie International Edition 44(32): 5083-5087.

9. Bäumler, H. and R. Georgieva (2010). "Coupled Enzyme Reactions in Multicompartment Microparticles." Biomacromolecules 11(6): 1480-1487.
10. White, S. R.; Sottos, N. R.; Geubelle, P. H.; Moore, J. S.; Kessler, M. R.; Sriram, S. R.; Brown, E. N.; Viswanathan, S., (2001). "Autonomic healing of polymer composites." Nature 409(6822): 794-797.
11. Janssen, L. and K. Tenijenhuis (1992). "Encapsulation by Interfacial Polycondensation .1. The Capsule Production and a Model for Wall Growth." Journal of Membrane Science 65(1-2): 59-68.
12. Janssen, L. J. J. M. and K. te Nijenhuis (1992). "Encapsulation by interfacial polycondensation. II. The membrane wall structure and the rate of the wall growth." Journal of Membrane Science 65(1,Äì2): 69-75.
13. Freger, V. (2005). "Kinetics of Film Formation by Interfacial Polycondensation." Langmuir 21(5): 1884-1894.
14. Freger, V. and S. Srebnik (2003). "Mathematical model of charge and density distributions in interfacial polymerization of thin films." Journal of Applied Polymer Science 88(5): 1162-1169.
15. Oizerovich-Honig, R.; Raim, V.; Srebnik, S., (2009). "Simulation of Thin Film Membranes Formed by Interfacial Polymerization." Langmuir 26(1): 299-306.
16. Yashin, V. V. and A. C. Balazs (2004). "Theoretical model of interfacial polymerization." Journal of Chemical Physics 121(22):11440-11454.

17. Ji, J.; Dickson, J. M.; Childs, R. F.; McCarry, B. E., (2000). "Mathematical model for the formation of thin-film composite membranes by interfacial polymerization: Porous and dense films." Macromolecules 33(2): 624-633.
18. Crank, J. (1979). The Mathematics of Diffusion, Clarendon Press.
19. Gibson, Q. H.; Massey, V.; Swoboda, B. E. P., (1964). "Kinetics and Mechanism of Action of Glucose Oxidase." Journal of Biological Chemistry 239(11): 3927-&.
20. Walling, C. (1975). "Fenton's reagent revisited." Accounts of Chemical Research 8(4): 125-131.
21. Tse, P. H. S. and D. A. Gough (1987). "Time-dependent inactivation of immobilized glucose oxidase and catalase." Biotechnology and Bioengineering 29(6): 705-713.
22. Malikkides, C. O. and R. H. Weiland (1982). "On the mechanism of immobilized glucose oxidase deactivation by hydrogen peroxide." Biotechnology and Bioengineering 24(11): 2419-2439.
23. Krishnaswamy, S. and J. R. Kittrell (1978). "Deactivation studies of immobilized glucose oxidase." Biotechnology and Bioengineering 20(6): 821-835.
24. Bourdillon, C.; Thomas, V.; Thomas, D., (1982). "Electrochemical study of d-glucose oxidase autoinactivation." Enzyme and Microbial Technology 4(3): 175-180.
25. Masaro, L. and X. X. Zhu (1999). "Physical models of diffusion for polymer solutions, gels and solids." Progress in Polymer Science 24(5): 731-775.
26. Cukier, R. I. (1984). "Diffusion of Brownian spheres in semidilute polymer solutions." Macromolecules 17(2): 252-255.

27. Waters, D. J. and C. W. Frank (2009). "Hindered diffusion of oligosaccharides in high strength poly(ethylene glycol)/poly(acrylic acid) interpenetrating network hydrogels: Hydrodynamic vs. obstruction models." Polymer 50(26): 6331-6339.
28. Kizilel, S. "Mathematical Model for Microencapsulation of Pancreatic Islets within a Biofunctional PEG Hydrogel." Macromolecular Theory and Simulations 19(8-9): 514-531.
29. Mavituna, F.; Park, J. M.; Gardner, D., (1987). "Determination of the Effective Diffusion-Coefficient of Glucose in Callus-Tissue." Chemical Engineering Journal and the Biochemical Engineering Journal 34(1): B1-B5.
30. Yuan-Hui, L. and S. Gregory (1974). "Diffusion of ions in sea water and in deep-sea sediments." Geochimica et Cosmochimica Acta 38(5): 703-714.
31. Kern, D. M. H. (1954). "The Polarography and Standard Potential of the Oxygen-Hydrogen Peroxide Couple." Journal of the American Chemical Society 76(16): 4208-4214.
32. Shimada, K.; Kato, H.; Saito, T.; Matsuyama, S.; Kinugasa, S., (2005). "Precise measurement of the self-diffusion coefficient for poly(ethylene glycol) in aqueous solution using uniform oligomers." Journal of Chemical Physics 122(24).
33. Bouchoux, A.; Roux-de Balmann, H.; Lutin, F., (2005). "Nanofiltration of glucose and sodium lactate solutions - Variations of retention between single- and mixed-solute solutions." Journal of Membrane Science 258(1-2): 123-132.
34. Nightingale, E. R. (1959). "Phenomenological Theory of Ion Solvation - Effective Radii of Hydrated Ions." Journal of Physical Chemistry 63(9): 1381-1387.

35. Dohmen, M. P. J.; Pereira, A. M.; Timmer, J. M. K.; Benes, N. E.; Keurentjes, J. T. F., (2008). "Hydrodynamic radii of polyethylene glycols in different solvents determined from viscosity measurements." Journal of Chemical and Engineering Data 53(1): 63-65.

36. Fogolari, F.; Corazza, A.; Toppo, S.; Tosatto, S. C. E.; Viglino, P.; Ursini, F.; Esposito, G., "Studying Interactions by Molecular Dynamics Simulations at High Concentration." Journal of Biomedicine and Biotechnology.

37. Collinson, E.; Dainton, F. S.; Mile, B.; Tazuke, S.; Smith, D. R., (1963). "Thermal Redox Reactions Between Metal Ions and Radicals in Aqueous Solutions." Nature 198(4875): 26-30.

Chapter 5

Formation of core-shell particles by interfacial radical polymerization initiated by a glucose oxidase-mediated redox system

A unique design paradigm to form core-shell particles based on interfacial radical polymerization is described. The interfacial initiation system is comprised of an enzymatic reaction between glucose and glucose oxidase (GOx) to generate hydrogen peroxide, which, in the presence of iron (Fe2+), generates hydroxyl radicals that initiate polymerization. Shell formation on pre-fabricated polymeric cores is achieved by localizing the initiation reaction to the interface of the core and a surrounding aqueous monomer formulation into which it is immersed. The interfacially-confined initiation reaction is accomplished by incorporating one or more of the initiating species in the particle core and the remainder of the complimentary initiating components in the surrounding media such that interactions and the resulting initiation reaction occur at the interface. This work is focused on engineering the reaction behavior and mass transport processes to promote interfacially-confined polymerization, controlling the rate of shell formation, and manipulating the structure of the core-shell particle. Specifically, incorporating GOx in the precursor solution used to fabricate cores ranging from 100 to 200 μm, and the remainder of the complementary initiating components and monomer in the bulk solution prior to interfacial polymerization yielded shells whose average thickness was 20 μm after 4 minutes of immersion and at a bulk iron concentration of 12.5 mM. When the locations of glucose and GOx are interchanged, the average thickness of the shell was 15 μm or 100 μm for bulk iron concentrations of 45 mM and 12.5 mM, respectively. The initial locations of glucose and GOx also determine the

degree of interpenetration of the core and the shell. Specifically, for a bulk iron concentration of 45 mM, the thickness of the interpenetrating layer averaged 12 μm when GOx was initially within the core, whereas no interpenetrating layer was observed when glucose was incorporated in the core. The polymeric shell formed by this technique is also demonstrated to be self-supporting following core degradation. This behavior is accomplished by fabricating the particle core hydrogel from monomers possessing degradable groups that can be irreversibly cleaved by light exposure following shell formation. When the coated particle was exposed to light, the shell remained intact while the core degraded as evidenced by a dramatic change in diffusion coefficient of fluorescent beads immobilized within the core.

5.1 Introduction

Microparticles composed of a distinct core and shell are useful in a variety of applications such as drug delivery,[1-4] tissue engineering,[1,5] catalysis,[6,7] autonomic healing[8] and pigments,[1] among others. The shell can function to isolate the core from harsh external environments, including pH, physiological, or biochemical stresses; serve as a barrier membrane that controls the release of encapsulated molecules; or provide a means to achieve integration of multiple components with spatial separation. A number of techniques have been reported in the literature that are capable of fabricating core-shell architectures such as layer-by-layer self-assembly of polyelectrolytes,[9] magnetic coatings,[10] selective withdrawal coatings,[11] and interfacial polymerization.[12,13] Here, we demonstrate a unique design paradigm for the fabrication of core-shell objects in the sub-millimeter range based on interfacial polymerization initiated by radical generating reactions. The initiation system consists of the specific reaction between glucose and

glucose oxidase to generate hydrogen peroxide (H_2O_2), which, in the presence of Fe^{2+},

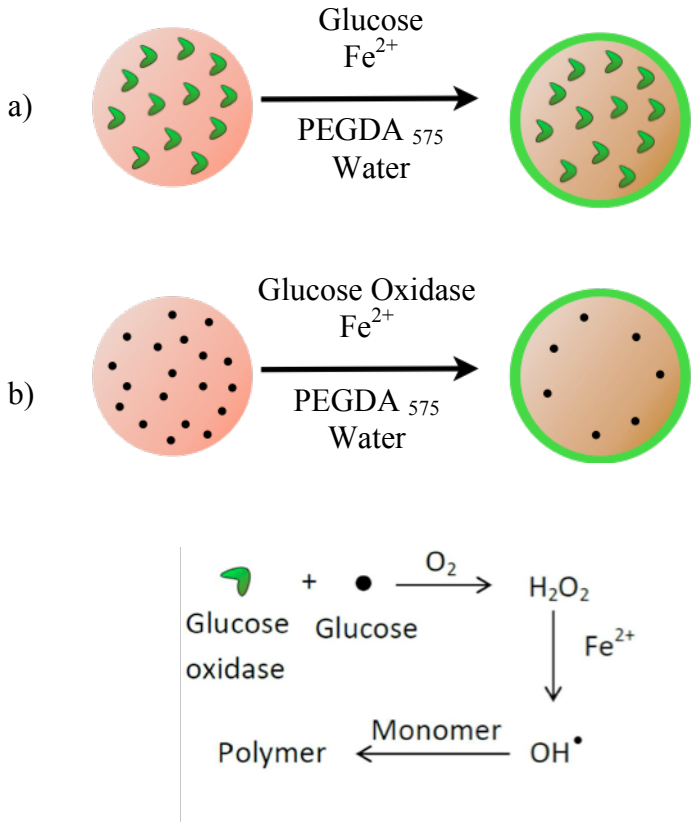

Figure 5.1: Schematic depicting the spatial organization of the initiating components in the hydrogel core and the bulk media prior to interfacial polymerization. a) Glucose oxidase is incorporated in the core and b) Glucose is incorporated in the core. The complementary initiating species are in the coating solution. The simplified reaction mechanism underpinning the interfacial polymerization is shown in c.

forms hydroxyl radicals capable of efficiently initiating (meth)acrylate monomer chain polymerization (**Figure 1c**). By confining one of the initiating species in a hydrogel core and the remaining initiating components and monomer in a coating solution, the formation of a shell or coating is accomplished (**Figure 1a and 1b**).

The mild conditions of temperature and pressure employed, as well as the use of aqueous monomer solutions, render this technique suitable for encapsulating biological moieties. Unlike other surface-initiated and interfacial radical polymerizations that

immobilize radicals or radical generating species at the surface or interface[12,14] prior to polymerization, this technique uses a simpler approach to achieve interfacially-confined initiating reactions. Here, the reaction is accomplished by mixing the initiating species into the precursor solutions used to fabricate the core and shell. Additionally, the coating that forms the shell is ideally conformal as a result of the isotropic mass transport properties of the core, which could enable cores with complex geometrical shapes to be coated uniformly. A particular implication of this approach is the ability to form liquid cores encapsulated in a shell of an unconventional geometry. This outcome is accomplished by dissolution of the core after the formation of the shell which is difficult to achieve when liquid cores are used directly as templates for the fabrication of the shell.

Johnson *et al.*[15] have demonstrated the formation of conformal coatings on 3D hydrogels of up to several millimeters in dimension and Hume *et al.*[23] used this approach to modify hydrogels with biological moieties to control dendritic cell activation.However, enabling interfacially-confined polymerization on hydrogel cores in the sub-millimeter range requires a highly reactive surrounding phase that prevents the rapid diffusion of the initiating species into the bulk media, which ultimately leads to unconfined bulk polymerization. In addition, the significantly smaller size of the hydrogel makes it difficult to physically remove these cores from the coating solution immediately after the desired thickness of the shell has formed. This challenge necessitates the establishment of a self-limiting reaction or stimulus-responsive termination of polymerization. A portion of this manuscript is focused on engineering the reaction behavior and mass transport conditions to promote interfacially-confined shell formation and enable control over the rate of shell growth and structure of the core-shell

particle. A subsequent portion of the work demonstrates the ability of the shell to be self-supporting in the absence of a core with a defined geometry. This behavior is accomplished by degrading an initially coated solid core to form a liquid core encapsulated within the shell. The transition of the core from a gelled to a liquid state is achieved by fabricating the hydrogel core from monomers that degrade upon exposure to light. [16]

5.2 Experimental

Materials: Glucose oxidase (GOx) from *aspergillus niger*, glucose, acrylamide/bisacrylamide (40%, 19:1), sorbitan monooleate (Span 80), poly(ethylene glycol) sorbitan monooleate (Tween 80), poly(ethylene glycol) diacrylate (PEGDA) (MW 575), ammonium persulfate, *N,N,N',N'*-tetramethylethylenediamine (TEMED), triethanolamine, and 2,2,6,6-tetramethyl-1-piperidinyloxy (TEMPO) used in this work were all obtained from Sigma Aldrich. Acryloxyethyl thiocarbamoyl rhodamine B (Rhodamine B acrylate) was obtained from Polysciences, and 2-(N-Morpholino)ethanesulfonic acid (MES) buffer pH 4.5 was obtained from Teknova. Yellow-green fluorescent particles 20 nm and 2 μm in diameter (excitation/emission, 505/515 nm) were obtained from Invitrogen.

5.2.1 Microparticle fabrication

The non-photodegradable hydrogel microparticles used in this work were synthesized by an inverse suspension polymerization described as follows: An aqueous phase (0.5 ml) consisting of the monomer was suspended in an organic phase (5 ml) that was purged with nitrogen for 5 minutes. The aqueous phase was formulated by dissolving in an acrylamide/bisacrylamide solution (0.5 ml), the following components; ammonium

persulfate (28 mg/ml), rhodamine B acrylate (0.005 wt%) and glucose oxidase (14 mg/ml) or glucose (0.1 M) depending on whether glucose or glucose oxidase is incorporated in the coating solution respectively. The organic phase consisted of Span 80 (200 μL) and Tween 80 (35 μL) and hexane to make up the organic phase (5 ml). The two phases were then emulsified by sonication for 10 seconds after which polymerization was initiated by the addition of TEMED (10 μL) followed by magnetic stirring for 10 minutes. Following this procedure, the supernatant was carefully removed and the remaining microparticles that settled at the bottom were re-suspended in hexane (water) when glucose (glucose oxidase) was present in the microparticles. Since glucose is negligibly soluble in hexane, most of it remains in the water-swollen microparticles. The glucose oxidase (GOx) is trapped in the microparticles due to the smaller mesh size of the network compared to the hydrodynamic radius of GOx, and therefore, does not diffuse into the bulk media when the microparticles are re-suspended in water.

5.2.2 Photodegradable microparticle fabrication

The monomers used in fabrication of photodegradable cores were poly(ethylene glycol) di-photodegradable-acrylate (PEGdiPDA; M_n 4070), synthesized as described earlier [16,17] and poly(ethylene glycol) tetrathiol (PEG4SH; M_n 5000) synthesized as described earlier [18]. Photodegradable microparticles were prepared via inverse suspension polymerization, in which, PEGdiPDA was copolymerized with PEG4SH via base-catalyzed michael addition in an aqueous phase that was suspended in an organic phase as previously reported [24]. The organic phase comprised hexane (5 mL) containing Span 80 and Tween 80 (150 mg of a 3:1 ratio by weight respectively). The aqueous phase (0.25 mL) consisted of triethanolamine (300 mM) at pH 8.0 with PEGdiPDA (6.2 wt%),

PEG4SH (3.8 wt%) and glucose (0.1 M). The polymerization reaction was allowed to proceed overnight. After the polymerization was completed, the suspension was centrifuged (Eppendorf Centrifuge Model 5702) at 1000 rcf for 10 min, and the supernatant was decanted. The microparticles were then washed twice with hexanes and recovered with the same centrifugation conditions.

5.2.3 Interfacial polymerization and particle characterization

Formation of the shell by interfacial polymerization was accomplished by injecting the coating solution (2 ml) into microparticle suspension (50 μL). The aqueous coating solution consisted of $PEGDA_{575}$ (15 wt%), glucose (0.1 M) or glucose oxidase (3μM) depending on whether GOx or glucose is present in the microparticle respectively, iron (II) sulfate at the desired concentration, MES buffer pH 4.5 (10 mM) , and either rhodamine B acrylate (0.005 wt%) or yellow-green fluorescent particles (0.01 vol%). The ensuing interfacial polymerization was allowed to continue for the desired time after which an aqueous solution (5ml) containing TEMPO (6 mM) was added to arrest the polymerization. The supernatant was carefully removed and the remaining particles were resuspended in deionized water before characterization. The fluorescence images of the coated particles were obtained by confocal microscopy using a Zeiss Pascal LSM 5 confocal microscope. The gels were excited with a 488 nm argon ion laser (543 nm helium neon laser) and fluorescence was monitored from 492-557 nm (547-680 nm).

5.3 Results and discussion

5.3.1 Reaction engineering at the interface

The spatial organization of the initiating components can be achieved in two ways as represented in **Figures 1a** and **1b** that differ in the initial location of the initiating

components, namely glucose or glucose oxidase, prior to interfacial polymerization. The difference in the location of the enzyme and glucose has significant implications in the ability to control the thickness and properties of the shell, the interpenetrating layer, and the immersion time required to accomplish shell formation with minimal bulk polymerization. These are discussed in the following sections.

5.3.2 GOx is located in the core and glucose in the bulk solution

In this design, glucose oxidase (GOx) is incorporated in the core precursor solution while glucose, Fe^{2+}, and the monomer, poly (ethylene glycol) diacrylate (MW 575) are included in the immersion phase (**Figure 1a**). Glucose oxidase is a bulky molecule (hydrodynamic radius, r_h ~43 Å) compared to the size of glucose (r_h ~ 3.5 Å). Therefore, GOx is effectively confined within the core on account of the smaller mesh size (<20 Å) of the polyacrylamide network, but glucose in the surrounding phase can diffuse into the core to initiate the reaction that generates hydrogen peroxide (H_2O_2). Interfacial polymerization occurs when the generated H_2O_2, whose locus of formation is always within the core, diffuses to the interface of the dynamically densifying shell and the surrounding media to react with the surrounding Fe^{2+} and generate hydroxyl radicals. This interplay of reaction behavior and the diffusion process results in shell growth in a self-limiting manner. The self-limiting growth results from H_2O_2, generated with the core, diffusing to the moving interface between the shell and the bulk monomer solution. In order to sustain shell growth, H_2O_2 must diffuse through the shell layer while avoiding reaction with Fe^{2+} that is diffusing into the shell to generate radicals at the shell-bulk interface.[21,22] Otherwise, hydroxyl radical production occurs within the shell instead of near the desired interface, thereby contributing negligibly to shell growth. The resistance

to diffusion of H_2O_2 increases with thickness and therefore decreases the likelihood of

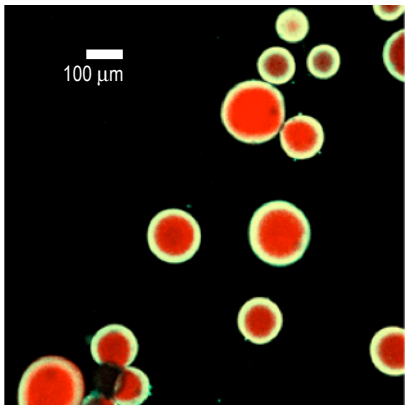

Figure 5.2: Representative fluorescence image of coated hydrogel cores when glucose oxidase is incorporated in the core. The concentration of GOx in the precursor solution used to fabricate the core was 14mg/ml. The condition used for coating solution was 0.1M Glucose, 12.5 mM Fe^{2+}, 0.01 vol% Yellow-green nanoparticles, 10 mM MES Buffer pH 4.5, 15wt% $PEGDA_{575}$. Immersion time was 4 min.

mass transport of initiating species into the bulk media. This approach results in minimal bulk polymerization when the microparticles are immersed in the coating solution for relatively long time periods. **Figure 2** shows a representative fluorescent image of core-shell microparticles fabricated using this design at the end of 4 minutes of immersion. Another implication of hydrogen peroxide being generated in the core is that the polymerization of monomer diffusing into the core forms an interpenetrating network. This results because of persistent generation of hydroxyl radicals within the core due to the redox reaction between H_2O_2 and Fe^{2+} that has diffused into the core.

Figure 3a provides evidence to support this hypothesis. In these experiments the core-shell particles were fabricated at two conditions, which differ in the fluorescent molecules that are used to render the shell fluorescent. In the first condition rhodamine B acrylate was used as the co-monomer for the shell formulation; thereby allowing diffusion of the dye into the core enabled by the smaller size of this dye relative to the network mesh size. In the second condition fluorescent nanoparticles, more than an order of magnitude larger than the mesh size of the core, were incorporated in the shell

formulation. Therefore, when rhodamine B acrylate is used, both the portion of the shell outside the core as well as the interpenetrating layer formed are observed in the fluorescent images. However, the interpenetrating layer is not observed when fluorescent nanoparticles are used; thereby enabling calculation of the interpenetrating layer thickness. Ensemble averaged thicknesses of the interpenetrating layer indicated that the thickness of the layer was ~ 12 µm (Figure 3c).

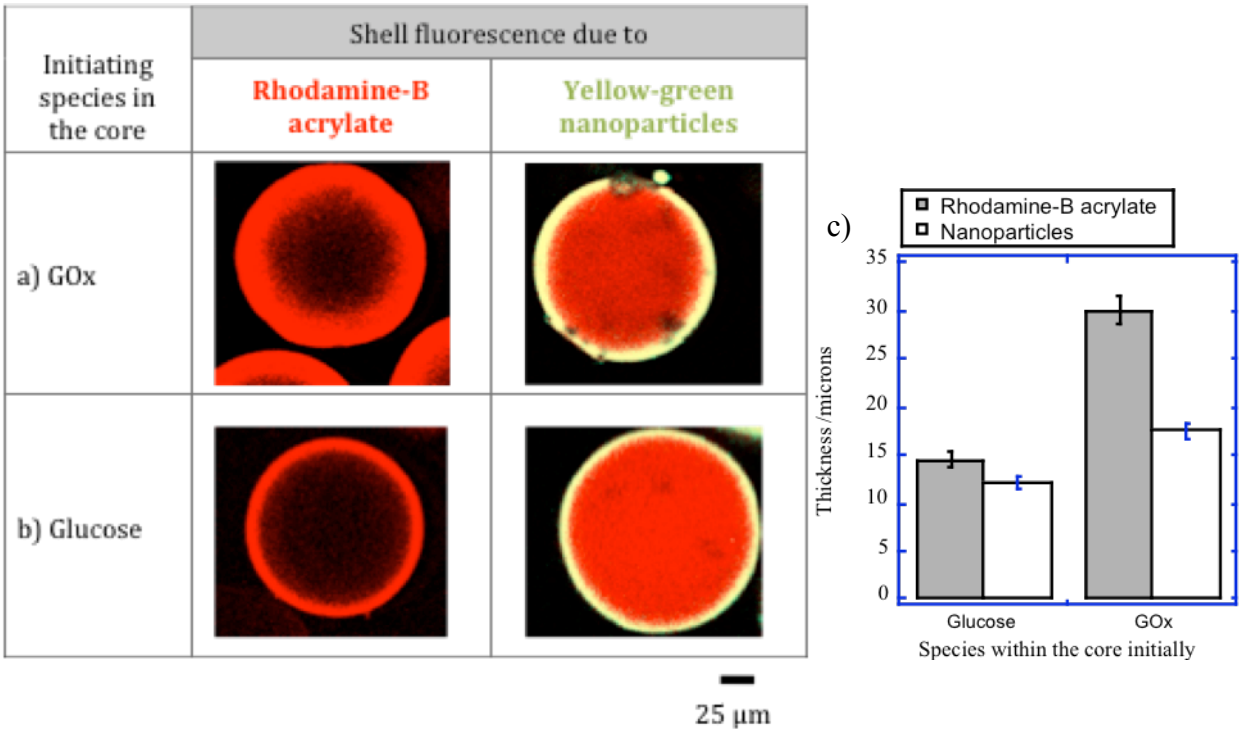

Figure 5.3: Representative fluorescence images of coated hydrogel cores when Rhodamine-B acrylate was used to render the shell fluorescent (left) and yellow-green nanoparticles were incorporated in the shell to render the shell fluorescent (right). The initiating species incorporated in the core prior to interfacial polymerization was a) GOx. The conditions used for the coating solution were 0.1M glucose , 45 mM Fe^2, 0.01 vol% Yellow-green nanoparticles (right), 0.005 wt% rhodamine-B acrylate (left), 10 mM MES Buffer pH 4.5, 15wt% $PEGDA_{575}$. Immersion time was 4 min. b) Glucose is within the core. The conditions used for the coating solution were 3µM GOx, 45 mM Fe^2, 0.01 vol% Yellow-green nanoparticles (right), 0.005 wt% rhodamine-B acrylate (left), 10 mM MES Buffer pH 4.5, 15wt% $PEGDA_{575}$. Immersion time was 30 s . The thickness of the shell in each of the cases is shown in (c).

5.3.3 Glucose is located in the core and GOx in the bulk solution.

In this design, the initial locations of glucose and GOx are interchanged such that glucose is located in the core and GOx in the bulk solution. The GOx cannot diffuse from the bulk media into the core, whereas glucose can rapidly diffuse into the bulk media to initiate the generation of hydrogen peroxide. This confinement of H_2O_2 generation into the bulk decreases the distances that H_2O_2 needs to diffuse to reach the non-stationary

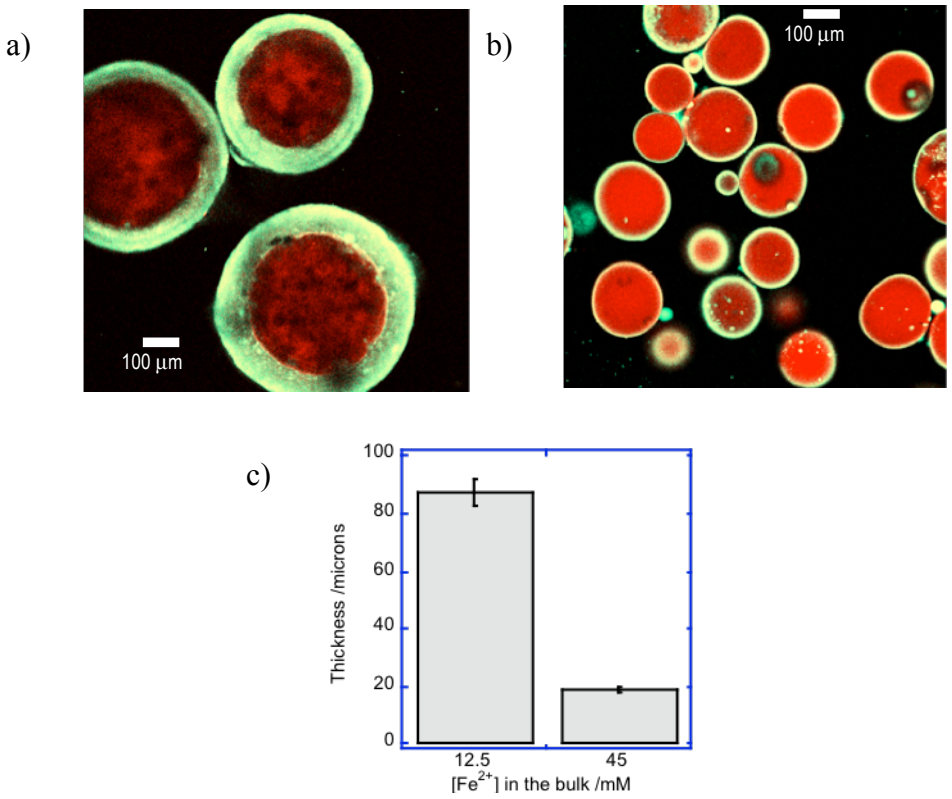

Figure 5.4: Representative fluorescence images of the coated hydrogel cores when glucose is incorporated in the core for two concentrations of iron (Fe^{2+}) in the precursor solution used to form the shell a) 12.5 mM b) 45 mM. Higher iron concentrations limit the shell's growth resulting in a thinner shell c) Glucose concentration in the precursor solution used to fabricate the core was 0.1 M. The conditions used for the coating solution were 3 µM GOx, 0.01 vol% yellow-green nanoparticles, 10 mM MES buffer pH = 4.5, 15 wt% $PEGDA_{575}$. Immersion time is 30 seconds.

interface and initiate polymerization. The rapid diffusion of glucose into the bulk media and the resulting delocalization of the initiation reaction into the bulk solution enable the formation of thicker shells. **Figure 4a** shows a representative fluorescence image of the coated microparticles for the same bulk iron concentration used earlier (**Figure 3**), but at the end of 30 seconds. The average thickness of the shell was calculated to be ~90 μm (**Figure 4c**). The significantly lower polymerization time employed decreases the likelihood of bulk polymerization resulting from the rapid diffusion of glucose into the bulk media. The polymerization was stopped after 30 seconds by injecting a high concentration of TEMPO, a powerful radical inhibitor, into the reacting mixture. Further, the thickness of the shell can be controlled by changing the bulk iron concentration, which acts to influence the degree of confinement of the initiation reaction. Previous work on the enzyme-mediated redox reaction mechanism has established that using higher concentrations of Fe^{2+} promotes localized polymerization by confining the redox reaction between H_2O_2 and Fe^{2+} to the interface as a result of enabling a highly reactive surrounding phase.[21,22] Therefore, the concentration of iron was increased by a factor of ~4 to enable inhibition in the bulk. However, the higher initiation rates adjacent to the interface, compared to the bulk media, allows interfacial polymerization to occur. This strategy resulted in the formation of shells ~20 μm thick after 30 seconds of immersion as shown in **Figure 4b** and quantified in **Figure 4c**. Additionally, this design approach eliminated the formation of any observable interpenetrating networks (**Figure 3b**). Since the locus of hydrogen peroxide generation is within the bulk media, the likelihood of radicals being generated within the core is decreased, resulting in negligible

polymerization of the monomer that diffuses into the core. The result is a distinct core and shell polymer network.

5.3.4 Self-supporting shells: Formation of core-shell particles with liquid cores

The ability of the shell to be self-supporting in the absence of a core with a well-defined geometry is demonstrated by using cores that possess photodegradable groups in the polymer network, as templates for shell formation. Irreversible, photoinduced cleavage of *o*-nitrobenzyl ether (NBE) moieties in the PEGdiPDA structure, [24] initiates the transition from a gelled state to a solution state and hence the formation of a liquid core (**Figure 5**). To form a shell around the photodegradable cores, glucose was incorporated into the core and glucose oxidase in the bulk coating formulation prior to

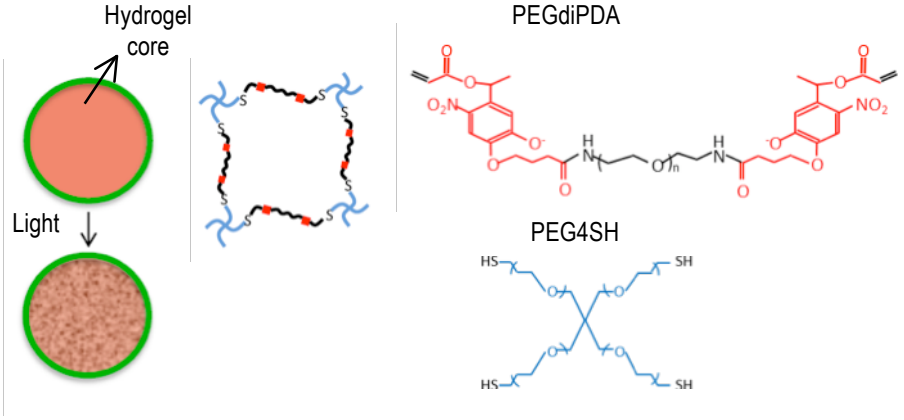

Figure 5.5: Schematic depicting photodegradation of the coated hydrogel core that possesses degradable groups in the polymer network. The core is fabricated by copolymerization of poly(ethylene glycol) di-photodegradable-acrylate (PEGdiPDA) and poly(ethylene glycol) tetrathiol (PEG4SH). The *o*-nitrobenzyl ether moieties (NBE) in the PEGdiPDA structure absorbs strongly at 365 nm, and the resulting irreversible cleavage causes degradation of the crosslinks and, ultimately, the formation a liquid core.

conducting interfacial polymerization. This strategy was chosen to increase the likelihood of formation of a distinct shell, thereby conserving the photodegradable properties of the hydrogel core. The fluorescent images of a core-shell particle prior to

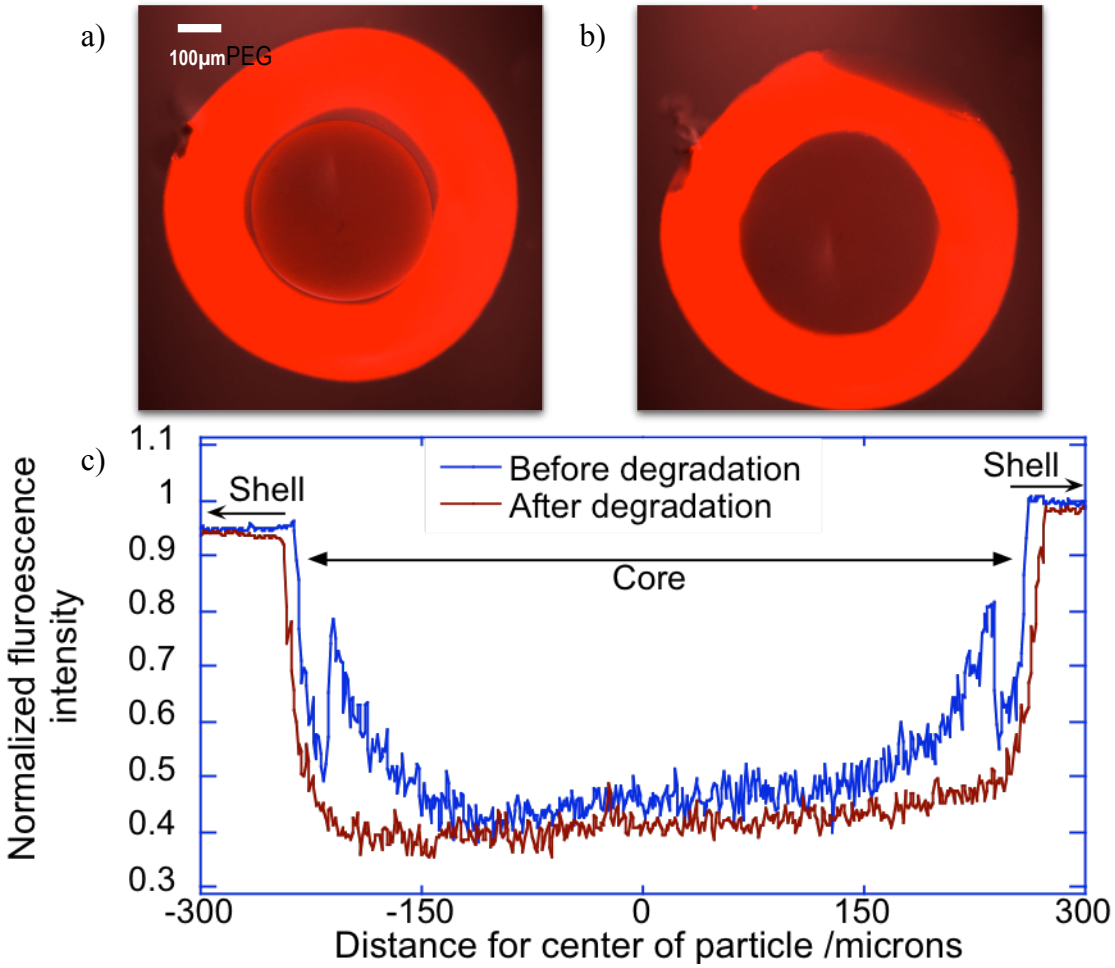

Figure 5.6: Representative fluorescence images of coated degradable hydrogel cores before (a) and after (b) exposing to light. The concentration of glucose in the precursor solution used to fabricate the core was 0.1 M. The conditions used for forming the shell were 3 µM GOx , 45 mM Fe^{2+}, 0.005 wt% rhodamine-B acrylate, 10 mM MES Buffer pH 4.5 and 15wt% $PEGDA_{575}$. Immersion time was 30s. The core was exposed to light of wavelength 365nm at an intensity of 20 mW/cm^2 for 2 minutes. The normalized fluorescence intensity as a function of distance from the center of the particle before and after degradation (c). The degradation of the core is indicated by the drop in fluorescence intensity at the core-shell interface.

and after photodegradation are shown in **Figures 6a** and **6b**, respectively. Before degradation (**Figure 6a**), the core can be distinctly seen, due to the higher background fluorescence resulting from the autofluorescence of photodegradable moieties, most notably of the interface of the core microsphere. The quantitative variation of fluorescence intensity, shown in **Figure 6c** highlights this idea. However, upon exposure to light, the photodegradable groups are cleaved and the resulting transition of the core from a crosslinked polymer to a degraded state (**Figure 6b**) decreased the fluorescence intensity (**Figure 6c**).

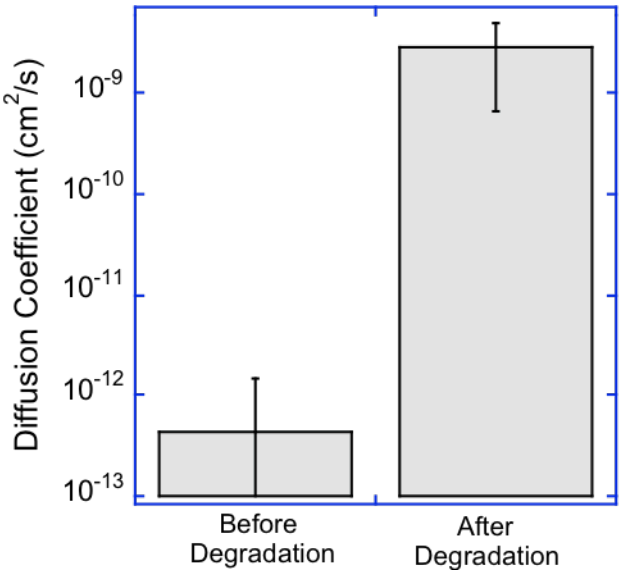

Figure 5.7: Average diffusion coefficient of fluorescent beads, 2µm in diameter, incorporated into the core, prior to (left) and after photodegradation (right). These values were calculated by tracking the 2D trajectory of the beads before and after photodegradation and using a random walk model to correlate the mean square displacement of the beads to the diffusion coefficient.

To provide direct evidence of the formation of a liquid core, the mass transport properties of the core were monitored before and after degradation. Monitoring was accomplished by incorporating fluorescent beads (2 μm in diameter) into the core formulation and using single particle tracking methodology[20] to correlate the trajectories of the beads to the diffusion coefficient in the core. **Figure 7** compares the average diffusion coefficient of the beads in the core before and after photodegradation. The diffusion coefficient before degradation is statistically insignificant from zero whereas the value after photodegradation takes a finite value indicating the significantly increased mobility of the beads resulting from the photodegradation-induced gel to sol transition of the core. Besides demonstrating the ability to form free-standing structures, this investigation also highlights the potential towards constructing photo-responsive controlled release architectures. The rapid light-induced production of cleavage products is subsequently released into the surrounding environment at a rate that is determined by the properties of the shell.

5.4 Conclusions

Reaction engineering of the glucose oxidase-mediated redox reaction to enable core-shell formation by interfacial polymerization was described. The initial sequestration of glucose or glucose oxidase in the initial core is an important factor that controls the interfacial polymerization rate and the ultimate structure of the core-shell particle. Incorporating GOx in the core precursor solution and the remainder of the complementary initiating species in the bulk media prior to polymerization results in thinner shells and self-limiting shell growth. This is because the locus of hydrogen peroxide generation is always within the confines of the core resulting in a decreased

likelihood of H_2O_2 diffusion to the non-stationary interface with increasing thickness to sustain shell growth. The presence of GOx in the core also leads to less distinct core and shell phases with a greater degree of interpenetration of the two caused by the necessity for glucose to diffuse into the core to form hydrogen peroxide. Switching the initial locations of glucose and GOx leads to rapid formation of thicker shells due to the delocalization of the hydrogen peroxide generation into the bulk solution resulting from diffusion of glucose into the bulk media. This switch also results in distinct core and shell phases as a result of negligible radical generation within the confines of the core. The polymeric shell formed by this technique is self-supporting when the initially solid core is photodegraded to form a liquid.

5.5 Acknowledgements

This work has been supported by the National Institutes of Health (Grant R21 EB 012188) and the National Science Foundation (DMR 1006711).

5.6 References

[1] R. Langer, Acc. Chem. Res. **2000**, 33, 94-101.

[2] F. Caruso, Adv. Mater. **2001**, 13, 11-22.

[3] S. Freiberg, X. X. Zhu, Int. J. Pharm. **2004**, 282, 1-18.

[4] Y. F. Zhu, J. L. Shi, W. H. Shen, X. P. Dong, J. W. Feng, M. L. Ruan, Y. S. Li, Angew. Chem., Int. Ed. **2005**, 44, 5083-5087.

[5] D. B. Shenoy, A. A. Antipov, G. B. Sukhorukov, H. Mohwald, Biomacromolecules **2003**, 4, 265-272.

[6] H. Baumler, R. Georgieva, Biomacromolecules **2010**, 11, 1480-1487.

[7] H. G. Zhu, M. J. McShane, Langmuir **2005**, 21, 424-430.

[8] S. R. White, N. R. Sottos, P. H. Geubelle, J. S. Moore, M. R. Kessler, S. R. Sriram, E. N. Brown, S. Viswanathan, Nature **2001**, 409, 794-797.

[9] W. Chen, T. J. McCarthy, Macromolecules **1997**, 30, 78-86.

[10] S. S. H. Tsai, J. S. Wexler, J. D. Wan, H. A. Stone, Appl. Phys. Lett. **2011**, 99, 153509

[11] I. Cohen, H. Li, J. L. Hougland, M. Mrksich, S. R. Nagel, Science **2001**, 292, 265-267.

[12] C. Scott, D. Wu, C.-C. Ho, C. C. Co, J. Am. Chem. Soc. **2005**, 127, 4160-4161.

[13] H. N. Yow, A. F. Routh, Soft Matter **2006**, 2, 940-949.

[14] Y. Luo, H. Gu, Macromol. Rapid Commun. **2006**, 27, 21-25.

[15] L. M. Johnson, C. A. DeForest, A. Pendurti, K. S. Anseth, C. N. Bowman, ACS Appl. Mater. Interfaces **2010**, 2, 1963-1972.

[16] A. M. Kloxin, M. W. Tibbitt, K. S. Anseth, Nat. Protoc. **2010**, 5, 1867-1887.

[17] A. M. Kloxin, A. M. Kasko, C. N. Salinas, K. S. Anseth, Science **2009**, 324, 59-63.

[18] B. D. Fairbanks, S. P. Singh, C. N. Bowman, K. S. Anseth, Macromolecules **2011**, 44, 2444-2450.

[19] L. M. Johnson, B. D. Fairbanks, K. S. Anseth, C. N. Bowman, Biomacromolecules **2009**, 10, 3114-3121.

[20] H. Qian, M. P. Sheetz, E. L. Elson, Biophys. J. **1991**, 60, 910-921.

[21] R. Shenoy, C. N. Bowman, *Biomaterials* **2012**, *33*, 6909-6914.

[22] R. Shenoy, C. N. Bowman, Macromol. Theory Simul. (in press), DOI : 10.1002/mats.201200062

[23] P. S. Hume, C. N. Bowman, K. S. Anseth, Biomaterials **2011**, 32, 6204-6212

[24] M. W. Tibbitt, B. W. Han, A. M. Kloxin, K. S. Anseth, J. Biomed. Mater. Res., Part A **2012,** 100A, 1647-1654.

Chapter 6

Oxygen inhibition suppression using a singlet oxygen sensitizer

Here, we report a novel method of suppressing oxygen inhibition while simultaneously performing photopolymerizations with a visible light photoinitiator. A singlet oxygen sensitizer, Zinc tetra (t-butyl) phthalocyanine (Znttp), is used to excite oxygen at a rate greatly exceeding the initiation rate to promote the reaction of ground state oxygen preferentially with Znttp. The inhibition times of such polymerizations decreased from 280 seconds for polymerization without Znttp to 40 seconds for Znttp-mediated polymerizations in air. Thermal polymerization studies shows that the suppression mechanism happens only when the formulation is exposed to visible light that is absorbed by Znttp. The excited state of Znttp resulting from light absorption transfers its energy to oxygen, consequently exciting it to the singlet state. Due to the presence of deactivating mechanisms, the singlet oxygen decays back to its ground state and a quasi-steady state is established between the ground state and singlet state oxygen species. Due to the high rate of light absorption by Znttp as compared to the photoinitiator, the singlet state oxygen becomes the predominant oxygen species, thereby resulting in significant suppression of radical scavenging by ground state oxygen. Experimental results are corroborated with a mathematical model to describe the variation in inhibition times with changing Znttp concentration. The value of the characteristic lifetime of singlet oxygen calculated from the model is 1 millisecond, consistent with that which is reported in the literature for several organic monomers. Finally, optimal initiating conditions are designed to suppress oxygen inhibition while achieving high conversions in the most challenging condition of a sample equilibrated

with a pure oxygen atmosphere.

6.1 Introduction

Oxygen inhibition is a commonly encountered issue while performing radical polymerizations. Many applications based on photopolymerizations namely paints, coatings, adhesives, photolithography and dental resins are severely affected by oxygen inhibition [1,2,3,4]. In particular, surface initiated polymerizations, performed with extremely low concentrations of surface-bound initiator [5,6,7,8], are highly susceptible to oxygen inhibition. Without an inert gas purge such systems are often devoid of any significant polymerization. Oxygen limits radical polymerizations by acting as a powerful radical scavenger, consuming radicals on a one radical to one oxygen molecule basis to form peroxy radicals that are practically incapable of continuing the polymerization, particularly in the absence of any chain transfer agents such as thiols or amines [9]. The final result is the presence of an induction period during which little polymerization occurs, and the initiating radicals consume oxygen. If diffusion of oxygen from the atmosphere or from non-initiating regions of the sample is more rapid than initiation, the inhibition time becomes effectively infinite and polymerization never proceeds to any significant extent. Otherwise, once the oxygen concentration drops to or below on the order of 10^{-6} M, the polymerization reaction begins in earnest [10].

There have been a number of creative approaches to overcoming the problems of inhibition resulting from dissolved oxygen. Use of amines [11,12], thiols [13,14], singlet oxygen scavengers [15,16,17], Organoboranes [18], Organosilanes [19] and reactive curing conditions [20] are some of the chemical means that have been employed to tackle

this issue. Physical means comprise degassing the monomer formulation prior to polymerization or use of an inert gas purge chamber to perform polymerizations in an oxygen free environment. In all of these approaches the focus has been either driving the oxygen out of the system physically, consuming the oxygen prior to polymerization or scavenging peroxy radicals and transforming them into a more potent polymerization-

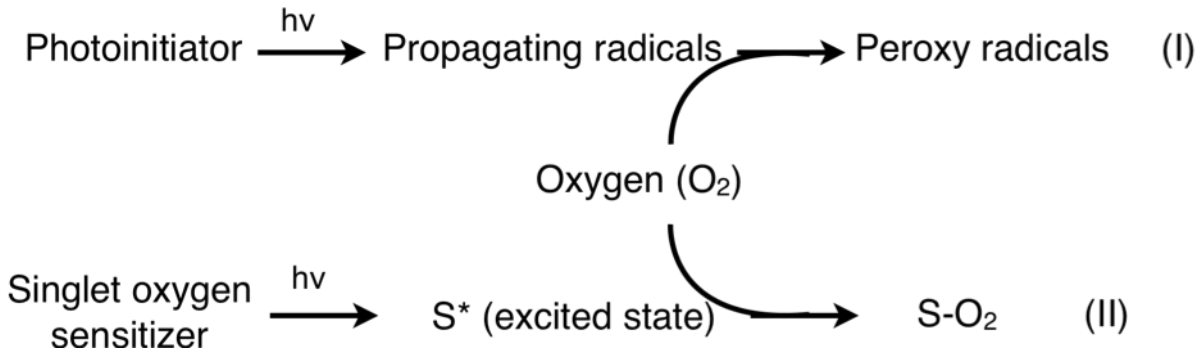

Scheme 6.1: Propagating radicals are consumed in pathway I by oxygen to form weakly initiating peroxy radicals. Oxygen is consumed in a competitive pathway II via photoexcitation of a singlet oxygen sensitizer to promote the elimination or reduction of the inhibition time.

capable radical.

Here, this work presents a scheme through which an alternative pathway for oxygen consumption is provided, thereby circumventing the reaction between oxygen and initiating radicals. This approach is illustrated in Scheme 1 where the competitive reaction pathway involving reaction of oxygen with the excited state singlet oxygen trapper occurs in parallel with the reaction of oxygen to form the peroxy radical that inhibits the polymerization. In the absence of the second parallel pathway, the rate of oxygen consumption by reaction with initiating radicals to form peroxy radicals is

equivalent to the slowest reaction (rate determining step) in the top reaction series, which is the initiation rate. By providing an alternative pathway for the reaction of oxygen that is much faster than the initiation rate, radical scavenging can be made negligible, and photoinitiator radicals are able to directly and efficiently initiate polymerization. It is precisely this technique that is employed in the present work to perform photopolymerizations in an oxygen rich environment.

Metallo-phthalocyanines (MPc) like Zinc and Aluminum phthalocyanines are used commonly in photodynamic tumor therapy because of their ability to produce reactive oxygen species (ROS) with a high quantum yield upon photoactivation [21,22,23]. Following photon absorption, the MPcs transition to their excited singlet state, which undergoes intersystem crossing to form the excited triplet state. Because the transition from the excited triplet state to the ground state is a spin forbidden process, the triplet lifetime is sufficient to enable energy transfer to oxygen resulting in excited singlet oxygen, also called singlet oxygen [24]. In contrast to ground state triplet oxygen, which by virtue of its biradical nature very efficiently reacts with radicals to form peroxy radicals, singlet oxygen is diamagnetic and not highly reactive with initiating or propagating radicals. Singlet state oxygen has a lifetime of about a millisecond in most acrylic monomers and decays back to its ground state [17]. Znttp has also been used previously as a photosensitizer of oxygen to increase the reactivity of oxygen towards reducing species like 9,10 Dimethylanthracene, which acts as a trapper for the singlet oxygen [17]. This technique was successfully used to consume oxygen prior to polymerization as a means for eliminating any oxygen inhibition period. The focus of the work here is to show that suppression of oxygen inhibition can be enabled simply by

direct photosensitization of oxygen. The fundamental mechanism of such a kinetic scheme is also elucidated.

6.2 Experimental

6.2.1 Materials

Poly(ethylene glycol) diacrylate (PEGDA) (Mn=575), 1-vinyl-2-pyrrolidinone (VP), N-Methyldiethanolamine (MDEA), Zinc 2,9,16,23-tetra-*tert*-butyl-29*H*,31*H*-phthalocyanine (Znttp), Zinc 1, 2, 3, 4, 8, 9, 10, 11, 15,16,17,18,22,23,24,25 -hexadecafluoro-29*H*,31*H*-phthalocyanine (ZnFPc), Zinc 1,4,8,11,15,18,22,25-octabutoxy-29*H*,31*H*-phthalocyanine (ZnoBPc), Aluminum phthalocyanine hydroxide (AlPcOH), 4-Hydroxy-2,2,6,6-tetramethylpiperidinyloxy (TEMPO) 2,2'-Azobis(2-methylpropionitrile) (AIBN), Riboflavin and Camphorquinone were obtained from Sigma Aldrich. PEGDA was purified twice using columns from Scientific Polymer Products that remove hydroquinone monomethyl ether (MEHQ). Irgacure-7

84 was purchased from CIBA.

6.2.2 Polymerizations

PEGDA was used as the monomer for all experiments. Small amounts of VP was also used to increase the mobility of the propagating radical as a result of the smaller size of VP while MDEA was used as the co-initiator in type II initiated systems. A Nicolet Magna-IR 760 E.S.P infrared spectrometer adapted with a horizontal sample holder was used to monitor polymerizations in real time tracking the 4465-4530 cm^{-1} peak . C=C conversion was calculated by measuring *in situ* changes in this peak area. Sample chambers were prepared using binder clips to clamp two glass slides on either side of a 100-micron thick sheet lining two edges. Where purging was performed, it was carried out by bubbling argon/oxygen through the monomer formulation before polymerization and transferred to the sample chamber quickly to prevent equilibration with the surroundings. Visible light irradiation of eosin was achieved with an in-house internal bandpass filter (350nm – 650 nm) and an external 480 nm longpass filter (Edmund optics) positioned at the end of a light guide and a collimating lens. A similar light

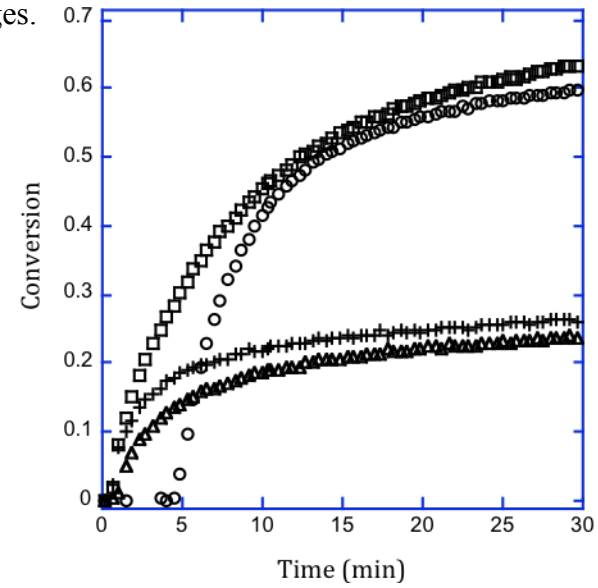

Figure 6.1: Conversion profiles for bulk polymerization of Poly(ethylene glycol) diacrylate (PEGDA) for various conditions: Addition of Znttp with(+) and without (Δ) argon purging, No Znttp added with ( ) and without (O) argon purging. The monomer formulation used was 1.8 M PEGDA, 0.23 M MDEA, 35 mM VP 0.87 µM Eosin, 2.9 x 10^{-4} M Znttp. Light Intensity was 75 mW/cm^2 of the wavelength range 480-650 nm

setup was used for irradiation of camphorquinone, Riboflavin and Irgacure-784, except that the internal filter was a 400-500 nm bandpass filter (Exfo). Light Intensities were measured by an International Light radiometer. Thermal polymerizations were initiated with AIBN at 60 °C.

6.3 Results and Discussion

6.3.1 Bulk polymerization studies

Eosin-initiated photopolymerizations were performed in laminated bulk samples both in purged and unpurged formulations both with and without the Znttp. The inhibition times for different scenarios were compared, and the double bond conversion as a function of the irradiation time for these various experiments is shown in Figure 1. It is seen that when dissolved oxygen is present in the monomer formulations which are not purged with argon, an inhibition time of

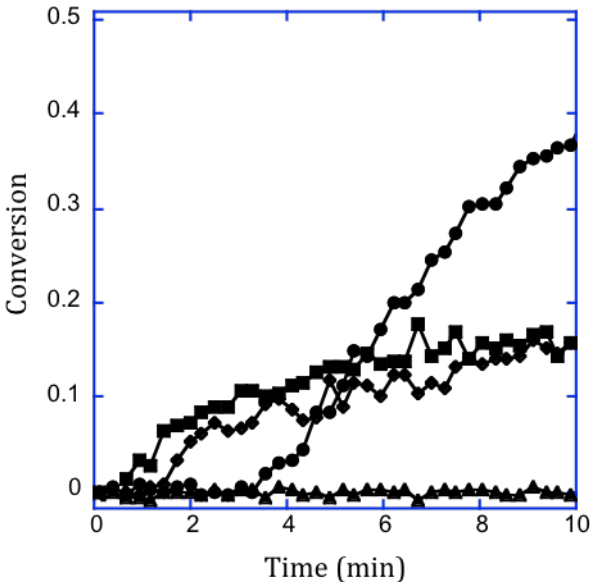

Figure 6.2: Behavior of Znttp mediated polymerization of PEGDA purged with pure oxygen to increase the dissolved concentration. The conditions are as follows: In the presence of Znttp with ( ) ◇ and without (□) an oxygen purge, No Znttp present with (Δ) and without (O) oxygen purge. The monomer formulation used was: 1.8M PEGDA, 0.23M Mdea, 35mM Vp, 0.87 µM Eosin, 2.9 x 10^{-4}M Znttp, Light intensity was 75 mW/cm^2 in the wavelength range 480-650 nm

approximately 280 seconds is seen in the sample without any Znttp. However, when Znttp is present in the monomer formulation the inhibition time is significantly decreased to approximately 40 seconds (Fig. 1). Bulk polymerization with only Znttp in the monomer formulation and no eosin (not shown) did not exhibit any polymerization on these timescales, indicating that Znttp and its excited state products do not initiate polymerization under these conditions. Therefore, the reduction in inhibition time has other origins. When oxygen was eliminated through purging and photopolymerizations were initiated in the presence of Znttp, the resulting conversion profile is very similar to the conversion profile of Znttp in the presence of oxygen. This behavior indicated that Znttp acts almost exclusively to suppress oxygen inhibition. In addition to its beneficial effects on overcoming oxygen inhibition, it is also observed from the results presented in Figure 1 that Znttp affects the

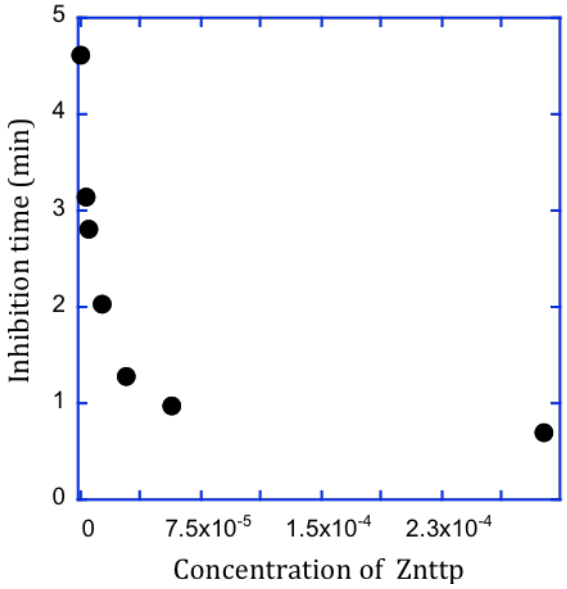

Figure 6.3: Effect of varying the concentration of Znttp on the bulk polymerization of PEGDA. Plotted is the inhibition time of polymerization in minuted (y axis) vs. Znttp added in Molar units (x axis). The monomer formulation used was: 1.8M PEGDA, 0.23M MDEA, 35mM VP, 0.87 μM Eosin, 2.9 x 10^{-4}M Znttp, Light intensity was 75 mW/cm^2 in the wavelength range 480-650 nm

continuing polymerization rate and particularly the maximum conversion. Comparing the photopolymerization conversion profiles for samples with and without Znttp in purged conditions (Fig. 1), it is observed that the initial polymerization rates are similar but at higher conversion the rate decreases for the Znttp formulation, likely due to the participation of Znttp in promoting radical termination. The effects of Znttp in oxygen rich conditions were also evaluated and the results are presented in Figure 2 where the conversion profiles are presented for the control and Znttp-containing formulations in formulations equilibrated with oxygen rich environments. Here, it is observed that oxygen purging results in complete inhibition of photopolymerization without Znttp. This result is significant because it accentuates the ability of Znttp to promote photopolymerization under conditions of excess oxygen compared to the photoinitiator where polymerization is otherwise infeasible to any extent.

To understand whether this ability to suppress inhibition is applicable to other inhibition mechanisms through one of a variety of possible alternative mechanisms, TEMPO, a known radical scavenger was added as an inhibitor to the monomer formulation. Table 1 includes the inhibition times for photopolymerizations in the presence of TEMPO with varying Znttp concentration. Within error, the inhibition times in samples containing TEMPO (Table 1) are not different when compared to the significant reduction in inhibition times seen in formulations performed without TEMPO, but in the presence of oxygen (Figure 3). This clearly highlights the specific ability of Znttp in improving initiation in oxygen-inhibited photopolymerizations. However, the mechanism of this behavior is not well understood, and it is the intention of the following sections to address this topic.

Znttp Concentration (M)	Inhibition time (sec)
0	126 +/- 10
2.9×10^{-6}	129 +/- 4
2.9×10^{-5}	135 +/- 4
2.9×10^{-4}	114 +/- 10

Table 6.1: Inhibition times for different Znttp concentrations in the presence of TEMPO. The monomer formulation used was: 1.8M PEGDA, 0.23M MDEA, 35mM VP, 2.9μM Eosin, 130μM TEMPO, Light intensity was 75 mW/cm^2 in the wavelength range 480-650nm.

6.3.2 Role of Photoactivation

Znttp is a light-absorbing compound, and its absorption characteristics are well known. Figure 4 shows the absorption spectra of Znttp in the visible range. The incident light spans 480- 650 nm and even though the peak light absorption of Znttp does not fall in this range, the quanta of light absorbed are significant when incorporating high concentrations of Znttp, as used in many of the experiments performed. To ascertain the importance of light, thermally initiated polymerizations were performed with and without Znttp for both simultaneous irradiation conditions as well as unexposed conditions.

Figure 5 shows the polymerization kinetic profiles for these experiments. It is seen that in the unpurged conditions Znttp reduces the inhibition time only when the monomer formulation is exposed to light. This behavior confirms the hypothesis that light absorption by Znttp is necessary for overcoming the oxygen inhibition, even during thermal initiation. It can also be concluded that the effect on termination kinetics is a non-photoactivated oxygen independent mechanism as the reduction in the long-term polymerization kinetics and final conversion are observed whether there is simultaneous irradiation or not.

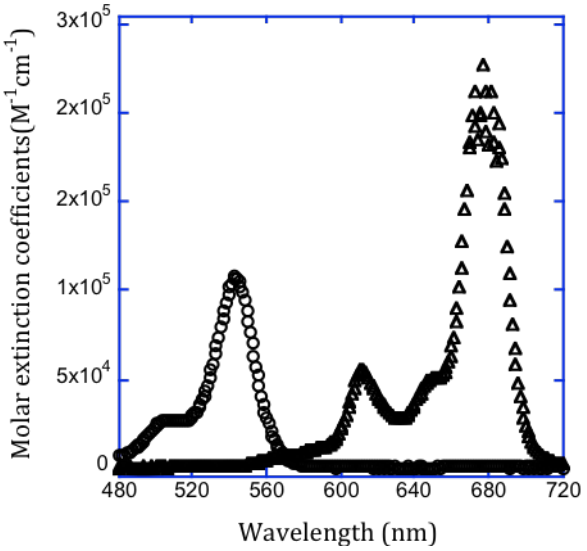

Figure 6.4: Absorption spectra of Znttp (Δ) and Eosin (O) in dimethyl sulfoxide.

6.3.3 Behavior with other photoinitiators and analogous phthalocyanines

Eosin-initiated photopolymerizations in the presence of Znttp are different from conventional photopolymerizations because of the presence of two light absorbing compounds. It is therefore possible that the Znttp could be sensitized by eosin to lead to the observed behavior. If eosin sensitization is the primary mode through which the Znttp acts, then photopolymerizations initiated by type I photoinitiators would not exhibit similar suppression since their excited state generally cleaves rapidly, making the sensitization event unlikely. As presented in

Figure 6, suppression of oxygen inhibition by the Znttp continues to be observed when

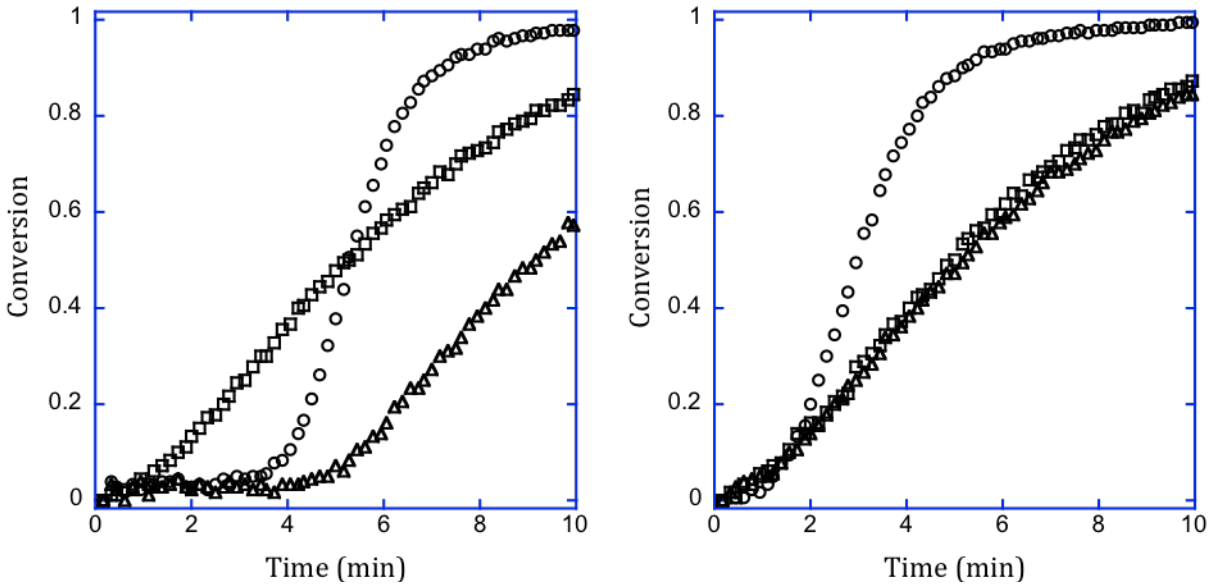

Figure 6.5: Thermal polymerization of PEGDA at 60 C with AIBN in unpurged (left) and purged (right) conditions. The conditions in both the conditions are as follows: No Znttp present with light exposure (O), in the presence of Znttp with ( ) and without (Δ) light exposure. The monomer formulation is 1.8M PEGDA, 0.23M MDEA, 35 mM VP, 0.85 wt% AIBN, 5.8 x 10^{-4} M Znttp, Light intensity was 75 mW/cm^2 in the wavelength range 480-650 nm

the initiator is a type I photoinitiator as it was with both thermal initiators and with type II photoinitiators. Also, as shown in Figure 7, Znttp is effective in suppressing the inhibition time in the presence of numerous other initiators as well, including riboflavin and camphorquinone. In all cases, as the Znttp concentration increases, the inhibition time decreases. It is common knowledge that metallo-phthalocyanines (MPc) like zinc and aluminum sensitize oxygen as a result of energy transfer from the triplet state of the MPc to ground state oxygen. Other Mpcs that have unfilled valence shells are poor oxygen sensitizers as a result of their very short triplet state. Figure 8 shows the conversion

profiles for zinc phthalocyanines

with different ring substituents as well as aluminum phthalocyanine for the same concentrations of MPc. It is evident that the inhibition times in each of the

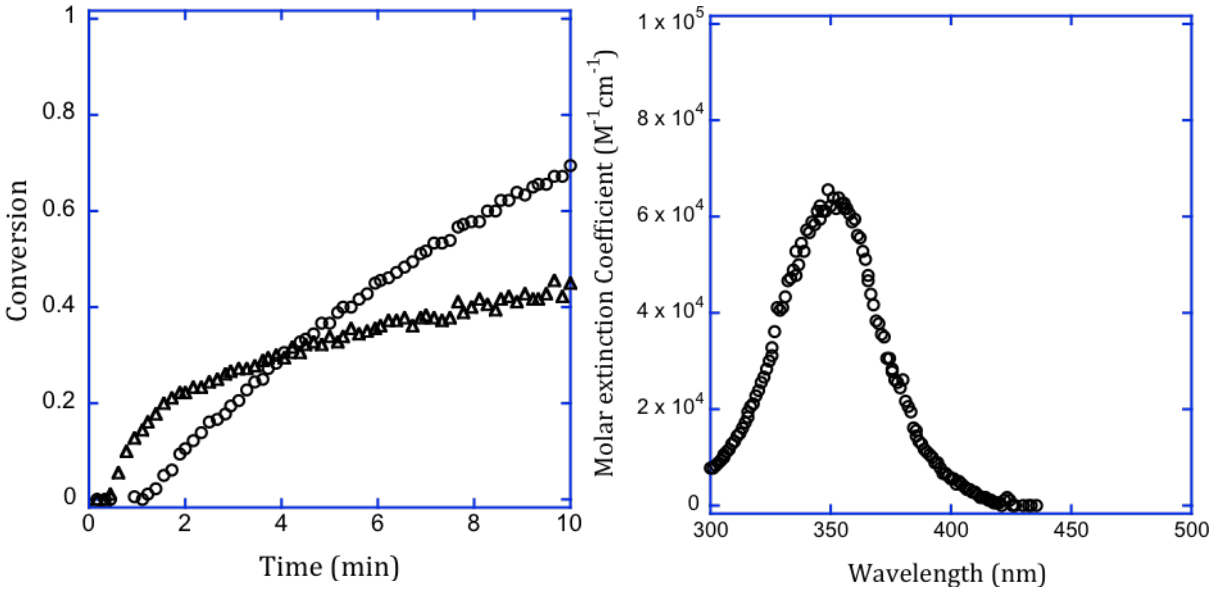

Figure 6.6: Bulk polymerization of PEGDA with (Δ) and without (O) the presence of Znttp. The photoinitiator used is Irgacure-784. The monomer formulation is 1.8 M PEGDA, 35 mM VP, 150 µM I-784, 2.9 x 10^{-4} M Znttp, Light intensity is 10 mW/cm^2 in the wavelength range 400-500 nm. Absorption spectra for Znttp (right) in the wavelength range 300-500 nm

phthalocyanines are significantly affected. In the Zinc-chelated Pcs, the magnitude of this change is observed to be in the same order as the total light absorbed by the Pc species (Table 2). Since varying the porphyrin ring substituents with the same metal center does not significantly affect the quantum yield of oxygen [25], it can be concluded that the rate of oxygen photosensitization by each of the Zinc-substituted phthalocyanines and hence the inhibition time follows the same order as their absorbances. Specifically the inhibition times for the Znttp, ZnOBPc and ZnFPc were found to be approximately 0.5, 1 and 2.9

minutes respectively while calculations

indicates that the total number of photons absorbed under these conditions is approximately 6 times greater for Znttp and 3 times greater for ZnOBPc compared to the

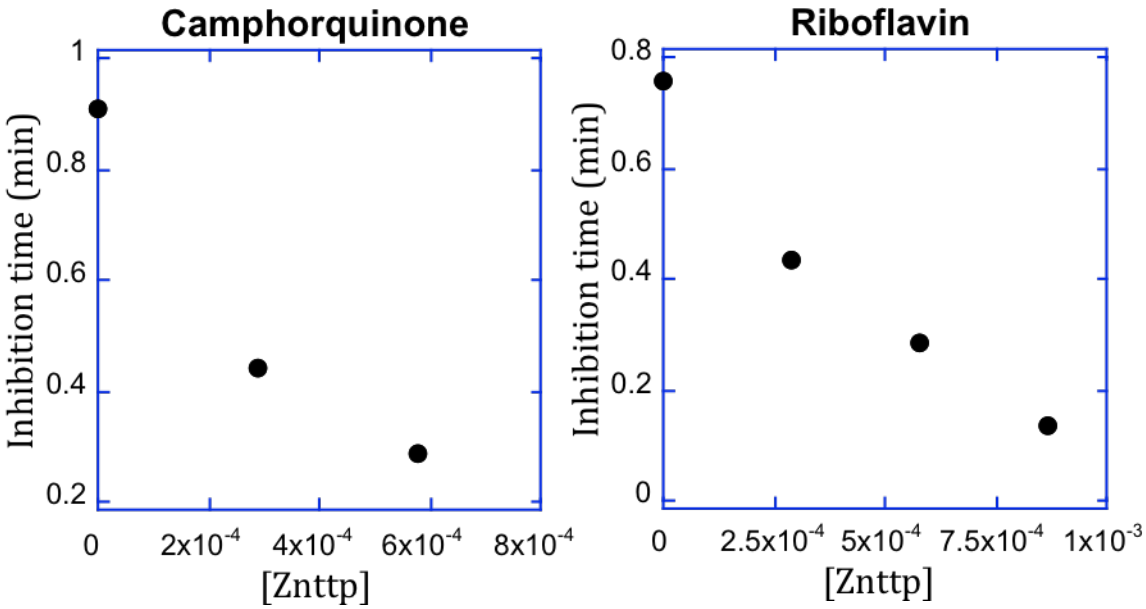

Figure 6.7: Effect of varying the concentration of Znttp on the inhibition time of polymerization of PEGDA for two different photoinitiators: Camphorquinone (left) at a concentration of 700µM and Riboflavin (right) at a concentration of 1.6 µM. The monomer formulation used is 1.8M PEGDA, 0.23M MDEA, 35mM VP, Light intensity is 50mW/cm^2 in the wavelength range 400-500 nm

ZnFPc. This latter calculation is based on the integration of light emission and absorption spectra of these three compounds in the wavelength range of interest. Distinctly, AlPcOH exhibits significantly enhanced termination which leads to lower final conversions.. Further, when incomplete valence shell metal chelated phthalocyanines like Cu^{2+}, Ni^{2+}, Fe^{2+}, Mn^{2+} were used (not shown), the suppression of oxygen inhibition was absent. This behavior further validates the idea that sensitization of oxygen is the primary mechanism

behind this remarkable suppression ability.

6.3.4 Kinetics of photoactivated suppression

To understand the mechanism of this photoactivated suppression, a quantitative study of the relationship between the inhibition time and the Znttp concentration was attempted. The simplified scheme of the proposed mechanism is shown in Scheme 2. Here, the phthalocyanine species (Pc) reacts with ground state oxygen upon absorption of light via its triplet state to form an excited complex (exciplex). This complex can return to the ground state through deactivating collisions or dissociate into singlet oxygen and ground state Pc. It is known that metal chelated phthalocyanines of transition metals are efficient quenchers of singlet oxygen [24,26]. Therefore, the singlet oxygen is either physically quenched by the phthalocyanine species, in this case Znttp, or loses energy to the surrounding media with a characteristic lifetime (= $1/k_d$). Overall, this mechanism results in a pseudo steady state between ground state and singlet state oxygen,

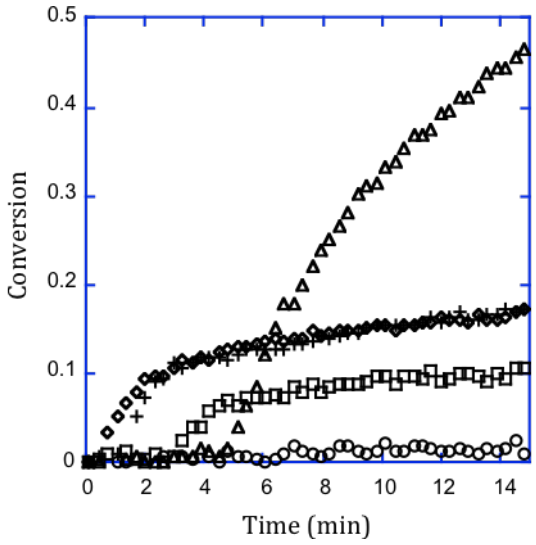

Figure 6.8: Conversion profiles for polymerization of PEGDA in the presence of different phthalocyanines - Znttp (◊), ZnoBPc (+), ZnFPc(□), AlPcOH (O) and without Phthalocyanine (Δ). The monomer formulation used was 1.8M PEGDA, 0.23M MDEA, 35mM VP, 0.87μM Eosin. 2.9 x 10^{-4}M Pc. Light Intensity used was 75mW/cm^2 of 480-650 nm light

and the position of this pseudo steady state is determined by the concentration of the phthalocyanine species, the photon absorption rate and several other factors.

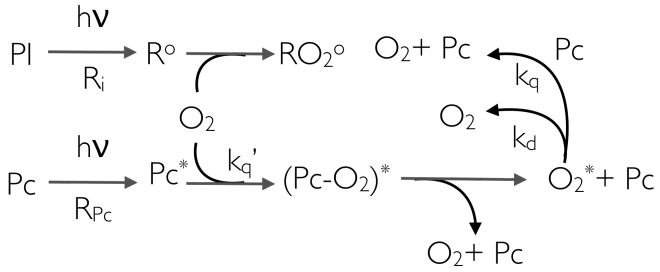

Scheme 2: Simplified photoactivated suppression of oxygen inhibition . Rpc is the rate of light absorption by the phthalocyanine and R_i is the rate of photoinitiation. kd (=1/τ) is the decay constant of singlet oxygen, kq is the quenching constant of singlet oxygen by the phthalocyanine and k_q' is the quenching constant of excited phthalocyanine by oxygen

The rate-determining step for sensitization of oxygen by Znttp is photon absorption by Znttp, since the oxygen quenching rate constant (k_q') is relatively large. The rate of photosensitization of oxygen by Znttp is calculated as,

$$R_{so} = \phi \sum_{\lambda} I_o(\lambda)\alpha(\lambda)C10^3 e^{-\alpha(\lambda)Ct} = A * C \qquad (1)$$

where R_{so} is the singlet oxygen photosensitization rate, I_o (λ) is the wavelength dependent incident light intensity, α(λ) is the wavelength dependent absorption coefficient, t is the thickness of sample , C is the concentration of Znttp and A is a constant. Based on previous work, the value for the singlet oxygen quantum yield is taken to be 0.4 and the oxygen quenching constant () by phthalocyanine species (kq') is 10^9 $M^{-1}s^{-1}$ [25].

The steady state is modeled by equating the generation rate of singlet oxygen, which is assumed to be the photosensitization rate of the singlet oxygen sensitizer, to the rate of disappearance of singlet oxygen as represented by the sum of the rates of singlet oxygen deactivation mechanisms mentioned earlier. The difference in inhibition time at a specific Znttp concentration, from its value at zero Znttp concentration provides a measure of the initial singlet oxygen concentration because it does not participate in radical scavenging. Although the concentration of singlet oxygen during the inhibition period changes as a result of small amounts of radical scavenging by oxygen, a single, approximate value is assumed to represent this concentration during the inhibition period. Based on this approach, the final form of the equations is given as,

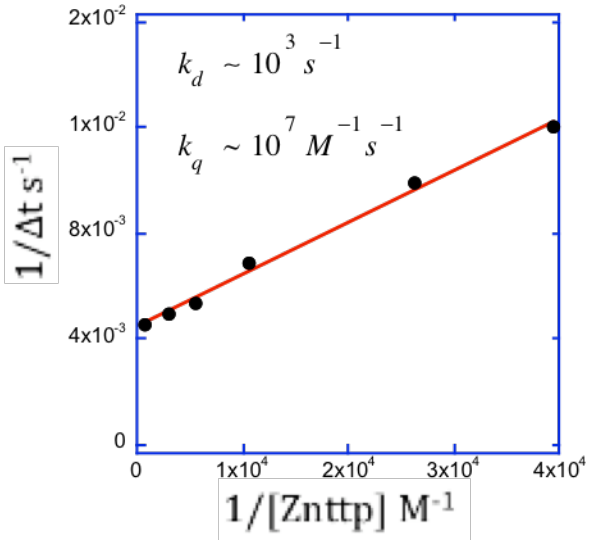

Figure 6.9: Validation of the mathematical representation of the proposed mechanism by fitting it with the experimental results. Δt represents the difference between the inhibition time for a specific concentration of Znttp and that at zero concentration of Znttp. kd and kq are calculated from the slope and intercept respectively

$$R_i \Delta t = [O_2^1]$$

$$\frac{1}{\Delta t} = \left(\frac{k_d R_i}{A} \right) \frac{1}{C} + \frac{k_q R_i}{A} \qquad (2)$$

where Δt is equal to the quantity, $t_{inh}(C=0)-t_{inh}(C)$, $[O_2^1]$ is the concentration of singlet oxygen. k_d is the singlet oxygen decay constant, k_q is the singlet oxygen deactivation constant and R_i is the photoinitiation rate. According to equation 2, if the inverse of the change in inhibition time is plotted against the inverse of the Znttp concentration, the resulting curve should be linear. Figure 9 shows that it is indeed the case. Moreover, the kinetic constants k_d and k_q are readily calculated from the slope and intercept. The calculated value of k_d corresponds to an oxygen excited state lifetime of approximately a millisecond, near that which is reported for oxygen in most organic liquids and monomers [17].

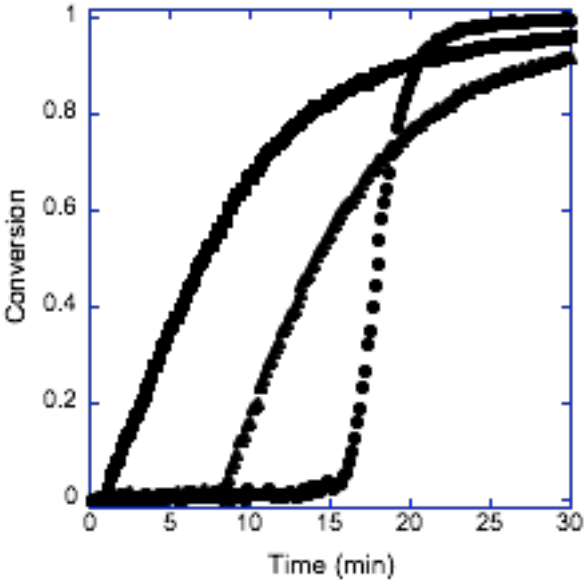

Figure 6.10: Conversion profiles for photopolymerization of PEGDA in oxygen saturated conditions: With Znttp and a single light source, 400-500 nm ( ), With Znttp and two light sources, 400-500 nm and 600-650 nm ( ), Without Znttp and two light sources, 400-500 nm and 600-650 nm (O). The monomer formulation used was 1.8M PEGDA, 0.23M MDEA, 35mM VP, 44 µM Eosin, 2.9 x 10^{-4} M Znttp. Light Intensity used was 7.5 mW/cm^2 of 400-500 nm light and 20 mW/cm^2 of 600-650 nm light. The monomer was purged with oxygen for 10 min prior to polymerization.

6.3.5 Optimization of curing conditions: Dual wavelength curing

In this section we demonstrate the capability of this technique to achieve high conversions and simultaneously suppress oxygen inhibition in highly inhibited environments. The primary effort was focused on making the undesirable termination reaction insignificant by altering the ratio of Znttp to propagating radicals. As a result, Znttp renders only a small fraction of the radicals inactive and most radicals continue to propagate, uninhibited by Znttp. This outcome is enabled by increasing the photoinitiator (Eosin) concentration and selecting wavelengths that promote effective singlet oxygen generation. Two independent light sources spanning 400-500 nm and 600-650 nm were chosen. The photoinitiator, eosin, has a negligible absorption in the 600-650 nm range whereas Znttp absorbs in both ranges, thereby providing an opportunity for nearly independent control of the oxygen photosensitization rates and the photoinitiation rate. Figure 10 shows the conversion profiles of oxygen saturated monomer formulations for various scenarios. It is clear that when Znttp is absent, the conversion profile is characterized by an extended inhibition time followed by polymerization to complete conversion. The conversion profiles for Znttp-mediated polymerizations sh

ow significantly lower inhibition times while also enabling conversions of higher than 90%, even before the inhibition period in the conventional polymerization is complete! The difference between dual and single wavelength curing is obvious in the degree of reduction in inhibition time.

6.4 Conclusions

The ability of Znttp to reduce or eliminate oxygen inhibition in radical-mediated

polymerizations has been shown. Moreover the suppression happens simultaneously with polymerization. In particular, this ability was demonstrated to be most significant in highly inhibited environments where the oxygen concentration exceeds the photoinitiator concentration, a condition under which polymerization without Znttp is practically impossible. This approach facilitates the use of low initiator concentrations, even in oxygen rich media. Furthermore, the mechanism of this suppression has been shown to occur by photosensitization of oxygen by Znttp. Therefore, with high rates of oxygen photosensitization, radical scavenging by oxygen and the associated polymerization inhibition are suppressed. Znttp also participates in increasing the termination kinetics via a non-photoactivated mechanism and as a result decreases the overall conversion significantly under some conditions. This result was overcome by appropriately designing curing conditions that relatively reduce the termination reaction while still promoting singlet oxygen generation.

6.5 References

1. Decker, C. Photoinitiated Curing of Multifunctional Monomers. Acta Polymerica **1994**, 45, 333-347.

2. Decker, C. Kinetic study and new applications of UV radiation curing. Macromolecular Rapid Communications **2002**, 23,1067-1093.

3. Andrzejewska, E. Photopolymerization kinetics of multifunctional monomers. Progress in Polymer Science **2001**, 26, 605-665.

4. Bowman, C. N.; Kloxin, C.J. Toward an enhanced understanding and implementation of photopolymerization reactions. AIChE Journal **2008,** 54, 2774-3037

5. Qian, T. C.; Li, Y. F.; Wu, Y.Z.; Zheng, B.; Ma, H.W. Superhydrophobic

poly(dimethylsiloxane) via surface-initiated polymerization with ultralow initiator density. Macromolecules **2008**, 41, 6641-6645.

6. Hansen, R. R.; Avens, H. J.; Shenoy, R.; Bowman, C.N. Quantitative evaluation of oligonucleotide surface concentrations using polymerization-based amplification. Analytical and Bioanalytical Chemistry **2008**, 392, 167-175.

7. Hansen, R. R.; Sikes, H. D.; Bowman, C.N. Visual detection of labeled oligonucleotides using visible-light-polymerization-based amplification. Biomacromolecules **2008**, 9, 355-362.

8. Sikes, H. D.; Hansen, R. R.; Johnson, L.M.; Jenison, R.; Birks, J.W.; Rowlen, K.L.; Bowman, C.N. Using polymeric materials to generate an amplified response to molecular recognition events. Nature Materials **2008**, 7, 52-56.

9. Hoyle, C. E.; Bowman, C.N. "Thiol-Ene Click Chemistry." Angewandte Chemie-International Edition **2010**, 49, 1540-1573.

10. Decker, C.; Jenkins, A.D. Kinetic Approach of O-2 Inhibition in Ultraviolet-Induced and Laser-Induced Polymerizations. Macromolecules **1985**, 18, 1241-1244.

11. Davidson, R.S. The role of amines in UV-curing; Chapman and Hall, 1993; Vol. III.

12. Miller, C.W.; Kess, R.; Iijima, T.; Hoyle, C.E. Polym. Prepr. **1997**, 38, 258

13. Hoyle, C. E.; Lee, T. Y.; Roper, T. M. Thiol-Enes: Chemistry of the past with promise for the future. J. Polym. Sci.: Polym. Chem. Ed., **2005,** 42, 530-5338

14. Gush, D. P.; Ketley, A. D. Modern paint and coatings **1978**, 11, 68

15. Studer, K.; Decker, C.; Beck, E.; Schwalm, R. Overcoming oxygen inhibition in UV-curing of acrylate coatings by carbon dioxide inerting, Part I. Progress in Organic

Coatings **2003**, 48, 92-100.

16. Decker, C. Novel Method for Consuming Oxygen Instantaneously in Photopolymerizable Films. Makromolekulare Chemie-Macromolecular Chemistry and Physics **1979**, 180, 2027-2030.

17. Gou, L. J.; B. Opheim, B.; Corestsopoulos., C.N.; Scranton, A.B. Consumption of the molecular oxygen in polymerization systems using photosensitized oxidation of dimethylanthracene. Chemical Engineering Communications **2006**, 193, 620-627.

18. Lalevee, J.; M. A. Tehfe, M.A.; Allonas, X.; Fouassier, J.P. Boryl Radicals as a New Photoinitiating Species: A Way to Reduce the Oxygen Inhibition. Macromolecules **2008**, 41, 9057-9062.

19. El-Roz, M.; J. Lalevee, J.; Allonas, X.; Fouassier, J.P. The silane-ene and silane-acrylate polymerization process: A new promising chemistry? Macromolecular Rapid Communications **2008**, 29, 804-808.

20. Awokola, M.; W. Lenhard, W.; Löffler, H.; Flosbach, C.; Frese, P. UV crosslinking of acryloyl functional polymersin the presence of oxygen. Progress in organic coatings **2002**, 44, 211- 216

21. Bonnett, R. Photosensitizers of the Porphyrin and Phthalocyanine Series for Photodynamic Therapy. Chemical Society Reviews **1995**, 24, 19-33.

22. Henderson, B. W.; Dougherty, T.J. How Does Photodynamic Therapy Work. Photochemistry and Photobiology **1992**, 55, 145-157.

23. Nelson, J. S.; Liaw, L.H.; Orenstein, A.; Roberts, W.G.; Berns, M.W. Mechanism of Tumor Destruction Following Photodynamic Therapy with

Hematoporphyrin Derivative, Chlorin, and Phthalocyanine. Journal of the National Cancer Institute **1988**, 80, 1599-1605.

24. Wasserman, H. H., Murray, R.W, Eds. Singlet Oxygen; Academic Press: New York, **1979**

25. Grofcsik, A.; Baranyai, N.; Bitter, I.; Csokai, V.; Kubinyi, M.; Szegletes, K.; Tatai, J.; Vidoczy, T. Triple state properties of tetrasubstituted zinc phthalocyanine derivatives. Journal of Molecular Structure **2004**, 704, 11-15.

26. Schweitzer, C.; Schmidt, R. Physical mechanisms of generation and deactivation of singlet oxygen. Chemical Reviews **2003**, 103, 1685-1757.

Chapter 7

Conclusions and recommendations

The glucose oxidase-mediated redox initiation is an ideal reaction to coat complex 3D substrates in a conformal fashion via interfacial polymerization given its light-independent initiation mechanism and inherent resistance to oxygen inhibition. Additionally, this initiation system also affords a high degree of reaction delocalization resulting in the ability to fabricate single and multilayer coatings that are hundreds of micrometers in thickness. This thesis discusses the relationship between the kinetics of interfacial polymerization and the macroscopic properties of the coating towards achieving heightened capabilities of the technique. The following sections summarize the findings as well as recommend future directions to expand upon this work.

The interplay of reaction behavior and mass transport processes dictates the kinetics of interfacial film growth and as a result influences the final properties of the coating such as permeability, structure and the degree of interpenetration with the substrate polymer network. To understand this interplay, the relationship between the coating thickness and the interfacial film was studied. The film growth was observed to follow two distinct kinetic regimes. An incipient growth phase that is primarily responsible for the dramatically different thicknesses between various concentrations of glucose and iron. Subsequent to this region, the film growth is nearly linear indicating that the diffusion of glucose and hydrogen peroxide to the polymerization front is sufficiently rapid to enable nearly constant polymerization rates. However, the reaction rates at this front is sufficiently rapid to prevent diffusion of initiating species into the bulk and reacting in isolation from the adhered coating, as indicated by the absence of

bulk polymerization. Stirring the bulk media caused bulk polymerization readily as a result of inducing higher mass transport rates of the initiating species into the bulk solution. These results highlight the importance of enabling a balance between the reaction and diffusion rates to minimize bulk polymerization. Therefore, factors that enable higher species diffusion rates such as substrate crosslinking density or molecular weight of monomers incorporated into the coating solution increases the tendency to cause bulk polymerization. This necessitates the means and understanding to control the delocalization process to enable interfacially confined coatings. The critical factors affecting this delocalization process were identified through a combination of experimental and mathematical modeling-based strategies. The bulk iron concentration was demonstrated to be an important factor that influences the delocalization of the redox reaction. Specifically, increasing the iron concentration in the bulk decreases the likelihood of hydrogen peroxide escaping reaction within the coating and diffusing into the bulk solution. This means that the decrease in the mass transfer resistance accompanying the use of substrates with lower crosslinking density or higher molecular weight monomers in the coating formulation can be compensated by increasing the iron concentration in the bulk media. Similarly, the degree of delocalization of the enzymatic reaction is controlled by the concentration of enzyme in the surrounding media. The enzyme, glucose oxidase has a hydrodynamic radius (~43Å) that is much greater than the mesh size of the polymer network formed using a monomer such as poly(ethylene glycol) diacrylate (MW 575) (< 20 Å). Since this monomer was used as the polymerizing precursor in the coating solution, the enzyme concentration within the coating after its formation would be different compared to the bulk enzyme concentration and is

determined by the enzyme trapping efficiency by the polymerization front since the enzyme cannot diffuse into the coating after its formation. To evaluate the trapping efficiency, the initial growth rates of a second polymeric layer on a coated hydrogel substrate with and without the presence of glucose oxidase in the bulk were compared. The significantly lower film growth rate when GOx was not present in the bulk indicated that concentration of the active enzyme trapped was dramatically lower than the bulk enzyme concentration. From the point of view of kinetics, this means that the enzymatic reaction rate within the coating is dramatically lower that bulk enzymatic reaction rates. Therefore the likelihood of glucose diffusing to the polymerization front without being significantly consumed within the coating is dramatically higher than if the trapped enzyme concentration was much higher.

To study the implications of the lower enzymatic activity within the coating, a mathematical model was developed by describing the reaction-diffusion process through representative partial differential equations that models the evolution of the species concentrations and incorporating a polymer concentration-dependent diffusion coefficient. Upon fitting the experimental data for the second layer film growth kinetics mentioned earlier to the model, the GOx concentration within the coating was evaluated to be 0.03% of the bulk enzyme concentration indicative of significant enzyme exclusion. The trapping efficiency will likely be influenced by the choice of monomer and its molecular weight and therefore must be given due consideration during material and process design. To understand the implications of this exclusion behavior, the simulation of growth kinetics and the polymer density gradients within the coating resulting from using the enzyme-mediated initiation system was compared to the same for an enzyme-

independent system such as a two-component redox system in which hydrogen peroxide is the initiating species within the core and Fe^{2+} is incorporated into the bulk media. The primary difference in the two-component redox system is the absence of a bulky initiating species that causes the exclusion behavior and hence profound differences in the reaction rate of the core species between the coating and the bulk solution. The rate of growth of film for the two-component redox system decreased dramatically with thickness unlike what was observed for the enzyme-mediated initiation system. This is because, for the two-component redox system, the likelihood of hydrogen peroxide diffusing to the polymerization front without being significantly consumed within the coating decreases with thickness. However, for the enzymatic system, glucose can readily escape reaction within the coating as a result of the dramatically lower reaction rates within the coating. This behavior also influenced the nature of polymer concentration gradients within the coating. The simulations indicated that for the enzyme-independent system, the polymerization contributed predominantly to increasing the crosslinking density of the coating after a certain coating thickness was formed. This is because hydrogen peroxide predominantly reacted within the coating and did not readily diffuse to the polymerization front where reaction would primarily increase the coating thickness. These results indicate that using an enzyme-mediated initiation system to conduct interfacial polymerization results in the ability to achieve a much higher degree of delocalization compared to an enzyme-independent system. This characteristic is advantageous in the ability to grow thicker coatings or multiple layers as both clearly depend on the ability of the initiating species to escape reaction within the coating.

The mathematical model also facilitated the characterization of the coating permeability and structure thereby providing insight into the relationship between the film growth kinetics and the macroscopic properties of the interfacial film. Particularly interesting was the influence of bulk iron concentration on the nature of the polymer density gradient within the coating. Decreasing the bulk iron concentration caused lower polymer formation adjacent to the hydrogel boundary than away from it. This was observed experimentally as significantly lower fluorescence emission adjacent to the hydrogel boundary when a fluorescent co-monomer such as rhodamine B acrylate was incorporated into the coating formulation, indicative of decreased immobilization in this region. This phenomenon primarily affects the interfacial adhesion leading to the sedimentation of the coating during the interfacial polymerization process. Investigations into the evolution of the coating permeability demonstrated that the average diffusion of a non-reactive molecule such as rhodamine B within the coating decreased with increasing coating thickness indicative of the gradual densification of the coating with time and hence thickness. This result is consistent with the rapid delocalization of the initiation reactions.

Understanding of the coating process was used to enable coatings on hydrogel microparticles towards the formation of core-shell particles with controllable properties. The self-limiting nature of film growth observed in the second layer thickness profiles as a function of time without GOx in the bulk media formed the basis for implementing a strategy that involved incorporating GOx in the microparticles and glucose in the coating solution prior to the coating process. This resulted in the decreased likelihood of bulk polymerization associated with the inevitable presence of multiple hydrogel cores with

significantly smaller dimensions in the coating solution. The incorporation of GOx into the microparticle results in hydrogen peroxide being generated only within the core thereby increasing the likelihood of polymerization occurring within the microparticle. This was observed as a quantifiable interpenetrating core and shell polymer network. To enable distinct core and shell networks, which is advantageous when conservation of the core properties is necessary, the initial locations of glucose and GOx were swapped. This action results in hydrogen peroxide generation to occur predominantly in the bulk media thereby decreasing the likelihood of formation of interpenetrating layers. However, bulk polymerization as a result of rapid diffusion of glucose into the bulk media was suppressed by using significantly shorter coating times and higher bulk iron concentration to enable localized redox reaction. This ability was implemented in the development of hollow particles by means of core photodegradation, which clearly depends on the ability to maintain the photodegradable properties of the core after the coating process. The transition of the core into a liquid was evidenced by the dramatic change in the diffusion coefficient of fluorescent microbeads incorporated into the core. Interestingly, the incorporation of GOx in the microparticle and glucose in the bulk solution resulted in dramatic alteration of the photodegradation properties of the core thereby highlighting the necessity to enable distinct coatings.

7.1 Recommendations for future work

7.1.1 Enzyme-based glucose generation

$$\text{Glucoside} \xrightarrow{\beta\text{-Glucosidase}} \text{Glucose}$$

$$\text{Glucose} + O_2 \xrightarrow[Fe^{2+}]{GOX} OH^{\circ} + \text{products}$$

This section discusses the advantages of using enzyme-mediated glucose generation to enable unique capabilities using the interfacial polymerization based coating technique. The enzyme β- Glucosidase catalyzes the hydrolysis of the glycosidic linkage in glucosides (e.g. Salicin) to form glucose. When coupled to the reaction between glucose and glucose oxidase, unique capabilities of this process, particularly in regard to coating architectures, would be enabled as discussed below.

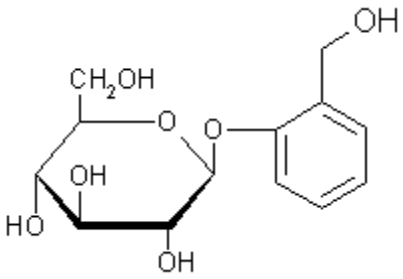

Salicin (o-(Hydroxymethyl)phenyl β-D-glucopyranoside)

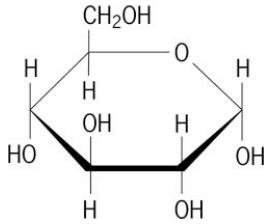

β-D Glucose

7.1.2 Formation of rupturable shells

The formation of core-shell microparticles by incorporating glucose into the core and GOx into the bulk solution prior to the coating process is advantageous in the fabrication of distinct shells as discussed earlier in this thesis. Incorporation of glucose into the core is typically enabled by its inclusion into the aqueous precursor solution used in the inverse emulsion polymerization process used to form the core. The result of this process

is a suspension of microparticles in hexane. The coating is subsequently formed by mixing the precursor coating solution into a small volume of the microparticle suspension for the desired time. The disadvantage of this process is the rapid flux of glucose into the bulk solution induced by the rapid intake of water by the hydrogel that can result in the increased likelihood of bulk polymerization or the inability to form thin coatings. This is especially pronounced when the cores are formed from monomers with molecular weights that result in high swelling ratios. For example, the molecular weight of PEG used to form the photodegradable cores discussed in the thesis is 4070 and the hydrogel formed using this monomer has a swelling ratio of around 20 after 10 minutes. An interesting application of core-shell particles with photodegradable cores is the ability to induce rupture due to swelling that accompanies degradation. However, this approach depends on the ability to generate sufficiently thin coatings. This outcome could not be obtained with the current strategy, likely because of the rapid diffusion of glucose due to a combination of higher diffusion coefficient within the core and swelling-assisted mass transport. One of the solutions is to suppress the swelling by equilibrating the cores in water prior to the coating process. However, this is not possible without causing the diffusion of glucose out of the microparticle thereby resulting in significant depletion in the core. This can be overcome by incorporating β- Glucosidase in the microparticle and salicin (and GOx, Fe^{2+}) into the coating solution. Since the bulky enzyme is trapped in the microparticle, equilibration in water prior to the coating process can be enabled without loss of the enzyme. The salicin in the bulk solution diffuses into the core to enzymatically generate glucose which subsequently diffuses into the bulk solution to initiate the GOx-mediated polymerization.

7.1.3 Formation of multilayers

Multilayered shells can be enabled by immersion of a coated microparticle into multiple coating solutions in succession. When glucose is incorporated into the core and GOx in the coating solution prior to interfacial polymerization, the challenge is to prevent premature depletion of glucose due to rapid diffusion into the bulk solution. When GOx is incorporated into the core and glucose in the bulk media prior to interfacial polymerization, the challenge is to prevent consumption of hydrogen peroxide within the coating which decreases the likelihood of formation of additional layers.

A potential solution is to incorporate β- Glucosidase in the core and salicin (and GOx, Fe^{2+}) in the coating solution. Glucose that is generated within the core as a result of reaction between β- Glucosidase and salicin diffuses into the bulk to initiate the GOx-mediated shell formation. Since GOx cannot diffuse into the coating, the reaction rate of glucose (with GOx) within the coating is sufficiently low to enable diffusion of glucose into a second coating solution without significant consumption within the first layer. This is also the case when a third layer is formed from the enzymatically generated glucose within the core.

An alternative solution is to incorporate GOx into the core and β- Glucosidase (and glucose, Fe^{2+}) in the coating solution. Here β- Glucosidase is a non-reactive component with the sole purpose of being included in the first layer. To form the second layer, the trapped β- Glucosidase in the first layer is used as the precursor along with salicin, GOx and Fe^{2+} that are incorporated in the coating solution. The second layer formed will inevitably trap the GOx in the bulk solution. To coat the third layer, GOx in

the second layer is used as the precursor and the process is repeated. The schematic is shown in Figure 1.

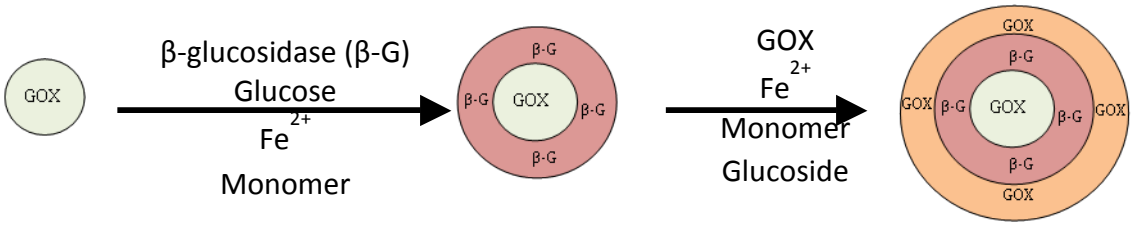

Figure 1: Schematic depicting the formation of multilayer coating using a modified scheme involving enzymatic generation of glucose

7.1.4 Alternative enzyme-substrate systems

The poor solubility of glucose and glucose oxidase in organic media restricts its use to aqueous systems. The use of enzymes or substrates that are both soluble and active in organic solvents enables the use of the enzymatic initiation system to conduct polymerization at the interface of organic media and water or in coating hydrophobic substrates. One such enzymatic system involves amine oxidase that uses amines, water and oxygen as substrates for the formation of hydrogen peroxide. Incorporating amines in an organic media and the remaining components and monomer in an aqueous phase, interfacial polymerization can be conducted without the necessity of a support substrate. However, very little is understood about the initiation kinetics or the proclivity of amine oxidase to be encapsulated within the coating.

The utilization of the glucose oxidase-mediated initiation system to enable interfacial polymerization-based coating in tissue engineering is limited to low concentrations of glucose because high levels of glucose can cause oxidative stress

on encapsulated cells. Alternative substrates such as galactose, mannose or xylose can be used with glucose oxidase to produce hydrogen peroxide. Characterization of the kinetics of polymerization in these systems is important to ascertain the feasibility of conducting interfacial polymerization at reasonable timescales.

Bibliography

1. Iwata H, Hata Y, Matsuda T, Ikada Y. Initiation of Radical Polymerization by Glucose-Oxidase Utilizing Dissolved-Oxygen. Journal of Polymer Science Part a-Polymer Chemistry 1991;29(8):1217-1218.
2. Decker C, Jenkins AD. Kinetic approach of oxygen inhibition in ultraviolet- and laser-induced polymerizations. Macromolecules 1985;18(6):1241-1244.
3. Johnson LM, Fairbanks BD, Anseth KS, Bowman CN. Enzyme-Mediated Redox Initiation for Hydrogel Generation and Cellular Encapsulation. Biomacromolecules 2009;10(11):3114-3121.
4. Berron BJ, Johnson LM, Ba X, McCall JD, Alvey NJ, Anseth KS, et al. Glucose Oxidase-Mediated Polymerization as a Platform for Dual-Mode Signal Amplification and Biodetection. Biotechnology and Bioengineering 2011;108(7):1521-1528.
5. Johnson LM, DeForest CA, Pendurti A, Anseth KS, Bowman CN. Formation of Three-Dimensional Hydrogel Multilayers Using Enzyme-Mediated Redox Chain Initiation. Acs Applied Materials & Interfaces 2010;2(7):1963-1972.
6. Hume PS, Bowman CN, Anseth KS. Functionalized PEG hydrogels through reactive dip-coating for the formation of immunoactive barriers. Biomaterials 2011;32(26):6204-6212.
7. Scott C, Wu D, Ho CC, Co CC. Liquid-core capsules via interfacial polymerization: A free-radical analogy of the nylon rope trick. Journal of the American Chemical Society 2005;127(12):4160-4161.
8. Luo YW, Gu HY. A general strategy for nano-encapsulation via interfacially confined living/controlled radical miniemulsion polymerization. Macromolecular

Rapid Communications 2006;27(1):21-25.

9. Jiang D, Huang X, Qiu F, Luo C, Huang LL. Synthesis of Polymer Thin Film Gradient with Nanometer Thickness through Water Diffusion Controlled Surface Polymerization. Macromolecules 2009;43(1):71-76.
10. von Werne TA, Germack DS, Hagberg EC, Sheares VV, Hawker CJ, Carter KR. A Versatile Method for Tuning the Chemistry and Size of Nanoscopic Features by Living Free Radical Polymerization. Journal of the American Chemical Society 2003;125(13):3831-3838.
11. Sikes HD, Hansen RR, Johnson LM, Jenison R, Birks JW, Rowlen KL, et al. Using polymeric materials to generate an amplified response to molecular recognition events. Nature Materials 2008;7(1):52-56.
12. Yoshikawa C, Goto A, Tsujii Y, Fukuda T, Yamamoto K, Kishida A. Fabrication of High-Density Polymer Brush on Polymer Substrate by Surface-Initiated Living Radical Polymerization. Macromolecules 2005;38(11):4604-4610.
13. Kizilel S, Perez-Luna VH, Teymour F. Photopolymerization of poly(ethylene glycol) diacrylate on eosin-functionalized surfaces. Langmuir 2004;20(20):8652-8658.
14. Fortier G, Belanger D. Characterization of the Biochemical Behavior of Glucose-Oxidase Entrapped in a Polypyrrole Film. Biotechnology and Bioengineering 1991;37(9):854-858.
15. Krishnaswamy S, Kittrell JR. Deactivation Studies of Immobilized Glucose Oxidase. Biotechnology and Bioengineering 1978;20(6):821-835.
16. Tse PHS, Gough DA. Time-Dependent Inactivation of Immobilized Glucose-Oxidase and Catalase. Biotechnology and Bioengineering 1987;29(6):705-713.

17. Greenfield PF, Kittrell JR, Lawrence RL. Inactivation of Immobilized Glucose Oxidase by Hydrogen-Peroxide. Analytical Biochemistry 1975;65(1-2):109-124.
18. Pryor WA. Oxyradicals and Related Species - Their Formation, Lifetimes, and Reactions. Annual Review of Physiology 1986;48:657-667.
19. Scott, C.; Wu, D.; Ho, C.-C.; Co, C. C., (2005). "Liquid-Core Capsules via Interfacial Polymerization:, A Free-Radical Analogy of the Nylon Rope Trick." Journal of the American Chemical Society 127(12): 4160-4161.
20. Luo, Y. W. and H. Y. Gu (2006). "A general strategy for nano-encapsulation via interfacially confined living/controlled radical miniemulsion polymerization." Macromolecular Rapid Communications 27(1): 21-25.
21. Shenoy R, Bowman CN, Kinetics of interfacial radical polymerization initiated by a glucose oxidase-mediated redox system, Biomaterials (2012), http://dx.doi.org/10.1016/j.biomaterials.2012.06.014
22. Langer, R. (1999). "Biomaterials in Drug Delivery and Tissue Engineering: One Laboratory's Experience." Accounts of Chemical Research 33(2): 94-101.
23. Freiberg, S. and X. X. Zhu (2004). "Polymer microspheres for controlled drug release." International Journal of Pharmaceutics 282(1–2): 1-18.
24. Zhu, Y.; Shi, J.; Shen, W.; Dong, X.; Feng, J.; Ruan, M.; Li, Y., (2005). "Stimuli-Responsive Controlled Drug Release from a Hollow Mesoporous Silica Sphere/Polyelectrolyte Multilayer Core–Shell Structure." Angewandte Chemie International Edition 44(32): 5083-5087.
25. Bäumler, H. and R. Georgieva (2010). "Coupled Enzyme Reactions in Multicompartment Microparticles." Biomacromolecules 11(6): 1480-1487.

26. White, S. R.; Sottos, N. R.; Geubelle, P. H.; Moore, J. S.; Kessler, M. R.; Sriram, S. R.; Brown, E. N.; Viswanathan, S., (2001). "Autonomic healing of polymer composites." Nature 409(6822): 794-797.
27. Janssen, L. and K. Tenijenhuis (1992). "Encapsulation by Interfacial Polycondensation .1. The Capsule Production and a Model for Wall Growth." Journal of Membrane Science 65(1-2): 59-68.
28. Janssen, L. J. J. M. and K. te Nijenhuis (1992). "Encapsulation by interfacial polycondensation. II. The membrane wall structure and the rate of the wall growth." Journal of Membrane Science 65(1,Äì2): 69-75.
29. Freger, V. (2005). "Kinetics of Film Formation by Interfacial Polycondensation." Langmuir 21(5): 1884-1894.
30. Freger, V. and S. Srebnik (2003). "Mathematical model of charge and density distributions in interfacial polymerization of thin films." Journal of Applied Polymer Science 88(5): 1162-1169.
31. Oizerovich-Honig, R.; Raim, V.; Srebnik, S., (2009). "Simulation of Thin Film Membranes Formed by Interfacial Polymerization." Langmuir 26(1): 299-306.
32. Yashin, V. V. and A. C. Balazs (2004). "Theoretical model of interfacial polymerization." Journal of Chemical Physics 121(22):11440-11454.
33. Ji, J.; Dickson, J. M.; Childs, R. F.; McCarry, B. E., (2000). "Mathematical model for the formation of thin-film composite membranes by interfacial polymerization: Porous and dense films." Macromolecules 33(2): 624-633.
34. Crank, J. (1979). The Mathematics of Diffusion, Clarendon Press.

35. Gibson, Q. H.; Massey, V.; Swoboda, B. E. P., (1964). "Kinetics and Mechanism of Action of Glucose Oxidase." Journal of Biological Chemistry 239(11): 3927-&.
36. Walling, C. (1975). "Fenton's reagent revisited." Accounts of Chemical Research 8(4): 125-131.
37. Malikkides, C. O. and R. H. Weiland (1982). "On the mechanism of immobilized glucose oxidase deactivation by hydrogen peroxide." Biotechnology and Bioengineering 24(11): 2419-2439.
38. Bourdillon, C.; Thomas, V.; Thomas, D., (1982). "Electrochemical study of d-glucose oxidase autoinactivation." Enzyme and Microbial Technology 4(3): 175-180.
39. Masaro, L. and X. X. Zhu (1999). "Physical models of diffusion for polymer solutions, gels and solids." Progress in Polymer Science 24(5): 731-775.
40. Cukier, R. I. (1984). "Diffusion of Brownian spheres in semidilute polymer solutions." Macromolecules 17(2): 252-255.
41. Waters, D. J. and C. W. Frank (2009). "Hindered diffusion of oligosaccharides in high strength poly(ethylene glycol)/poly(acrylic acid) interpenetrating network hydrogels: Hydrodynamic vs. obstruction models." Polymer 50(26): 6331-6339.
42. Mavituna, F.; Park, J. M.; Gardner, D., (1987). "Determination of the Effective Diffusion-Coefficient of Glucose in Callus-Tissue." Chemical Engineering Journal and the Biochemical Engineering Journal 34(1): B1-B5.
43. Yuan-Hui, L. and S. Gregory (1974). "Diffusion of ions in sea water and in deep-sea sediments." Geochimica et Cosmochimica Acta 38(5): 703-714.

44. Kern, D. M. H. (1954). "The Polarography and Standard Potential of the Oxygen-Hydrogen Peroxide Couple." Journal of the American Chemical Society 76(16): 4208-4214.

45. Shimada, K.; Kato, H.; Saito, T.; Matsuyama, S.; Kinugasa, S., (2005). "Precise measurement of the self-diffusion coefficient for poly(ethylene glycol) in aqueous solution using uniform oligomers." Journal of Chemical Physics 122(24).

46. Bouchoux, A.; Roux-de Balmann, H.; Lutin, F., (2005). "Nanofiltration of glucose and sodium lactate solutions - Variations of retention between single- and mixed-solute solutions." Journal of Membrane Science 258(1-2): 123-132.

47. Nightingale, E. R. (1959). "Phenomenological Theory of Ion Solvation - Effective Radii of Hydrated Ions." Journal of Physical Chemistry 63(9): 1381-1387.

48. Dohmen, M. P. J.; Pereira, A. M.; Timmer, J. M. K.; Benes, N. E.; Keurentjes, J. T. F., (2008). "Hydrodynamic radii of polyethylene glycols in different solvents determined from viscosity measurements." Journal of Chemical and Engineering Data 53(1): 63-65.

49. Fogolari, F.; Corazza, A.; Toppo, S.; Tosatto, S. C. E.; Viglino, P.; Ursini, F.; Esposito, G., "Studying Interactions by Molecular Dynamics Simulations at High Concentration." Journal of Biomedicine and Biotechnology.

50. Collinson, E.; Dainton, F. S.; Mile, B.; Tazuke, S.; Smith, D. R., (1963). "Thermal Redox Reactions Between Metal Ions and Radicals in Aqueous Solutions." Nature 198(4875): 26-30.

51. Decker, C. Photoinitiated Curing of Multifunctional Monomers. Acta Polymerica **1994**, 45, 333-347.

52. Decker, C. Kinetic study and new applications of UV radiation curing. Macromolecular Rapid Communications **2002**, 23,1067-1093.
53. Andrzejewska, E. Photopolymerization kinetics of multifunctional monomers. Progress in Polymer Science **2001**, 26, 605-665.
54. Bowman, C. N.; Kloxin, C.J. Toward an enhanced understanding and implementation of photopolymerization reactions. AIChE Journal **2008,** 54, 2774-3037
55. Qian, T. C.; Li, Y. F.; Wu, Y.Z.; Zheng, B.; Ma, H.W. Superhydrophobic poly(dimethylsiloxane) via surface-initiated polymerization with ultralow initiator density. Macromolecules **2008**, 41, 6641-6645.
56. Hansen, R. R.; Avens, H. J.; Shenoy, R.; Bowman, C.N. Quantitative evaluation of oligonucleotide surface concentrations using polymerization-based amplification. Analytical and Bioanalytical Chemistry **2008**, 392, 167-175.
57. Hansen, R. R.; Sikes, H. D.; Bowman, C.N. Visual detection of labeled oligonucleotides using visible-light-polymerization-based amplification. Biomacromolecules **2008**, 9, 355-362.
58. Sikes, H. D.; Hansen, R. R.; Johnson, L.M.; Jenison, R.; Birks, J.W.; Rowlen, K.L.; Bowman, C.N. Using polymeric materials to generate an amplified response to molecular recognition events. Nature Materials **2008**, 7, 52-56.
59. Hoyle, C. E.; Bowman, C.N. "Thiol-Ene Click Chemistry." Angewandte Chemie-International Edition **2010**, 49, 1540-1573.
60. Decker, C.; Jenkins, A.D. Kinetic Approach of O-2 Inhibition in Ultraviolet-Induced and Laser-Induced Polymerizations. Macromolecules **1985**, 18, 1241-1244.

61. Davidson, R.S. The role of amines in UV-curing; Chapman and Hall, 1993; Vol. III.

62. Miller, C.W.; Kess, R.; Iijima, T.; Hoyle, C.E. Polym. Prepr. **1997**, 38, 258

63. Hoyle, C. E.; Lee, T. Y.; Roper, T. M. Thiol-Enes: Chemistry of the past with promise for the future. J. Polym. Sci.: Polym. Chem. Ed., **2005,** 42, 530-5338

64. Gush, D. P.; Ketley, A. D. Modern paint and coatings **1978**, 11, 68

65. Studer, K.; Decker, C.; Beck, E.; Schwalm, R. Overcoming oxygen inhibition in UV-curing of acrylate coatings by carbon dioxide inerting, Part I. Progress in Organic Coatings **2003**, 48, 92-100.

66. Decker, C. Novel Method for Consuming Oxygen Instantaneously in Photopolymerizable Films. Makromolekulare Chemie-Macromolecular Chemistry and Physics **1979**, 180, 2027-2030.

67. Gou, L. J.; B. Opheim, B.; Corestsopoulos., C.N.; Scranton, A.B. Consumption of the molecular oxygen in polymerization systems using photosensitized oxidation of dimethylanthracene. Chemical Engineering Communications **2006**, 193, 620-627.

68. Lalevee, J.; M. A. Tehfe, M.A.; Allonas, X.; Fouassier, J.P. Boryl Radicals as a New Photoinitiating Species: A Way to Reduce the Oxygen Inhibition. Macromolecules **2008**, 41, 9057-9062.

69. El-Roz, M.; J. Lalevee, J.; Allonas, X.; Fouassier, J.P. The silane-ene and silane-acrylate polymerization process: A new promising chemistry? Macromolecular Rapid Communications **2008**, 29, 804-808.

70. Awokola, M.; W. Lenhard, W.; Löffler, H.; Flosbach, C.; Frese, P. UV crosslinking of acryloyl functional polymersin the presence of oxygen. Progress in organic coatings **2002**, 44, 211- 216

71. Bonnett, R. Photosensitizers of the Porphyrin and Phthalocyanine Series for Photodynamic Therapy. Chemical Society Reviews **1995**, 24, 19-33.

72. Henderson, B. W.; Dougherty, T.J. How Does Photodynamic Therapy Work. Photochemistry and Photobiology **1992**, 55, 145-157.

73. Nelson, J. S.; Liaw, L.H.; Orenstein, A.; Roberts, W.G.; Berns, M.W. Mechanism of Tumor Destruction Following Photodynamic Therapy with Hematoporphyrin Derivative, Chlorin, and Phthalocyanine. Journal of the National Cancer Institute **1988**, 80, 1599-1605.

74. Wasserman, H. H., Murray, R.W, Eds. Singlet Oxygen; Academic Press: New York, **1979**

75. Grofcsik, A.; Baranyai, N.; Bitter, I.; Csokai, V.; Kubinyi, M.; Szegletes, K.; Tatai, J.; Vidoczy, T. Triple state properties of tetrasubstituted zinc phthalocyanine derivatives. Journal of Molecular Structure **2004**, 704, 11-15.

76. Schweitzer, C.; Schmidt, R. Physical mechanisms of generation and deactivation of singlet oxygen. Chemical Reviews **2003**, 103, 1685-1757.